Stony Brook University

OFFICIAL COPY

The official electronic file of this thesis or dissertation is maintained by the University Libraries on behalf of The Graduate School at Stony Brook University.

© All Rights Reserved by Author.

The binding and release of oxygen and hydrogen peroxide are directed through a hydrophobic tunnel in cholesterol oxidase

A Dissertation Presented

by

Lin Chen

to

The Graduate School

in Partial Fulfillment of the

Requirements

for the Degree of

Doctor of Philosophy

in

Chemistry

Stony Brook University

August 2007

Stony Brook University

The Graduate School

Lin Chen

We, the dissertation committee for the above candidate for the Doctor of Philosophy degree, hereby recommend acceptance of this dissertation.

Nicole S. Sampson, Professor, Dissertation Advisor, Department of Chemistry

Carlos Simmerling, Associate Professor, Chairperson of defense, Department of Chemistry

Stanislaus S. Wong, Associate Professor, Third member of defense, Department of Chemistry

John Shanklin, Senior Biochemist, Outside member of defense, Biology Department, Brookhaven National Laboratory

This dissertation is accepted by the Graduate School

Lawrence Martin

Dean of the Graduate School

Abstract of the Dissertation

The binding and release of oxygen and hydrogen peroxide are directed through a hydrophobic tunnel in cholesterol oxidase

by

Lin Chen

Doctor of Philosophy

in

Chemistry

Stony Brook University

2007

The catalytic mechanism of cholesterol oxidase has been extensively studied, but the steps involving the usage of molecular oxygen are still not fully understood. Recently, a crystal structure of cholesterol oxidase was solved at sub-Ångstrom resolution (Lario PI, Sampson N and Vrielink A, J Mol. Biol. 2003; 326:1635-50). Multiple side-chain conformations were observed for the active site residues. The conformations of Asn485 suggested that it acts as a gate to modulate oxygen entry through a tunnel. The tunnel residues adopt multiple conformations as well. In this work, validation of the catalytic function for other

tunnels was sought. Mutations of tunnel residues result in 30-60 fold reductions in the rate of oxidation, but the rate of isomerization is almost unchanged. Hydride transfer from sterol to flavin adenine dinucleotide (FAD) is no longer rate limiting in the tunnel mutants. The wild-type enzyme forms a ternary complex with both substrates, cholesterol and oxygen. The mutant enzymes are kinetically cooperative with respect to oxygen. A mnemonic model was constructed to explain the observed kinetic cooperativity. As predicted by the model, The mutant reactions are not cooperative with respect to cholesterol and kinetic cooperativity increases with increasing cholesterol concentration. Also consistent with the model, positive cooperativity is lost when a poor substrate reduces the rate of subsequent catalytic steps. The crystal structure of the mutant, F359W, supports the kinetic interpretation.

Dedicate to my loving family

and

to Prof. Marian Stankovich, who gave critical advice on Chapter 3 of this dissertation but passed away recently

Table of Contents

Chapter 2

The catalysis of cholesterol oxidase can be controlled by a hydrophobic tunnel that allows the access of molecular oxygen to the active site as well as the output of hydrogen peroxide

Chapter 3

The interplay between potentiometry and structural biology: probing the role of Asn485 in the catalysis of cholesterol oxidase by two mutant enzymes: N485L and N485D

Chapter 4

Experimental methods

List of Figures

Figure **Page**

Chapter 1

Chapter 2

Chapter 3

Chapter 4

List of Tables

Table **Page**

Chapter 1

Chapter 2

Chapter 3

List of Schemes

Scheme **Page**

Chapter 1

Chapter 3

Chapter 4

List of Abbreviations

2×YT	2×yeast-tryptone broth
3BHSD	3β-hydroxysterol dehydrogenase
Ala, A	Alanine
Asp, D	Aspartic acid
AO_Cb	alcohol oxidase from *Candida boidinii*
bCD_Ec	β-choline dehydrogenase from *Escherichia coli*
BSA	Bovine Serum Albumin
Cys, C	Cysteine
ChoA	*Streptomyces* cholesterol oxidase
ChoB	*Brevibacterium sterolicum* cholesterol oxidase
ChoD	Cholesterol oxidase-like enzyme from *Rhodococcus equi*
ChoE	*Rhodococcus equi* cholesterol oxidase
CO_Re	cholesterol oxidase from *Rhodococcus equi*
CO_St	cholesterol oxidase from *Streptomyces* spp.
ddiH_2O	distilled, deionized water
DHEA	dehydroepiandrosterone
DTT	dithiothreitol
FAD	flavin adenine dinucleotide
$FADH_2$	1,5 dihydroflavin adenine dinucleotide
Gln, Q	Glutamine
Glu, E	Glutamic Acid
GMC	glucose-methanol-choline
GO_An	*Aspergillus niger* glucose oxidase
h	hour
H	histidine
HRP	horseradish peroxidase
HPAA	p-hydroxyphenyl acetic acid
I.E.	isotope effects
IPTG	isopropyl α-D-thiogalactoside
K.I.E.	kinetic isotope effects
L	liter
LB	Luria broth
Leu, L	Leucine
ML_Ps	(*R*)-(1)-mandelonitrile lyase from *Prunus serotina*
PEG	Polyethyleneglycol
RPM	Rotation Per Minute
SDS-PAGE	Sodium Dodecyl Sulphate- Polyacrylamide Gel Electrophoresis
Thr, T	Threonine
Tyr, Y	Tyrosine

UV	UltraViolet
vis	visible
Val, V	Valine
WT	Wild Type

Acknowledgement

It has been an exciting and yet rewarding journey - one that I had never dreamed of. The knowledge and experience I gained here in Prof. Sampson's lab have been invaluable to my career. I am deeply indebted to Prof. Sampson for her encouragement, advice, mentoring, and research support throughout my master's and doctoral studies. I also truly appreciate her patience and tolerance during my numerous mishaps. This dissertation is part of the research carried out through her vision throughout last six years.

Ever since I accepted the offer from Stony Brook I have been warmly welcomed and hosted by the Chemistry community. I would like to gratefully thank all members of the department who help me going through all the teaching assignments and courses. Especially, I want to address Prof. Carlos Simmerling and Prof. Stanislaus Wong for their patience and advice in serving as my committee members.

I am fortunate to have the opportunity to work with a group of energetic people in Prof. Sampson's Lab. I have enjoyed every moment that we have worked together. I appreciate all their friendships and their collective encouragement to finish this dissertation.

To all of you, thank you.

Chapter 1

Overview of cholesterol oxidase

I. Cholesterol oxidase and other enzymes in the family

1. Overview

Cholesterol oxidases are a class of enzymes that are capable of oxidizing a number of steroids including cholesterol. The ability of some microbes to utilize cholesterol and other sterols as their carbon source was noted [**1**]. Studies demonstrated the conversion of cholesterol to 17-keto steroids [**2**] and coprostanol [**3**]. However, due to limitation of techniques available, researchers were not able to purify a single enzyme of cholesterol oxidase at that time. Meanwhile, cholesterol oxidase attracted more attention in the field of insecticide discovery in the 1960's. A finding that insects could use sterols to support larva development led scientists to examine the role of cholesterol oxidase in insect physiology [**4**]. Boll weevil, the bug that fed on cotton buds and flowers, were devastating to farm crops for decades. The fact that its larva development was inhibited by a protein that is homologous in sequence to cholesterol oxidase from *Streptomyces* triggered a series of studies [**5, 6**] aiming to find alternative to DTT (dichlorodiphenyltrichloroethane, an organochlorine) which is a major environmental threat [**7**].

The first pure cholesterol oxidase was isolated from a gram-positive bacteria, *Rhodococcus equi* in 1973 [**8**]. It brought the research of cholesterol oxidases to molecular level. A significant application following this work was the detection of serum cholesterol level by an assay, the major active component of which was cholesterol oxidase [**9**]. This method quickly gained

its popularity due to the increasing number of patients suffering cardiovascular diseases which will often result in abnormal serum cholesterol levels. With the improvements of molecular biology techniques, cholesterol oxidases were found in a number of other gram-positive bacterium such as *Streptomyces*, *Nocardia,* and *Pseudomonas* [**10, 11**]. Discoveries related to cholesterol oxidase are summarized in **Table 1-1**.

With an increasing interest in the catalytic mechanism of cholesterol oxidase, as well as advances in crystallography, a crystal structure of cholesterol oxidase became necessary. The first crystal structure of cholesterol oxidase (from *Rhodococcus equi*) was available in 1991 when it was refined to 1.8 Å [**12**]. This marked the start of atomic level research on cholesterol oxidase which extends to the study covered in this dissertation. Depending on a much more thorough and in-depth understanding of the mechanism of cholesterol oxidase catalysis, people found various applications of cholesterol oxidase in other fields such as membrane probe [**13**] and biosensor development [**14**] More importantly, a 3β-hydroxysterol dehydrogenase which catalyzes similar reactions to cholesterol oxidase is coded by a gene in the completed genome of *Mycobacterium Tuberculosis* [**15**]. In the rest of this section, details regarding the biology and applications of cholesterol oxidases will be reviewed and possible inhibitor design will be discussed.

Year	Milestone
1944~ 1967	Cholesterol and other sterols were oxidized by microbes as their carbon source [**1, 2**]
1973	First cholesterol oxidase isolated and crystallized from *Brevibacterium* [**8**]
1973	A method was developed to detect serum cholesterol level by cholesterol oxidase [**9, 16**]
1976	Cholesterol oxidase was found in *Nocardia, Pseudomonas* and *Rhodococcus* [**10**]
1989	Cholesterol oxidase found in *Streptomyces* [**11**]
1990	Immobilized cholesterol oxidase can be used as biosensor [**14**]
1991	Cholesterol oxidase crystal structure was solved [**17**]
1992	Membrane structure can be detected by using cholesterol oxidase as a probe [**13**]
1993	Boll weevil's growth was inhibited by an enzyme which was suggested as a cholesterol oxidase [**5**]
1997	Cholesterol oxidase was discovered to be associated with the pathogenesis of *Rhodococcus. equi* [**18**]
2005	Alzheimer disease beta-amyloid had similar mode of action as cholesterol oxidase [**19**]

Table 1-1 Milestones of cholesterol oxidase related discoveries

2. ChoA and ChoB

Based on the site of formation, non-pathogenic cholesterol oxidases can be classified into two groups: in one of the groups the enzymes are formed intracellularly or membrane associated, for example, *Rhodococcus erythropolis* [**20**] and *Nocardia rhodochrous* [**21**]; the other group of cholesterol oxidases are secreted into the growth media by the host organism, such as *Rhodococcus equi* [**22**] and *Streptomyces violascens* [**23**]. In this dissertation, all enzymes including original and mutated forms are derived from *Streptomyces* SA-COO strain [**24**], commonly recognized as ChoA. There are two distinct forms of cholesterol oxidase. These two forms bind the FAD cofactor in two different ways: non-covalently and covalently, respectively. They also differ in terms of structure, folding, kinetic and thermodynamic properties. Based on structure homology, cholesterol oxidases can be classified into two types. One example of the type II enzyme is the cholesterol oxidase from *Brevibacterium Sterolicum* which binds FAD covalently [**25**].

ChoA is secrected by *Streptomyces* bacteria into the environment (often soil) to break down steroids into an ingestible carbon source. *Streptomycetes* are among the many microbes that inhabit soil. In fact, the earthy smell of the soil is mainly due to the chemicals released by *Streptomyces* [**26**]. Their shapes are represented by long, helical filaments [**27**]. The most notable usage of *Streptomyces* bacteria is for the production of antibiotics and generation of potential drug leads [**28, 29**]. For example, one of the antibiotics derived from streptomycetes, bleomycin, has been an early tool in cancer

treatment [**30**].

The genome of *Streptomyces* can respond to changes in the environment and the expression of secondary metabaolism genes is conditionally regulated [**31**]. This feature has enabled *Streptomyces* to metabolize a wide range of materials including sugar, amino acids and steroids. This property is also useful in turning streptomycetes into a decomposing agent of some hazardous materials [**32**].

3. ChoD, ChoE and 3BHSD

These three enzymes have potential roles in assisting bacteria to infect their host. ChoD is from *Nocardia farcinica* which can cause an infectious disease called nocardiosis, especially during lung infection (Vet. Microbiol. 110, 1-2, p131-40 – will add to bibliography after all revision) [**33**]. This type of virulence is similar to the reported lung infection by *Rhodococcus equi*. ChoE (from *Rhodococcus equi*) has been suggested to act as a membrane-damaging toxin [**34**] while the role of ChoD in the virulence of *Nocardia farcinica* remains unclear. One enzyme from *Mycobacterium tuberculosis* 3β-hydroxysterol dehydrogenase (3BHSD), though not a cholesterol oxidase it uses NAD^+ instead of FAD as the cofactor, catalyzes similar oxidation and isomerization reactions [**35**]. All these three pathogenic bacteria target lung cells as their infection site.

The fact that cholesterol oxidase can be used as an insecticide by lysing endothelial cells of boll weevil (**Figure 1-1**) [**36**] has led to the proposal that the role of this enzyme is to break down membrane during pathogenesis. In *Mycobacterium tuberculosis*, this has been supported by the finding that the bacteria do not feed on sterols which suggests that cholesterol oxidases are not genetically generated for the purpose of primary metabolizm [**37**].

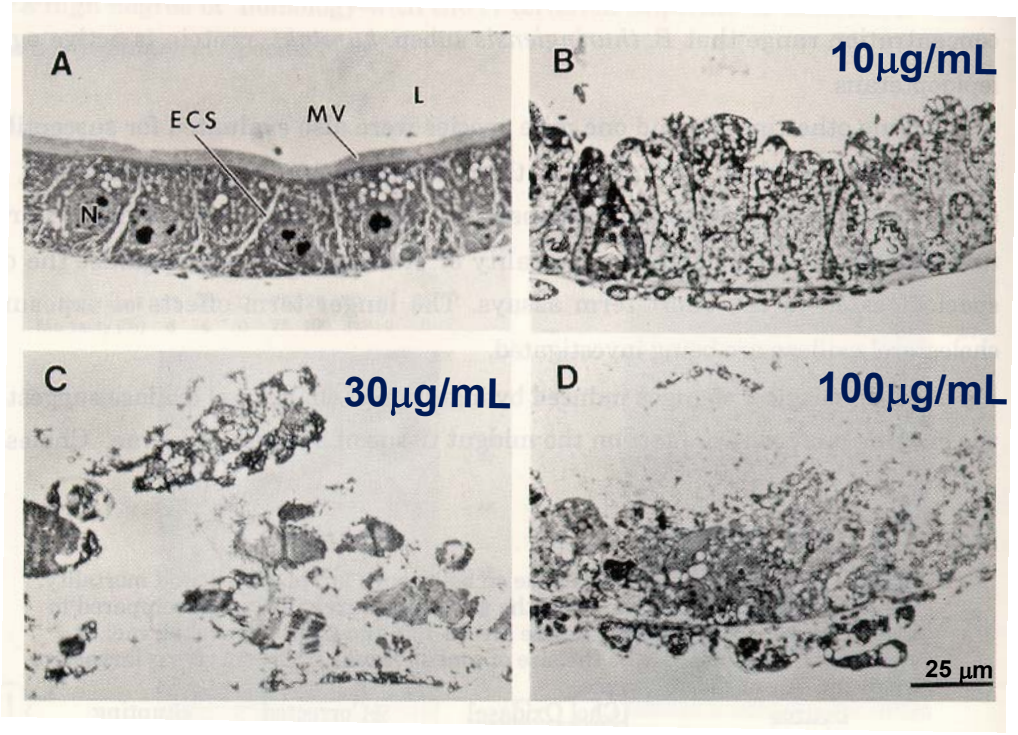

Figure 1-1 Midgut endothelial membranes of boll weevil larvae are lysed by cholesterol oxidase. Different concentrations of cholesterol oxidase used are labeled in each picture. A, control larvae, no cholesterol oxidase was added; B, partial lysis was induced by 10 μg/mL enzyme; Complete disruption of the membrane was observed at 30 μg/mL and 100 μg/mL for larvae (C) and second instar larvae (D), respectively. Reprinted from [**36**] with permission from Elsevier.

II. Physical and structural properties of type I cholesterol oxidase

1. Physical properties

Cholesterol oxidases are interfacial enzymes. They are water-soluble but their substrates, mostly steroids, are lipid-soluble and often localize in the lipid bilayer. The enzyme will need to bind to the lipid membrane in order to extract the steroids substrates. Cholesterol oxidase from different species possesses different molecular weight, substrate specificity, temperature, pH optimum and cofactor binding. For example, cholesterol oxidase from *Nocardia* is mostly active at 32 °C instead of 37 °C for most other cholesterol oxidases [**38**]. ChoA has a molecular weight of ~57 kDa.

2. Sequences

The amino acid sequence of ChoA has very low sequence identity with type II enzyme but overlap most with that of ChoE. The structure of glucose oxidase from *Aspergillus niger* (GO) is more similar to ChoA and ChoE (**Figure 1-2**). His447 (from ChoA) is conserved from ChoA, ChoE to GO. All four proteins contain a consensus Phe residue which in the case of ChoA is at 359 position. The active site Asn485 residue in ChoA is common in ChoE but not GO.

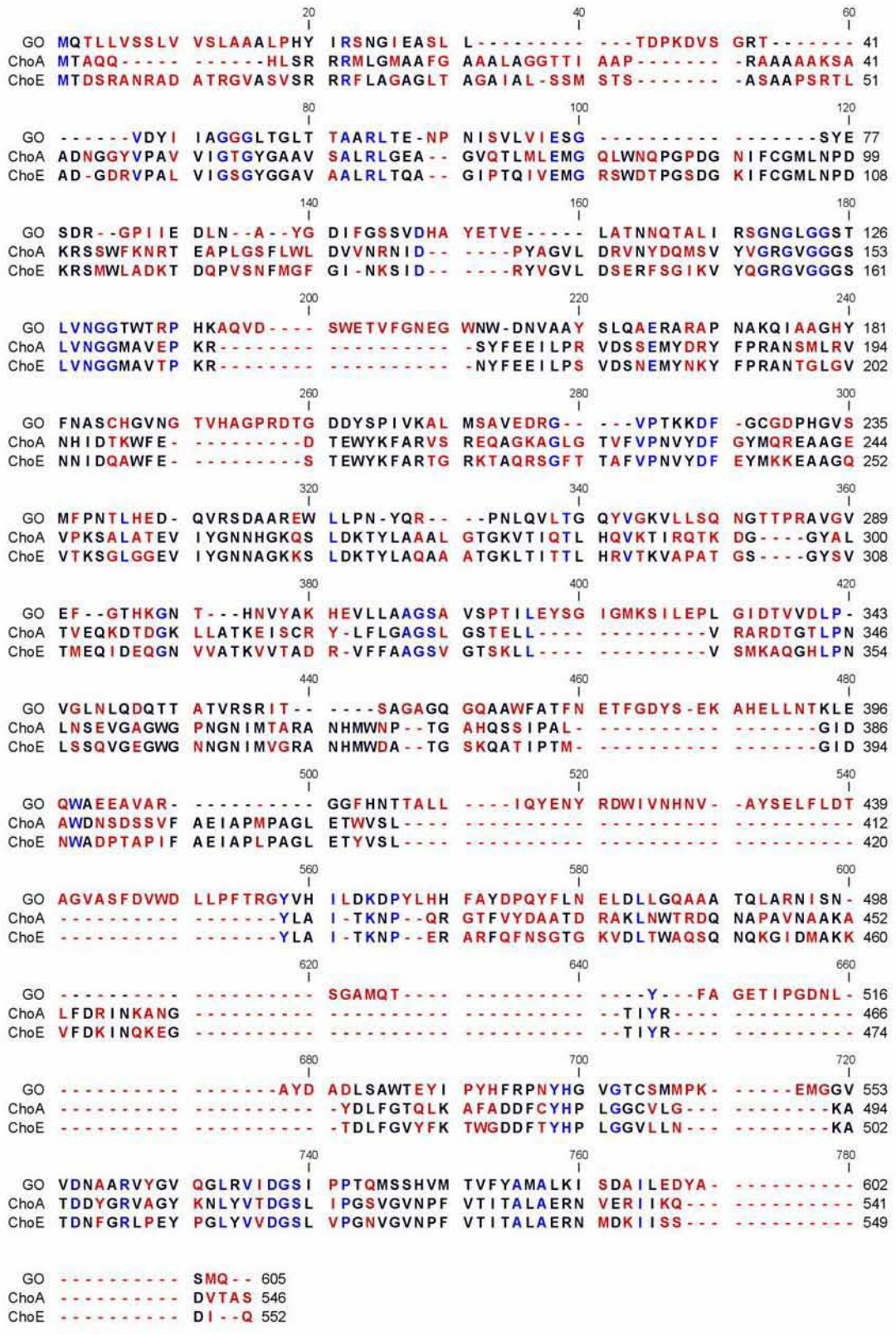
GO MQTLLVSSLV VSLAAALPHY IRSNGIEASL L--------- ---TDPKDVS GRT------- 41
ChoA MTAQQ----- ------HLSR RRMLGMAAFG AAALAGGTTI AAP------- -RAAAAAKSA 41
ChoE MTDSRANRAD ATRGVASVSR RRFLAGAGLT AGAIAL-SSM STS------- -ASAAPSRTL 51
GO ------VDYI IAGGGLTGLT TAARLTE-NP NISVLVIESG ---------- -------SYE 77
ChoA ADNGGYVPAV VIGTGYGAAV SALRLGEA-- GVQTLMLEMG QLWNQPGPDG NIFCGMLNPD 99
ChoE AD-GDRVPAL VIGSGYGGAV AALRLTQA-- GIPTQIVEMG RSWDTPGSDG KIFCGMLNPD 108
GO SDR--GPIIE DLN--A--YG DIFGSSVDHA YETVE----- LATNNQTALI RSGNGLGGST 126
ChoA KRSSWFKNRT EAPLGSFLWL DVVNRNID-- ----PYAGVL DRVNYDQMSV YVGRGVGGGS 153
ChoE KRSMWLADKT DQPVSNFMGF GI-NKSID-- ----RYVGVL DSERFSGIKV YQGRGVGGGS 161
GO LVNGGTWTRP HKAQVD---- SWETVFGNEG WNW-DNVAAY SLQAERARAP NAKQIAAGHY 181
ChoA LVNGGMAVEP KR-------- ---------- -SYFEEILPR VDSSEMYDRY FPRANSMLRV 194
ChoE LVNGGMAVTP KR-------- ---------- -NYFEEILPS VDSNEMYNKY FPRANTGLGV 202
GO FNASCHGVNG TVHAGPRDTG DDYSPIVKAL MSAVEDRG-- ---VPTKKDF -GCGDPHGVS 235
ChoA NHIDTKWFE- ---------D TEWYKFARVS REQAGKAGLG TVFVPNVYDF GYMQREAAGE 244
ChoE NNIDQAWFE- ---------S TEWYKFARTG RKTAQRSGFT TAFVPNVYDF EYMKKEAAGQ 252
GO MFPNTLHED- QVRSDAAREW LLPN-YQR-- --PNLQVLTG QYVGKVLLSQ NGTTPRAVGV 289
ChoA VPKSALATEV IYGNNHGKQS LDKTYLAAAL GTGKVTIQTL HQVKTIRQTK DG----GYAL 300
ChoE VTKSGLGGEV IYGNNAGKKS LDKTYLAQAA ATGKLTITTL HRVTKVAPAT GS----GYSV 308
GO EF--GTHKGN T---HNVYAK HEVLLAAGSA VSPTILEYSG IGMKSILEPL GIDTVVDLP- 343
ChoA TVEQKDTDGK LLATKEISCR Y-LFLGAGSL GSTELL---- ---------V RARDTGTLPN 346
ChoE TMEQIDEQGN VVATKVVTAD R-VFFAAGSV GTSKLL---- ---------V SMKAQGHLPN 354
GO VGLNLQDQTT ATVRSRIT-- ----SAGAGQ GQAAWFATFN ETFGDYS-EK AHELLNTKLE 396
ChoA LNSEVGAGWG PNGNIMTARA NHMWNP--TG AHQSSIPAL- ---------- -------GID 386
ChoE LSSQVGEGWG NNGNIMVGRA NHMWDA--TG SKQATIPTM- ---------- -------GID 394
GO QWAEEAVAR- ---------- GGFHNTTALL ----IQYENY RDWIVNHNV- -AYSELFLDT 439
ChoA AWDNSDSSVF AEIAPMPAGL ETWVSL---- ---------- ---------- ---------- 412
ChoE NWADPTAPIF AEIAPLPAGL ETYVSL---- ---------- ---------- ---------- 420
GO AGVASFDVWD LLPFTRGYVH ILDKDPYLHH FAYDPQYFLN ELDLLGQAAA TQLARNISN- 498
ChoA ---------- -------YLA I-TKNP--QR GTFVYDAATD RAKLNWTRDQ NAPAVNAAKA 452
ChoE ---------- -------YLA I-TKNP--ER ARFQFNSGTG KVDLTWAQSQ NQKGIDMAKK 460
GO ---------- ---------- SGAMQT---- ---------- ----Y---FA GETIPGDNL- 516
ChoA LFDRINKANG ---------- ---------- ---------- --TIYR---- ---------- 466
ChoE VFDKINQKEG ---------- ---------- ---------- --TIYR---- ---------- 474
GO ---------- -------AYD ADLSAWTEYI PYHFRPNYHG VGTCSMMPK- -----EMGGV 553
ChoA ---------- ---------- -YDLFGTQLK AFADDFCYHP LGGCVLG--- --------KA 494
ChoE ---------- ---------- -TDLFGVYFK TWGDDFTYHP LGGVLLN--- --------KA 502
GO VDNAARVYGV QGLRVIDGSI PPTQMSSHVM TVFYAMALKI SDAILEDYA- ---------- 602
ChoA TDDYGRVAGY KNLYVTDGSL IPGSVGVNPF VTITALAERN VERIIKQ--- ---------- 541
ChoE TDNFGRLPEY PGLYVVDGSL VPGNVGVNPF VTITALAERN MDKIISS--- ---------- 549
GO ---------- SMQ-- 605
ChoA ---------- DVTAS 546
ChoE ---------- DI--Q 552

Figure 1-2 Sequence alignment of cholesterol oxidases. ChoA, type I cholesterol oxidase from *Streptomyces*; ChoE, type I cholesterol oxidase from *Rhodococcus*; GO, glucose oxidase from *Aspergillus niger*. Residues highlighted in blue, 100% identical; Black, 75%; Red, <50%. Alignment was computed using CLC protein workbench [**39**].

3. Reactions catalyzed by cholesterol oxidase

ChoA is a bi-functional enzyme that catalyzes two reactions in one active site: an oxidation reaction which converts cholesterol into cholest-5-en-3-one followed by an isomerization reaction that converts the intermediate to the more thermodynamically stable cholest-4-en-3-one (**Scheme 1-1**). Meanwhile, one molecule of FAD cofactor is needed during the oxidation reaction to accept one hydride from the substrate. FAD is thus reduced. It is cycled back to its oxidized state by one molecule of oxygen, which is reduced to H_2O_2.

ChoA belongs to the glucose-methanol-choline (GMC) oxidoreductase family of enzymes [**40**]. Other enzymes in this family include methanol oxidase from the yeast *Hansenula polymorpha*, glucose oxidase from *Aspergillus niger* and choline dehydrogenase from *E. Coli*. These enzymes use the same cofactor (FAD) and catalyze similar reactions: oxidation of a hydroxy group to a ketone. For example, glucose oxidase catalyzes the oxidation of β-D-glucose to glucono-δ-lactone (**Scheme 1-2**) [**41**]. Glucose oxidase is homologous to cholesterol oxidase in structure and the oxidation reaction catalyzed. It undergoes a ping-pong Bi Bi mechanism to catalyze two-substrate enzymatic reactions [**42**]. More details about the kinetic aspects of glucose oxidase will be reviewed in Chapter 2.

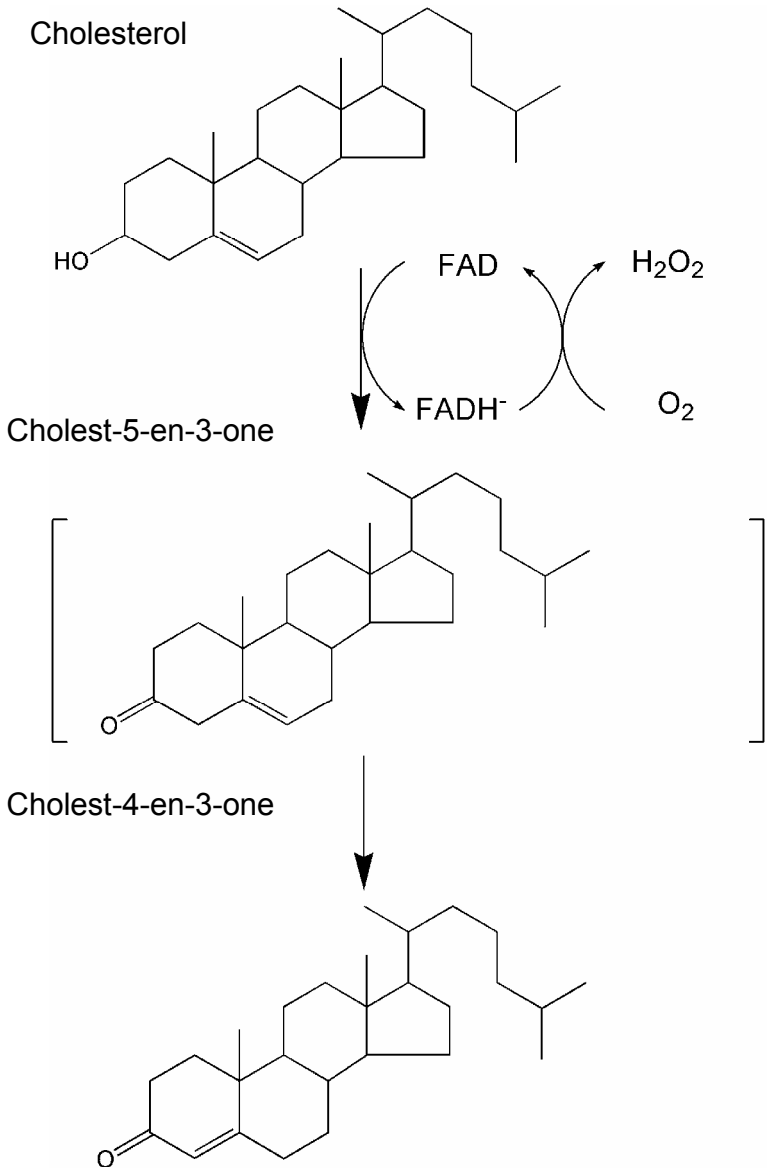

Scheme 1-1 Reaction catalyzed by cholesterol oxidase

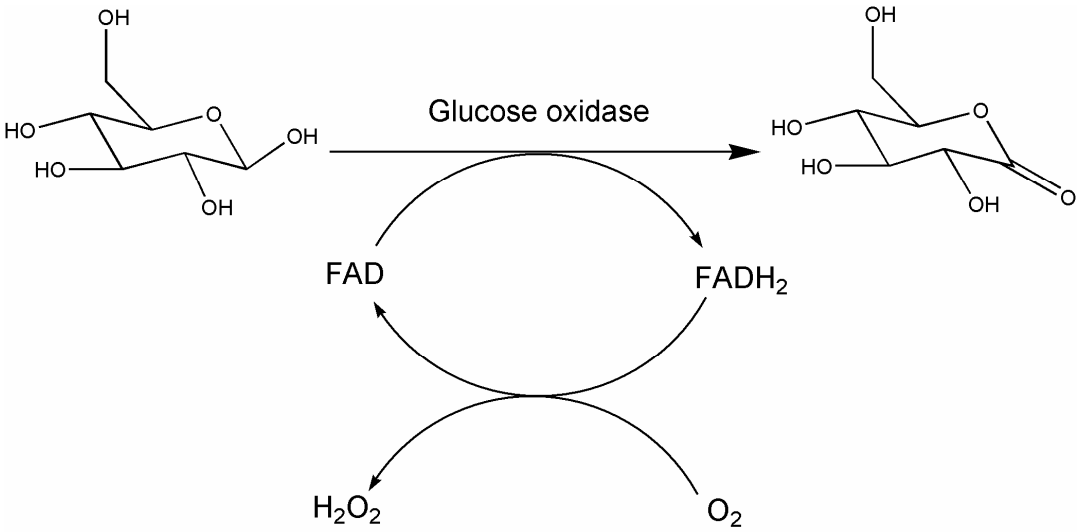

Scheme 1-2 Glucose oxidase oxidizes β-D-glucose into glucono-δ-lactone

An important application derived from the oxidation reaction catalyzed by cholesterol oxidase is the detection of serum cholesterol levels by monitoring product H_2O_2 formation by coupling to horseradish peroxidase in the visible wavelength region (**Scheme 1-3**). This assay is of interest because serum cholesterol levels are tightly associated with the risk of developing coronary heart disease [**43**]. The molecular basis of this serum cholesterol assay is that the horseradish peroxidase product, quinoneimine, has a significant absorbance at 505 nm which can be quantified.

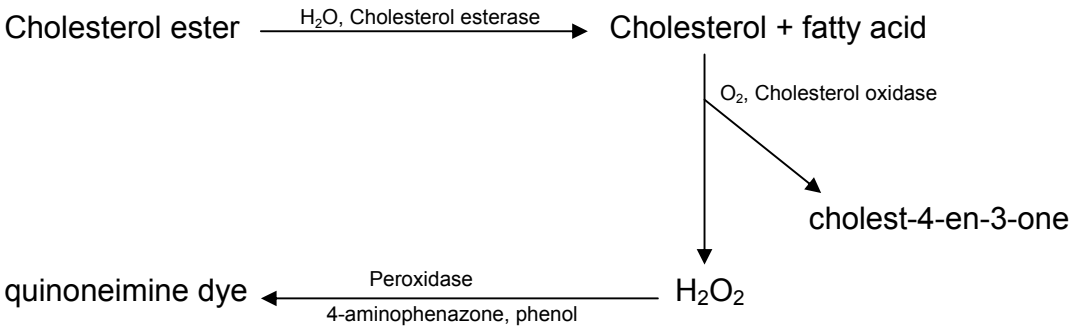

Scheme 1-3 Reaction basis of serum cholesterol assays

In addition to the oxidation reaction, ChoA also catalyzes a unique isomerization reaction that distinguishes it from the other GMC enzymes. The intermediate, cholest-5-en-3-one, is barely stable under normal physiological conditions. It slowly isomerizes to cholest-4-en-3-one at room temperature and neutral pH. However, it is subject to auto-catalyzed radical peroxidation and side products such as cholest-4-en-6-hydroperoxy-3-one are formed [**44, 45**]. The existence of this additional step can thus be attributed to the need to protect the intermediate from side reactions and better yield of the final products. This type of enzymatic isomerization of steroids is catalyzed by other enzymes such as ketosteroid isomerase [**46**] and especially 3β-hydroxy dehydrogenase [**47**], because the latter catalyzes a similar oxidation reaction preceding the isomerization, but in a different active site [**48**].

3β-Hydroxy steroid dehydrogenase (3BHSD) is one of the most important enzymes in the mammalian steroid metabolism pathways. One of the pathways that requires this enzyme, bile acid biosynthesis, has been given more attention recently due to its association with obesity treatment [**49**]. Bile acid is synthesized from cholesterol in the liver and is secreted into the intestine to enhance digestion of fat, as well as up-regulating a number of other genes the products of which are involved in energy metabolism. In short, 3BHSD is critical in regulating bile acid biosynthesis and thus affecting body cholesterol and fat level. Although 3BHSD catalyzes reactions similar to its bacterial counterpart, ChoA, their sequences and structures share little homology.

4. Tertiary structure of cholesterol oxidase

ChoA is structurally homologous to type I cholesterol oxidase from *Rhodococcus equi* (ChoE). Residues that are related to cofactor binding, as well as active site formation, are mostly conserved between ChoA and type I ChoE [**50**]. As a result, their native structures are almost identical. Residues 441-491 have been categorized as GMC oxidoreductase domain (CDD # 45101) that are involved in forming the catalytic center of the enzymes. The substrate-binding domain is mainly composed of alternative α helixes and β sheets. The substrate binding loops reside on a single face of the enzyme. A substrate analog has been crystallized with type I ChoE and the structure is shown in **Figure 1-2B**. This structure has allowed a detailed observation of the substrate binding loops which consist of two loops: loop 1 made up of residues 78-87 and loop 2 that is residues 433 to 436. Poor electron density in these regions has led to the suggestion that these loops are quite flexible structurally in type I ChoE, while in ChoA loop 2 is an ordered α helix (colored yellow, **Figure 1-2 A** and **B**).

On the other hand, type II ChoB has little structural homology with ChoA [**51**]. In this enzyme, the FAD cofactor is covalently linked to the protein via a histidine residue, and thus its physical and catalytic properties vary significantly from ChoA whose cofactor is non-covalently bound. ChoB contains two major domains that are similar to ChoA and ChoB: a substrate binding domain and a FAD binding domain. In between these two domains, lie the steroid binding loops.

The features that cholesterol oxidase share in common with the GMC oxidoreductases include a FAD-binding domain and a unique histidine residue. However, each cholesterol oxidase has distinct substrate-binding domain that shares little similarity to other GMC oxidoreductases. A representative crystal structure of one of the GMC oxidoreductases, glucose oxidase, is depicted in ribbon form in **Figure 1-2 D**.

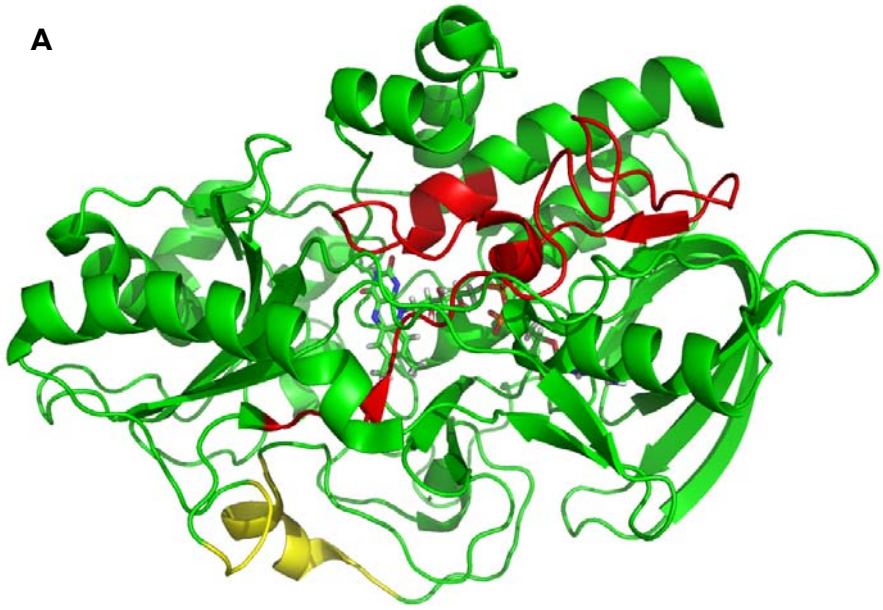

B

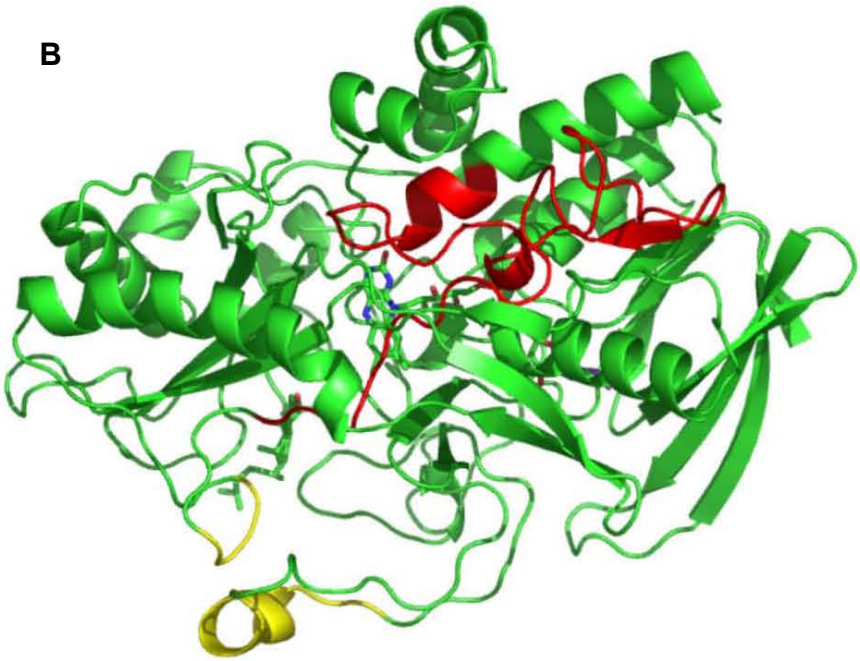

C

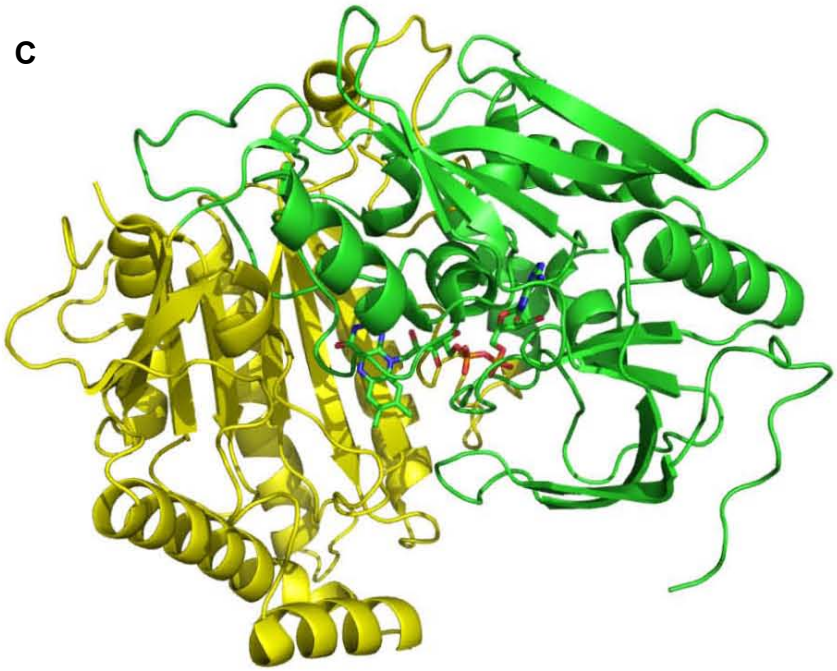

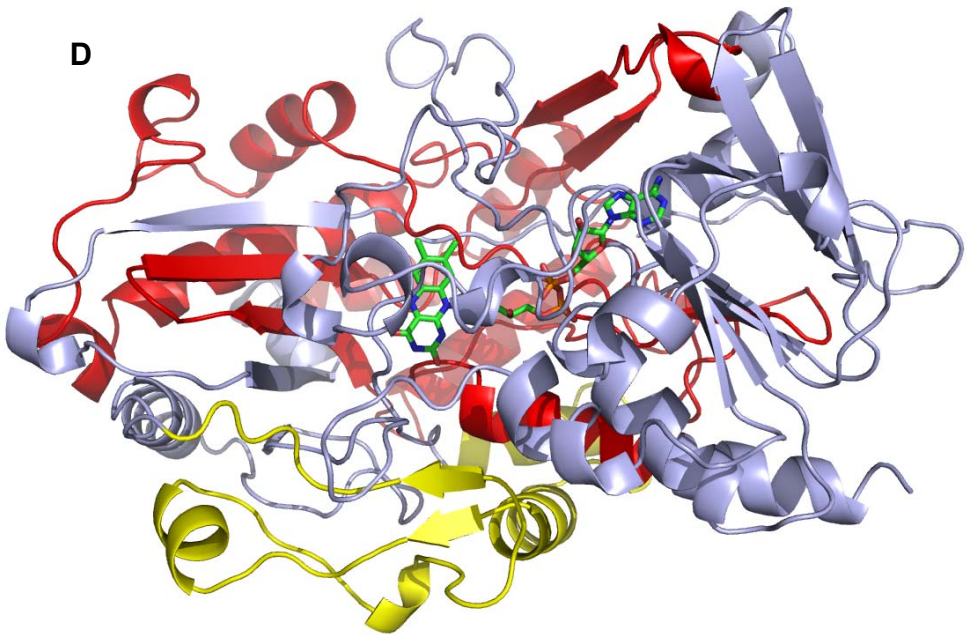

Figure 1-3 Crystal structures of various enzymes that catalyze homologous reactions shown as ribbon diagrams. The corresponding cofactors are shown in stick mode. The conserved GMC oxidoreductase domains are marked red, the substrate binding domain and loops in yellow. A. Cholesterol oxidase from *Streptomyces* (PDB entry 1MXT); B. type I cholesterol oxidase from *Brevibacterium* complexed with dehydroisoandrosterone (PDB entry 1COY); C. type II cholesterol oxidase from *Rhodococcus equi* (PDB entry 1I19); D. glucose oxidase from *Aspergillus niger* (PDB entry 1CF3).

III. Substrate specificity and Inhibition of the enzyme

Detailed substrate specificity studies have been carried out in the 1970s for cholesterol oxidases from *Nocardia* [**52**], *Rhodoccocus equi* [**53**] and *Streptomyces* [**23**]. Cholesterol displays maximum reactivity among these three species with the *Nocardia* cholesterol oxidase showing preference of C17 tailed steroids. It should be noted that the substrates of above experiments were dissolved in detergent micelles instead of lipid vesicles, which are much better mimics of lipid bilayers. As a matter of fact, the acitivities of ChoA against different substrates had no significant differences when liposomes were used [**54**]. In this study, WT and mutant proteins hardly discriminate between cholesterol and these two steroids under condition of 25 mol% sterol/DOPC unilamellar vesicles. Mutated residues do not have interactions with the tail of the sterols and these residues might form hydrophobic channel that lead the substrate into the active site. The same substrates were tested similarly in another study for cholesterol oxidase from *Rhodococcous equi* and their activities relative to cholesterol (100%) are: β-sitosterol (70%) and stigmasterol (40%) [**55**].

A few cholesterol derivatives were studied for multiple purposes including probing active site flexibility, searching for inhibitor and mechanistic implications. 4α,5α-cyclopropanocholestan-3β-ol and 4β,5β-cyclopropanocholestan-3β-ol are oxidized by ChoA 1000 times slower than cholesterol but they are substrates for ChoA [**56**]. It was also suggested that the active site and the substrate-binding domain is flexible since these two

substrates have rigid rings. Another conformational restrained derivative of cholesterol, 2α,3α-cyclopropanocholestan-3β-ol, was found to inhibit ChoA irreversibly resulting in two adducts of FAD-steroid [**57**]. This finding has more significance in inhibitor design because the flavin cofactor can now be accessed by cyclopropoxide ring-opening mechanism.

In an inhibitor screen study done by Witholt et al. [**58**]. they were able to specifically target the isomerization reaction of cholesterol oxidase from *Rhodoccocus*, *Streptomyces* and two other species using morpholine derivatives as inhibitors. In particular, fenpropimorph showed wide spectrum inhibition against all 4 enzymes. 50% of the enzyme activity could be inhibited with 50 mg/l concentration of fenpropimorph. A reversible competitive mechanism was suggested for the inhibition of cholesterol oxidase from *Steptomyces*.

IV. Summary

This dissertation aims to provide functional evidences for the catalytic studies of reactions catalyzed by cholesterol oxidase. In Chapter 2 the catalytic steps involving the usage of molecular oxygen will be discussed in detail. In particular, molecular oxygen was proposed to access the active site through a hydrophobic tunnel. Tunnel mutants will be used as probes to study the kinetic and thermodynamic properties of the enzyme. The role of residue Asn485 in the catalysis will be discussed in Chapter 3 by mutating it into Leu and Asp. In the WT enzyme the side chain of Asn makes an NH · · · π contact with the reduced form of the FAD cofactor. In order to further probe the role of the amide side chain in the catalysis, a N485D mutant will be constructed. The kinetic and redox potential profiles of all three enzymes (WT, N485D and N485L) will be reviewed together with the atomic resolution structure of the mutant enzymes to reveal how the stabilization of the reduced FAD cofactor is disrupted in the mutants.

V. References

1. G. E. Turfitt, The microbiological degradation of steroids: 2. Oxidation of cholesterol by proactinomyces spp, *Biochem. J.* **38** (1944), no. 5, 492-496.

2. C. J. Sih, H. H. Tai and Y. Y. Tsong, The mechanism of microbial conversion of cholesterol into 17-keto steroids, *J. Am. Chem. Soc.* **89** (1967), no. 8, 1957-1958.

3. I. Bjorkhem and J. A. Gustafsson, Mechanism of microbial transformation of cholesterol into coprostanol, *Eur. J. of Biochem. / FEBS* **21** (1971), no. 3, 428-432.

4. R. B. Clayton, The utilization of sterols by insects, *J. Lipid Res.* **5** (1964), 3-19.

5. J. P. Purcell, J. T. Greenplate, M. G. Jennings, J. S. Ryerse, J. C. Pershing, S. R. Sims, M. J. Prinsen, D. R. Corbin, M. Tran, R. D. Sammons and et al., Cholesterol oxidase: A potent insecticidal protein active against boll weevil larvae, *Biochem. Biophys. Res. Comm.* **196** (1993), no. 3, 1406-1413.

6. D. R. Corbin, J. T. Greenplate, E. Y. Wong and J. P. Purcell, Cloning of an insecticidal cholesterol oxidase gene and its expression in bacteria and in plant protoplasts, *Appl. Environ. Microbiol.* **60** (1994), no. 12, 4239-4244.

7. N. W. Earle, E. N. Lambremont, M. L. Burks, B. H. Slatten and A. F. Bennett, Conversion of β-sitosterol to cholesterol in the boll weevil and the inhibition of larval development by two aza sterols, *J. Econ. Ent.* **60** (1967), 291-293.

8. T. Uwajima, H. Yagi, S. Nakamura and O. Terada, Isolation and crystallization of extracellular 3β-hydroxysteroid oxidase of *brevibacterium sterolicum* nov. Sp., *Agr. Biol. Chem.* **37** (1973), no. 10, 2345-2350.

9. H. M. Flegg, Determination of serum cholesterol by an enzymic method, *Ann. Clin. Biochem.* **10** (1973), 79-84.

10. A. G. Smith and C. J. W. Brooks, Cholesterol oxidases: Properties and applications, *J. Steroid Biochem.* **7** (1976), 705-713.

11. T. Ishizaki, N. Hirayama, H. Shinkawa, O. Nimi and Y. Murooka, Nucleotide sequence of the gene for cholesterol oxidase from a *streptomyces* sp., *J. Bacteriol.* **171** (1989), 596-601.

12. A. Vrielink, L. F. Lloyd and D. M. Blow, Crystal structure of cholesterol oxidase from *Brevibacterium sterolicum* refined at 1.8 Å Resolution, *J. Mol. Biol.* **219** (1991), 533-554.

13. Y. Lange, Tracking cell cholesterol with cholesterol oxidase, *J. Lipid Res.* **33** (1992), 315-321.

14. W. Trettnak and O. S. Wolfbeis, A fiberoptic cholesterol biosensor with an oxygen optrode as the transducer, *Anal. Biochem.* **184** (1990), no. 1, 124-127.

15. S. T. Cole, R. Brosch, J. Parkhill, T. Garnier, C. Churcher, D. Harris, S. V. Gordon, K. Eiglmeier, S. Gas, C. E. Barry, 3rd, F. Tekaia, K. Badcock, D. Basham, D. Brown, T. Chillingworth, R. Connor, R. Davies, K. Devlin, T. Feltwell, S. Gentles, N. Hamlin, S. Holroyd, T. Hornsby, K. Jagels, A. Krogh, J. McLean, S. Moule, L. Murphy, K. Oliver, J. Osborne, M. A. Quail, M. A. Rajandream, J. Rogers, S. Rutter, K. Seeger, J. Skelton, R. Squares, S. Squares, J. E. Sulston, K. Taylor, S. Whitehead and B. G. Barrell, Deciphering the biology of mycobacterium tuberculosis from the complete genome sequence, *Nature* **393** (1998), no. 6685, 537-544.

16. W. Richmond, Preparation and properties of a cholesterol oxidase from nocardia sp. And its application to the enzymatic assay of total cholesterol in serum, *Clin. Chem.* **19** (1973), no. 12, 1350-1356.

17. A. Vrielink, L. F. Lloyd and D. M. Blow, Crystal structure of cholesterol oxidase from brevibacterium sterolicum refined at 1.8 a resolution, *J. Mol. Biol.* **219** (1991), no. 3, 533-554.

18. R. Linder and A. W. Bernheimer, Oxidation of macrophage membrane cholesterol by intracellular rhodococcus equi, *Vet. Microbiol.* **56** (1997), no. 3-4, 269-276.

19. L. Puglielli, A. L. Friedlich, K. D. Setchell, S. Nagano, C. Opazo, R. A. Cherny, K. J. Barnham, J. D. Wade, S. Melov, D. M. Kovacs and A. I. Bush, Alzheimer disease beta-amyloid activity mimics cholesterol oxidase, *J. Clin. Invest.* **115** (2005), no. 9, 2556-2563.

20. P. G. Atrat, B. Wagner, M. Wagner and G. Schumann, Localization of the cholesterol oxidase in rhodococcus erythropolis imet 7185 studied by immunoelectron microscopy, *J. Steroid Biochem. Mol. Biol.* **42** (1992), no. 2, 193-200.

21. T. Minuth, J. Thommes and M. Kula, Extraction of cholesterol oxidase from nocardia rhodochrous using a nonionic surfactant-bases aqueous two-phase system, *J. Biotech.* **38** (1995), no. 2, 151.

22. K. Watanabe, H. Aihara, Y. Nakagawa, R. Nakamura and T. Sasaki, Properties of the purified extracellular cholesterol oxidase from rhodococcus equi no-23, *J. Agri. Food Chem.* **37** (1989), no. 4, 1178-1182.

23. H. Tomioka, M. Kagawa and S. Nakamura, Some enzymatic properties of 3beta-hydroxysteroid oxidase produced by streptomyces violascens, *J. of Biochem.* **79** (1976), no. 5, 903-915.

24. Y. Murooka, T. Ishizaki, O. Nimi and N. Maekawa, Cloning and expression of a streptomyces cholesterol oxidase gene in streptomyces lividans with plasmid pij702, *Appl. Environ. Microbiol.* **52** (1986), no. 6, 1382-1385.

25. L. Pollegioni, G. Wels, M. S. Pilone and S. Ghisla, Kinetic mechanisms of cholesterol oxidase from *Streptomyces hygroscopicus* and *Brevibacterium sterolicum*, *Eur. J. of Biochem. / FEBS* **264** (1999), no. 1, 140-151.

26. R. Bentley and R. Meganathan, Geosmin and methylisoborneol biosynthesis in streptomycetes. Evidence for an isoprenoid pathway and its absence in non-differentiating isolates, *FEBS let.* **125** (1981), no. 2, 220-222.

27. Http://www.Nih.Go.Jp/saj/atlas/sample.Html

28. H. Umezawa, Microbial secondary metabolites with potential use in cancer treatment. (plasmid involvement in biosynthesis and compounds, *Biomedicine* **26** (1977), no. 4, 236-249.

29. Http://www.Hero.Ac.Uk/sites/hero/uk/research/archives/2002/genome_keys_unlock_nature1588.Cfm.

30. S. S. Cohen and J. I, Synthesis and the lethality of bleomycin in bacteria, *Cancer Res.* **36** (1976), no. 8, 2768-2774.

31. G. C. Uguru, K. E. Stephens, J. A. Stead, J. E. Towle, S. Baumberg and K. J. McDowall, Transcriptional activation of the pathway-specific regulator of the actinorhodin biosynthetic genes in streptomyces coelicolor, *Mole. Microbiol.* **58** (2005), no. 1, 131-150.

32. D. L. Crawford, Lignocellulose decomposition by selected streptomyces strains, *Appl. Environ. Microbiol.* **35** (1978), no. 6, 1041-1045.

33. M. Tsukamura and M. Ohta, Nocardia farcinica as a pathogen of lung infection, *Microbiol. Immu.* **24** (1980), no. 3, 237-241.

34. R. Linder and A. W. Bernheimer, Enzymatic oxidation of membrane cholesterol in relation to lysis of sheep erythrocytes by corynebacterial enzymes, *Arch. Biochem. Biophy.* **213** (1982), no. 2, 395-404.

35. K. Kishi, Y. Watazu, Y. Katayama and H. Okabe, The characteristics and applications of recombinant cholesterol dehydrogenase, *Biosci. Biotechnol. Biochem.* **64** (2000), no. 7, 1352-1358.

36. J. P. Purcell, J. T. Greenplate, M. G. Jennings, J. S. Ryerse, J. C. Pershing, S. R. Sims, M. J. Prinsen, D. R. Corbin, M. Tran, R. D. Sammons and R. J. Stonard, Cholesterol oxidase: A potent insecticidal protein active against boll weevil larvae, *Biochem. Biophys. Res. Commun.* **196** (1993), no. 3, 1406-1413.

37. Y. Av-Gay and R. Sobouti, Cholesterol is accumulated by mycobacteria but its degradation is limited to non-pathogenic fast-growing mycobacteria, *Can. J. Microbiol*. **46** (2000), no. 9, 826-831.

38. A. G. Smith and C. J. Brooks, Cholesterol oxidases: Properties and applications, *J. Steroid Biochem.* **7** (1976), no. 9, 705-713.

39. T. K. Bjarne Knudsen, Mikael Flensborg, Henrik Sandmann, Michael Heltzen, Alex Andersen, Mikkel Dickenson, Jakob Bardram, Peter J. Steffensen, Søren Mønsted, Torben Lauritzen, Roald Forsberg, Agnes Thanbichler, Jannick D. Bendtsen, Lasse Görlitz, Jane Rasmussen, David Tordrup, Morten Værum, Mikkel Nygaard Ravn, Clc protein workbench, (25. jun 2007).

40. D. R. Cavener, GMC oxidoreductases. A newly defined family of homologous proteins with diverse catalytic activities, *J. Mol. Biol.* **223** (1992), 811-814.

41. V. Leskovac, S. Trivic, G. Wohlfahrt, J. Kandrac and D. Pericin, Glucose oxidase from aspergillus niger: The mechanism of action with molecular oxygen, quinones, and one-electron acceptors, *Int. J. Biochem. Cell. Biol.* **37** (2005), no. 4, 731-750.

42. Q. H. Gibson, B. E. Swoboda and V. Massey, Kinetics and mechanism of action of glucose oxidase, *J. Biol. Chem.* **239** (1964), 3927-3934.

43. Detection, evaluation, and treatment of high blood cholesterol in adults, *Pan Am. J. Pub. Health* **9** (2001), no. 5, 338-344.

44. I. J. Kass and N. S. Sampson, The isomerization catalyzed by *Brevibacterium sterolicum* cholesterol oxidase proceeds stereospecifically with one base, *Biochem. Biophys. Res. Commun.* **206** (1995), 688-693.

45. N. S. Sampson and I. J. Kass, Isomerization, but not oxidation, is suppressed by a single point mutation, E361Q, in the reaction catalyzed by cholesterol oxidase, *J. Am. Chem. Soc.* **119** (1997), 855-862.

46. R. M. Pollack, Enzymatic mechanisms for catalysis of enolization: Ketosteroid isomerase, *Bioorg, Chem.* **32** (2004), no. 5, 341-353.

47. J. Simard, M. L. Ricketts, S. Gingras, P. Soucy, F. A. Feltus and M. H. Melner, Molecular biology of the 3beta-hydroxysteroid dehydrogenase/delta5-delta4 isomerase gene family, *Endocrine Rev.* **26** (2005), no. 4, 525-582.

48. J. L. Thomas, W. L. Duax, A. Addlagatta, S. Brandt, R. R. Fuller and W. Norris, Structure/function relationships responsible for coenzyme specificity and the isomerase activity of human type 1 3 beta-hydroxysteroid dehydrogenase/isomerase, *J. Biol. Chem.* **278** (2003), no. 37, 35483-35490.

49. J. D. Baxter and P. Webb, Metabolism: Bile acids heat things up, *Nature* **439** (2006), no. 7075, 402-403.

50. Q. K. Yue, I. J. Kass, N. S. Sampson and A. Vrielink, Crystal structure determination of cholesterol oxidase from streptomyces and structural characterization of key active site mutants, *Biochemistry* **38** (1999), no. 14, 4277-4286.

51. R. Coulombe, K. Q. Yue, S. Ghisla and A. Vrielink, Oxygen access to the active site of cholesterol oxidase through a narrow channel is gated by an arg-glu pair, *J. Biol. Chem.* **276** (2001), 30435-30441.

52. A. G. Smith and C. J. Brooks, Application of cholesterol oxidase in the analysis of steroids, *J. Chroma.* **101** (1974), no. 2, 373-378.

53. S. Ikawa, M. Takita and M. Ogura, Steroids as substrates for cholesterol: Oxygen oxidoreductase, with special reference to 3beta-hydroxy bile acids, *J. Biochem.* **85** (1979), no. 6, 1447-1452.

54. J. Xiang and N. S. Sampson, Library screening studies to investigate substrate specificity in the reaction catalyzed by cholesterol oxidase, *Protein Eng. Des. Sel*.**17** (2004), no. 4, 341-348.

55. J. Kreit, G. Lefebvre and P. Germain, Membrane-bound cholesterol oxidase from *Rhodococcus sp.* Cells. Production and extraction, *J. Biotechnol.* **33** (1994), no. 3, 271-282.

56. N. S. Sampson and A. E. McCann, 4,5-cyclopropanocholestan-3β-ol substrates for cholesterol oxidase and their ^{1}h nmr assignments, *J. Org.*

Chem. **62** (1997), no. 17, 5893-5897.

57. A. E. McCann and N. S. Sampson, A c_6-flavin adduct is the major product of irreversible inactivation of cholesterol oxidase by 2α,3α–cyclopropano-5αcholestan-3β-ol, *J. Am. Chem. Soc.* **122** (2000), 35-39.

58. P. G. Hesselink, A. Kerkenaar and B. Witholt, Inhibition of microbial cholesterol oxidases by dimethylmorpholines, *J. Steroid Biochem.* **35** (1990), no. 1, 107-113.

Chapter 2

The catalysis of cholesterol oxidase can be controlled by a hydrophobic tunnel that allows the access of molecular oxygen to the active site

I. Introduction

1. Overview of tunnels involved in transporting molecules within enzymes

Enzymes often catalyze reactions in which one or more of the substrates is a gas, often a small diatomic molecule, for example oxygen or hydrogen. Due to the small, non-polar nature of these molecules, the requirements for their specific binding have long been debated. It is possible that these gasses may reach the active sites of enzymes by passive diffusion through proteins as they undergo "breathing" vibrations. The passive diffusion of small gasses could occur along many different trajectories through a protein. However, there are many atomic resolution structures of enzymes and proteins in which possible binding cavities, and even tunnels have been visualized. In some cases, these tunnels have been saturated with xenon, an efficient diffractor of X-rays to demonstrate that a gas may diffuse through the channel or tunnel. Here we present functional evidence that the observed hydrophobic tunnel in type I cholesterol oxidase works as an oxygen-binding moiety.

Enzymes that channel an intermediate between two active sites are the best characterized examples of functional tunnels.[**1**] These tunnels sequester a gaseous or reactive intermediate that is generated at one active site, and direct its diffusion to a second active site. For example, tryptophan synthase channels indole generated in one subunit to the adjacent subunit where it is converted to tryptophan.[**2**] The amidotransferase family, of which carbamoyl phosphate synthetase is an exemplary member, channels ammonia produced from

substrate, e.g. glutamine, from one active site to a second where the ammonia is utilized in a second reaction. In the case of carbamoyl phosphate synthetases, carbamate is subsequently channeled to a third active site.[**3, 4**] In these examples, blocking diffusion of an intermediate into bulk solution and the ensuing improvement in catalytic efficiency is the primary mechanistic advantage that results from tunneling of metabolites. In the reaction catalyzed by carbon monoxide dehydrogenase/acetyl coenzyme A synthase A, a channel between subunits is proposed to allow transport of CO or CO_2 to the active site and between active sites.[**5**] Mutation of amino acids to block this channel appear to block CO and CO_2 acess to the active site.[**6**] These enzymes are primarily multimeric and require a tunnel or channel to pass the intermediate from one subunit to the next.

Enzymes that utilize a gas as a substrate, as opposed to as an intermediate, have different mechanistic requirements. In these cases, the substrate is already present in the bulk solution and must reach the active site. Binding gaseous substrate through a tunnel allows temporal and regiocontrol of its reaction with a second substrate, thus conferring a mechanistic advantage. For example, soybean lipoxygenase generates an alkyl radical intermediate. If activated oxygen is not directed at a specific carbon, many regioisomers could result. A channel has been proposed to act as a reservoir for O_2 that directs it through the protein to react predominantly at C-13 of the linoleyl radical.[**7, 8**] Mutation of Ile553 to Phe in this channel reduces oxygen access (k_{cat}/K_m^{O2}) to the radical intermediate without altering the rate of other steps in the catalytic cycle. The

classic example of oxygen binding is that of oxygen to the heme proteins myoglobin and hemoglobin.[**9**] Although, not enzymes, several low affinity binding sites for oxygen (or CO) have been observed by crystallographic and spectroscopic methods.[**10-12**]

In other cases, tunnels have been observed in enzymes, but their utilization has not been functionally demonstrated. For example, 3-hydroxybenzoate hydroxylase has a hydrophobic tunnel that leads to a discrete binding pocket that is proposed to be the oxygen binding site.[14] The structure of L-amino acid oxidase in the presence of L-phenylalanine reveals a Y-shaped channel that may bind the substrate oxygen and release the product hydrogen peroxide.[**13**] A hydrophobic tunnel proposed to bind oxygen and hydrogen peroxide is also present in the type II cholesterol oxidase.[**14**] Hydrophobic channels that could bind hydrogen gas were observed in the xenon-saturated structure of Ni-Fe hydrogenase.[**15**]

2. The catalysis of cholesterol oxidase is potentially controlled by a hydrophobic tunnel

The atomic structure of type I cholesterol oxidase has been solved to 0.95 Å resolution.[**16**] At this resolution, the two conformations of approximately 80 amino acid residues are resolved. In one conformation, several amino acids are oriented such that a narrow, hydrophobic tunnel extending from the outside surface of the enzyme to the buried active site is formed. In the alternate conformation the tunnel is closed (**Figure 2-1**). The orientation and size of this tunnel suggests that it provides a passageway for oxygen access to the active

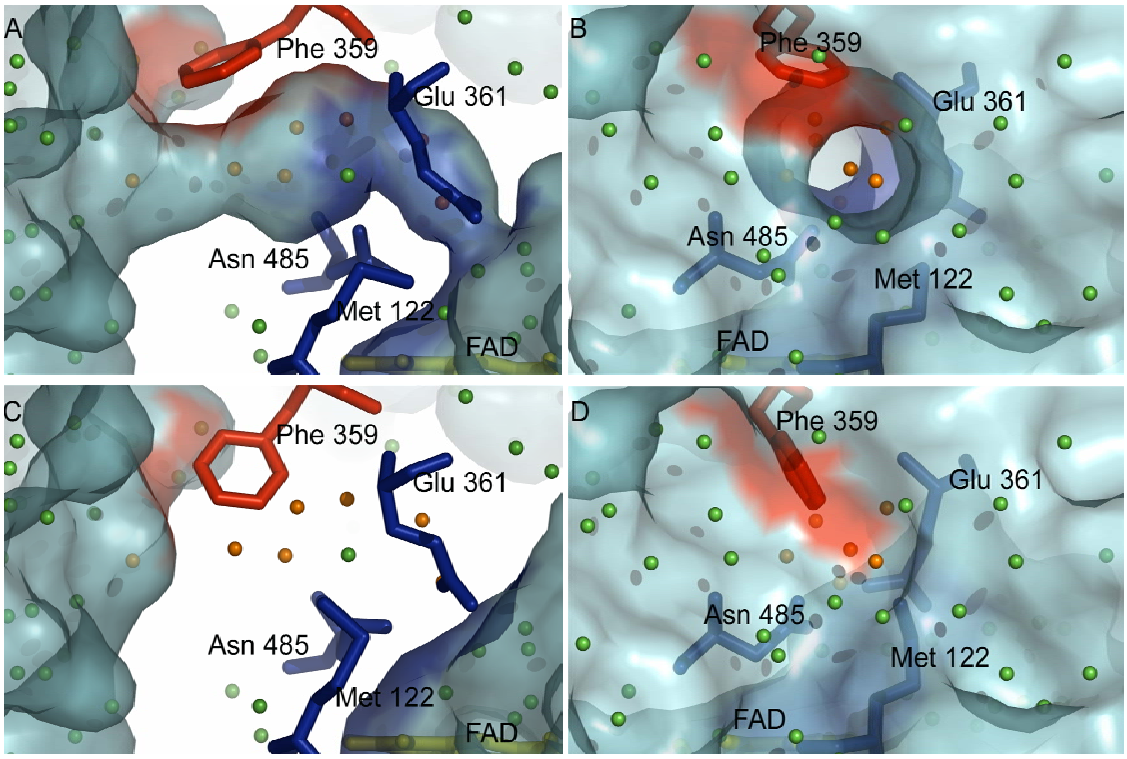

Figure 2-1 Atomic resolution structure of type I cholesterol oxidase. Light blue, surface; Lawn green, water molecules; Orange, water molecules that are in the tunnel. Key tunnel residues were labeled in blue and red. The hydrophobic tunnel is present when the tunnel residues are in their open conformations (A,B) but blocked in the closed conformations (C,D). Images were created using Pymol[**17**]. A and C were rotated 90° along the Y axis to produce B and D, respectively.

site and hydrogen peroxide release to the aqueous solvent. Phe359, Val189 and Gly347 frame the entrance to the tunnel. At the other end of the tunnel, Asn485 and Met122 form a gate between the tunnel and the isoalloxazine ring of the flavin. The tunnel is only long enough to house two oxygen molecules.

Cholesterol oxidases are bacterial, monomeric flavoenzymes that catalyze the oxidation of cholesterol to cholest-5-en-3-one. The flavin dinucleotide cofactor is simultaneously reduced. The reduced flavin is in turn oxidized by oxygen with concomitant formation of hydrogen peroxide. The cholest-5-en-3-one that is formed is isomerized to cholest-4-en-3-one in the same active site.

An amide-π interaction between the side chain of Asn485 in cholesterol oxidase and the pyrimidine ring of the FAD stabilizes the reduced flavin.[**18**] When the substrate is oxidized and the FAD cofactor is reduced, the side chain of Asn485 rotates toward the cofactor and a series of conformational changes involving other tunnel residues are initiated. These conformational changes result in the tunnel open conformation, suggesting that the conformation of Asn485, and, by implication, the oxidation state of the flavin regulate access of oxygen to the active site from this tunnel.

Despite the structural observation of a tunnel in this enzyme as well as other oxygen requiring enzymes, no functional evidence that there is a specific binding pathway, e.g., a tunnel, has been forthcoming. To test the functional importance of the tunnel, we investigated the effects of mutating tunnel residues, Phe359, Met122, Asn485 and Gly347. The kinetics of the reactions catalyzed by mutant

cholesterol oxidases were interpreted with respect to the mutant enzyme atomic structures.

II. Results

1. Construction and purification of WT and mutant cholesterol oxidases

The mutant cholesterol oxidase genes were constructed, and the corresponding proteins were heterologously expressed in *E. coli* and purified as previously described for other mutants and wild-type enzyme.[**19**] The isolated proteins were determined to be greater than 99% pure by SDS-PAGE analysis and UV/vis spectroscopy.

2. Kinetic characterization of tunnel mutants

Using cholesterol as a substrate at a fixed O_2 concentration of 256 μM (buffer saturated with air), steady-state kinetic assays were used to initially characterize the wild-type and mutant cholesterol oxidases. Individual mutation of the tunnel residues reduced k_{cat}^{app} for substrate conversion 30- to 575-fold and had little effect on the K_m^{app} (**Table 2-1**).

Cholesterol oxidase catalyzes the oxidation of cholesterol to cholest-5-en-3-one followed by its isomerization to cholest-4-en-3-one. Two steady-state kinetic assays were used to elucidate the individual effect of the mutations on these two chemical steps. One assay follows the formation of product cholest-4-en-3-one, and the second assay follows the formation of product H_2O_2. If the isomerization reaction is slowed or cholestenone binding is weakened by mutation, the intermediate cholest-5-en-3-one is released before it is isomerized,[**20**] and

Table 2-1. Assessment of mutation impact on oxidation, isomerization and steroid binding by measurement of apparent steady-state Michaelis-Menten rate constants for cholesterol turnover.[a]

	Substrate turnover[b] H_2O_2 detection		Substrate turnover[b] Cholest-4-en-3-one detection		Intermediate turnover[c] Cholest-4-en-3-one detection	
Enzyme	k_{cat}^{app} (s^{-1})	K_m^{app} (μM)	k_{cat}^{app} (s^{-1})	K_m^{app} (μM)	k_{cat}^{app} (s^{-1})	K_m^{app} (μM)
WT	47 ± 4	2.7 ± 0.3	42 ± 1	2.7 ± 0.3	61 ± 4	7 ± 1
F359W	1.3 ± 0.1	4 ± 1	0.86 ± 0.05	2.7 ± 0.8	23 ± 1	7 ± 1
M122V	1.6 ± 0.2	2 ± 1	1.8 ± 0.1	1.3 ± 0.2	32 ± 3	5 ± 2
G347N	0.85 ± 0.04	5 ± 1	1.0 ± 0.1	1.5 ± 0.6	12.0 ± 0.5	5.0 ± 0.8
N485D[d]	35 ± 4.4 x 10^{-3}	6.2 ± 2.2	73 ± 5 x 10^{-3}	7 ± 1	10 ± 1	7.2 ± 0.9
V189M	38 ± 10	15 ± 10	n.m.	n.m.	n.m.	n.m.

[a]Initial velocity data were fit to the Michaelis-Menten equation for a single substrate, equation (1). Values reported are the mean of three independent measurements, and errors are the standard deviation of the mean. [b]Cholesterol was used as a substrate at an ambient O_2 concentration of 256 μM. [c]Cholest-5-en-3-one was used as a substrate at an ambient O_2 concentration of 256 μM. [d]Taken from Lyubimov et al.[**21**]

different rates will be measured by the two assays. Comparison of the rate constants from the two assays shows that the intermediate is not released by any of the mutants. Direct measurement of the rate of isomerization using the intermediate cholest-5-en-3-one as a substrate confirmed that isomerization is not perturbed more than 6-fold in k_{cat}^{app} by mutation (**Table 2-1**) and the K_m^{app}'s are unaffected. Thus, reduced rates of steroid binding and release, or a reduced

rate of isomerization are not responsible for the 30- to 565-fold rate reductions caused by these mutations.

These data suggested mutation of the tunnel residues primarily affected the oxidation chemistry catalyzed by cholesterol oxidase. The oxidation reaction consists of two half-reactions: oxidation of cholesterol to cholest-5-en-3-one concomitant with reduction of FAD to $FADH^-$, and reduction of O_2 to H_2O_2 simultaneous with oxidation of $FADH^-$ to FAD. In the wild type catalyzed reaction, a primary kinetic isotope effect on hydride transfer from cholesterol to $FADH^-$ is observed on both k_{cat}^{app} and $(k_{cat}/K_m)^{app}$, requiring that oxidation of cholesterol is at least partially rate limiting at both sub-saturating and saturating cholesterol concentrations. The primary kinetic isotope effects on hydride transfer are greatly reduced in the cholesterol oxidation reactions catalyzed by all of the mutants except N485D (**Table 2-2**). The combination of reduced catalytic activity in the redox step, reduced sensitivity to deuterium substitution, and marginally reduced rates of isomerization suggests that either oxygen binding or $FADH^-$ oxidation have become rate limiting in the reactions catalyzed by the F359W, M122V and G347N mutants. The effect of asparagine 485 mutation on catalytic efficiency has been previously investigated and found to be pleiotropic. The majority of the rate reduction upon asparagine mutation is due to lessening the oxidation power of the flavin cofactor (reference [**19, 21**] and more details to be discussed in Chapter 3)

Table 2-2. Assessment of mutation impact on the kinetic isotope effect for hydride transfer from cholesterol to FAD by measurement of apparent steady-state Michaelis-Menten rate constants for cholesterol turnover.[a]

Enzyme	^{D}V & $^{D}V/K$
WT[b]	2.2 ± 0.1
F359W	1.2 ± 0.2
M122V	1.5 ± 0.1
G347N	1.7 ± 0.2
N485D[d]	2.5 ± 0.2

[a]Initial velocity data were measured for cholesterol or [3-^{2}H]-cholesterol as a substrate at a fixed O_2 concentration of 256 μM and fit to equation (2) for the same isotope effect on k_{cat}^{app} (V) and $(k_{cat}/K_m)^{app}$ (V/K). Values reported are the mean of three independent measurements, and errors are the standard deviation of the mean. [b]Taken from Ye et al.[**19**] [c]Taken from Lyubimov et al.[**21**]

Table 2-3. Steady-state rate constants for wild-type and mutant cholesterol oxidases.

Enzyme	K_{iO2} (μM)	K_m^{O2} (μM)	K_m^{chol} (μM)	k_{cat}(s^{-1})	h_{max}	$(k_{cat}/K_m^{O2})^{wt}/(k_{cat}/K_m^{O2})^{mut}$
WT[a]	1383 ± 120	300 ± 35	4.0 ± 0.5	96 ± 6	1.0[c]	1
F359W[b]	1381 ± 1649	617 ± 15	2.1 ± 2.5	7.4 ± 1	2.8[c]	27
M122V[b]	1931 ± 2146	655 ± 93	2.3 ± 2.5	23 ± 3	3.4[c]	9

[a]A compulsory order ternary-complex mechanism as described in equation (3) was fit to the initial velocity data to yield K_{ia}, K_{mB}, and K_{mA}. [b]Secondary plots of V_m^{O2app} and $(V_m/K_m)^{O2app}$ versus [cholesterol] were fit to equations (5) and (6), respectively to yield V_m, K_{ia}, K_{mB}, and K_{mA}. V_m^{O2app} and $(V_m/K_m)^{O2app}$ were obtained by fitting initial velocity data for varied oxygen concentrations at fixed cholesterol concentrations to equation (4). [c]h_{max} was determined by plotting h versus [cholesterol] as shown in **Figure 2-5**. Values reported are the mean of two independent measurements, and errors are the standard deviation of the mean.

Further steady-state assays were performed to identify the source of the rate decrease. The oxygen concentration was varied in addition to varying the cholesterol concentration and the formation of product cholest-4-en-3-one was followed. The dependence of wild-type rate on varied oxygen concentrations fit a classical hyperbolic saturation curve (**Figure 2-2a**), as did the dependence of rate on varied cholesterol. The combined oxygen and cholesterol data fit a model in which a ternary complex of steroid, oxygen and enzyme is formed (**Figure 2-2b**). The data were inconsistent with a ping-pong model in which cholest-4-en-3-one, the first product, is released before binding of O_2, the second substrate.

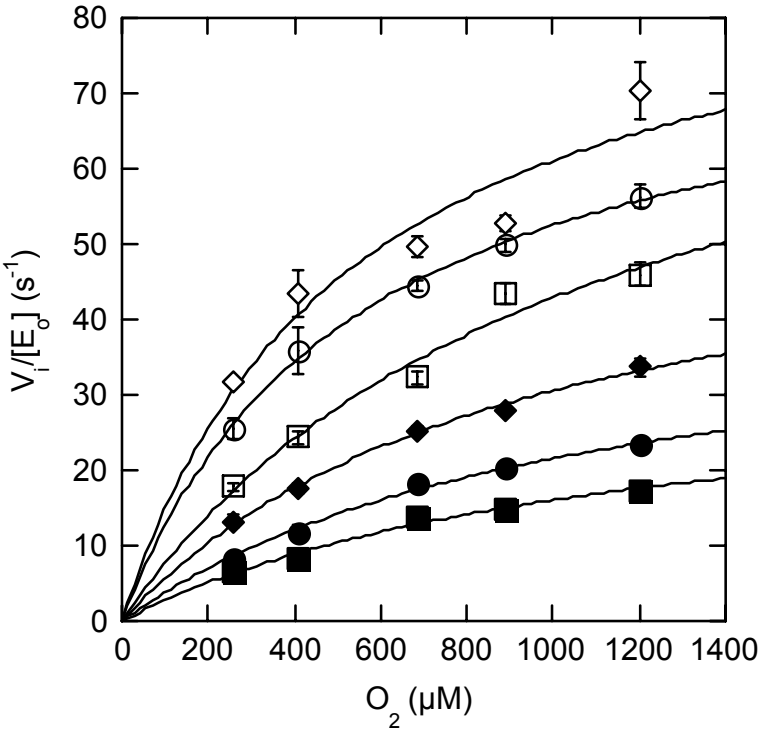
80
70
60
50
40
30
20
10
0
0
200
400
600
800
1000
1200
1400
$V_i/[E_o]$ (s^{-1})
O_2 (μM)

Figure 2-2a

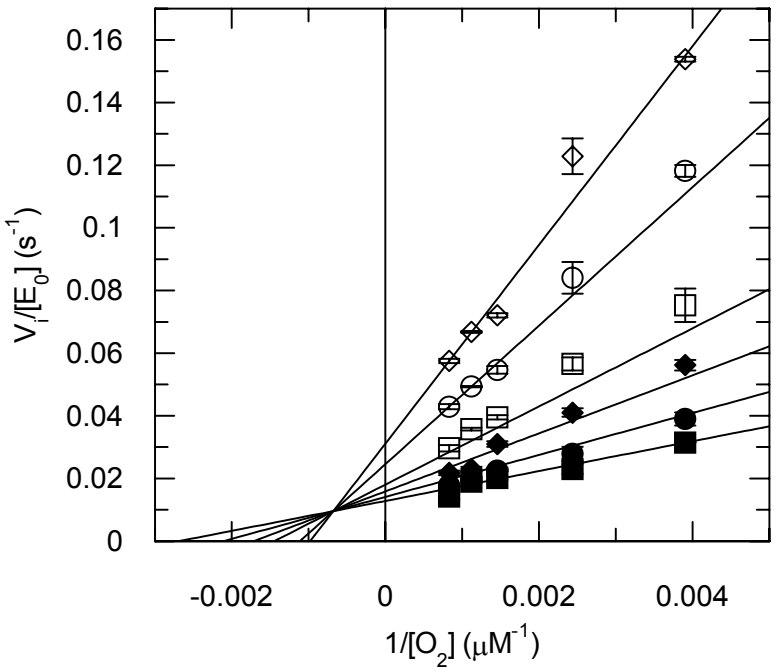
0.16
0.14
0.12
0.1
0.08
0.06
0.04
0.02
0
-0.002
0
0.002
0.004
$V_i/[E_0]$ (s^{-1})
$1/[O_2]$ (μM^{-1})

b

Figure 2-2: Ternary model of substrate binding. Initial velocities for wild-type cholesterol oxidase were measured over a range of O_2 concentrations with varied cholesterol concentrations. The data were globally fit to equation (3) for a sequential ternary mechanism or they were fit to equation (4) for a cooperative mechanism at each individual cholesterol concentration. For the fit to equation (4), the Hill coefficient, h, was 1.0 at all cholesterol concentration. The data shown are the average of two independent experiments, and the errors are the standard deviation of measurement. (a) Michaelis-Menten plots for $v_i/[E_o]$ versus $[O_2]$ at varied cholesterol concentrations: △, 30 μM ; ○, 15 μM; □, 9 μM; ▲, 6 μM; ●, 3 μM; and ■, 2 μM. (b) Double-reciprocal plot of the data in panel (a). The intersecting line pattern is consistent with the formation of a ternary complex between the enzyme, oxygen and steroid.

The rate dependencies on oxygen concentration of the mutant-catalyzed reactions were strikingly different than the wild-type catalyzed reaction. The N485D catalyzed reaction was linearly dependent on oxygen concentration within the experimentally accessible range of oxygen concentration (**Figure 2-3a**). In this concentration range, the reaction catalyzed by N485D is second order, i.e., dependent on both oxygen and enzyme concentration, suggesting that the K_m for oxygen has been increased to a concentration above the solubility limit of oxygen in aqueous buffer. The plots of initial rate catalyzed by F359W, M122V, and G347N versus oxygen concentration were sigmoid and were fit to the Hill equation for cooperativity (Figures 4B, 4C, and 4D). The Hill coefficients for the reactions-catalyzed by F359W and M122V ranged from 1.6 to 2.9 and were dependent on cholesterol concentration (**Figure 2-4**). Although, the reaction catalyzed by G347N appears cooperative, the data could not be fit reliably because the K_m^{app} for O_2 is close to the aqueous solubility limit of oxygen. Therefore these data were not analyzed further. Reanalysis of the wild-type data utilizing the Hill equation confirmed that there was no apparent oxygen cooperativity in the wild-type catalyzed reaction; the Hill coefficients at all cholesterol concentrations were 1 (**Figure 2-2a**).

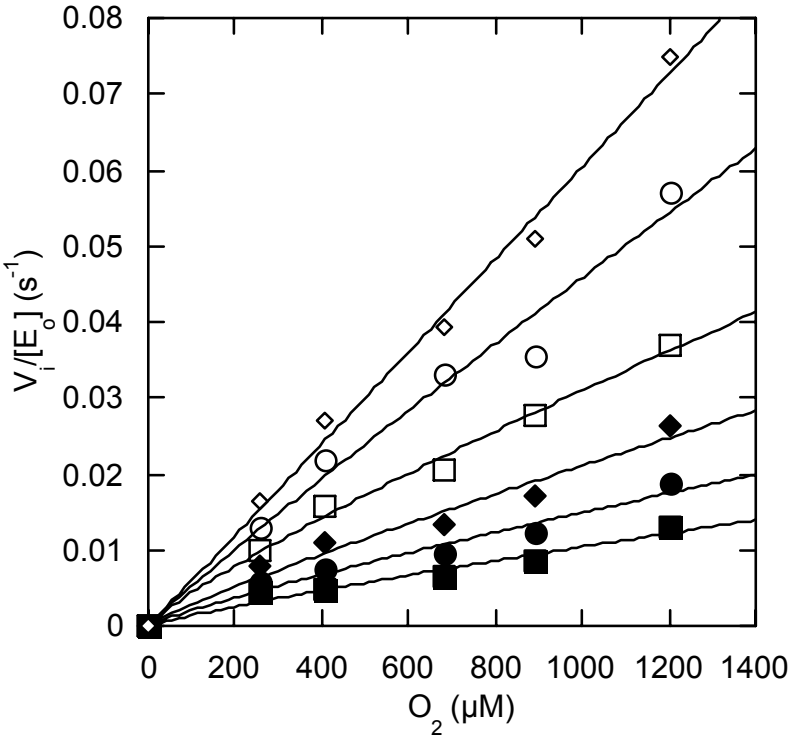
0.08
0.07
0.06
0.05
0.04
0.03
0.02
0.01
0
$V_i/[E_o]$ (s^{-1})
0
200
400
600
800
1000
1200
1400
O_2 (μM)

Figure 2-3a

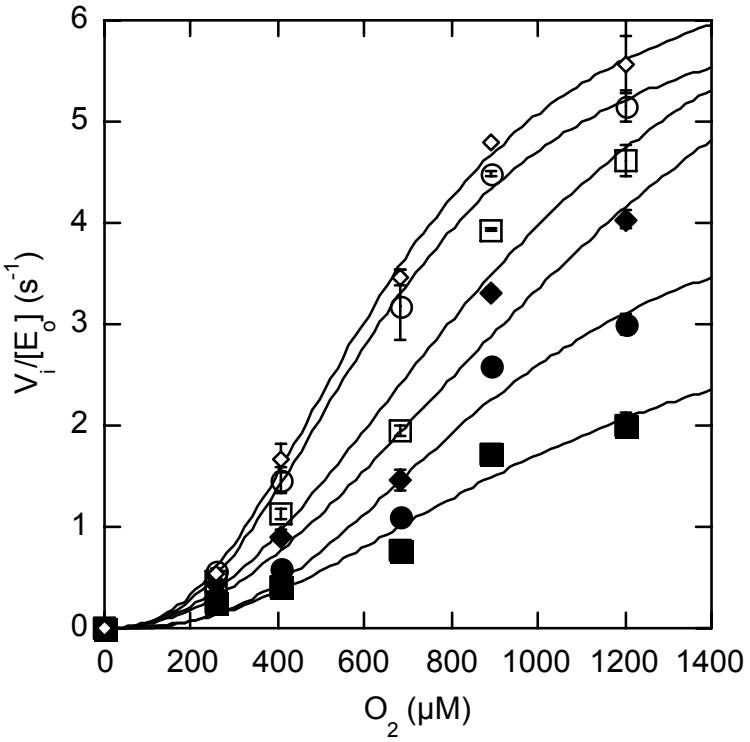
6
5
4
3
2
1
0
$V_i/[E_o]$ (s^{-1})
0
200
400
600
800
1000
1200
1400
O_2 (μM)

b

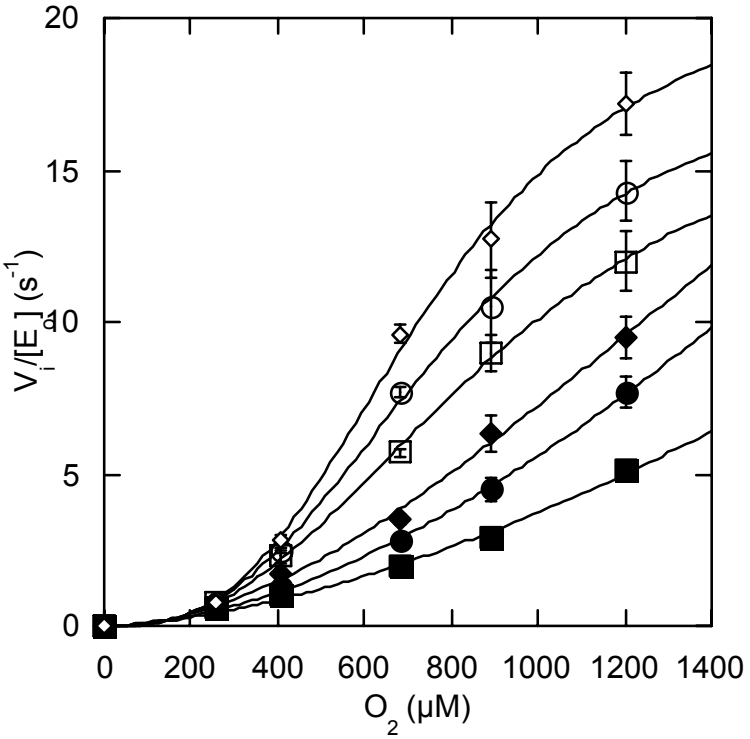
20
15
10
5
0
0
200
400
600
800
1000
1200
1400
$V_i/[E]_o$ (s^{-1})
O_2 (μM)

c

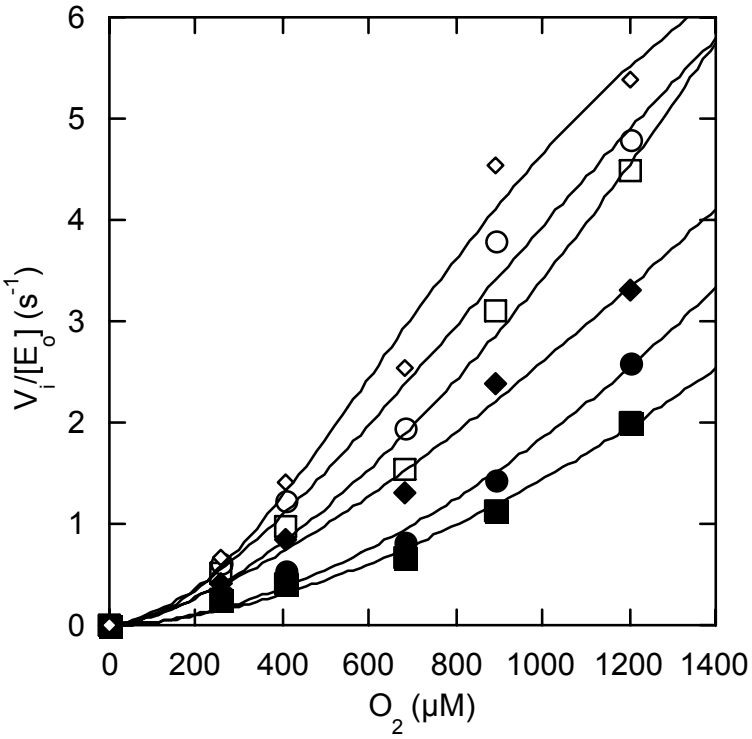
6
5
4
3
2
1
0
0
200
400
600
800
1000
1200
1400
$V_i/[E]_o$ (s^{-1})
O_2 (μM)

d

Figure 2-3: Oxygen cooperativity of mutants. $v_i/[E_o]$ was plotted versus $[O_2]$ at varied cholesterol concentrations and fit to equation (4): △, 30 μM ; ○, 15 μM; □, 9 μM; ▲, 6 μM; ●, 3 μM; and ■, 2 μM. (a) N485D; (b) F359W; (c) M122V; (d) G347N. The data shown are the average of two independent experiments, and the errors are the standard deviation of measurement.

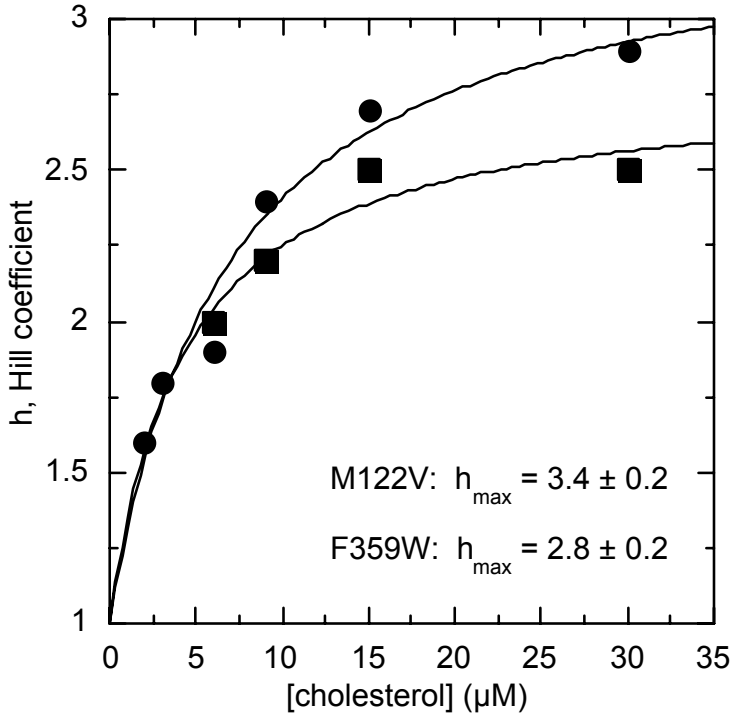

Figure 2-4: Dependence of F359W and M122V oxygen cooperativity on cholesterol concentration. V_m^{O2app} and $(V_m/K_m)^{O2app}$ were obtained by fitting initial velocity data for varied oxygen concentrations at six fixed cholesterol concentrations to equation (4). The Hill coefficients, *h,* thus obtained were plotted versus [cholesterol] and fit to a rectangular hyperbola with $h = 1$ at [chol] = 0. The data shown are the average of two independent experiments, and the errors are the standard deviation of measurement.

The kinetic cooperativity of oxygen reaction was investigated with a poor substrate, dehydroepiandrosterone. In the wild-type catalyzed reaction, k_{cat} is 50 times slower with dehydroepiandrosterone as substrate than with cholesterol. The wild-type catalyzed reaction has a hyperbolic dependence on oxygen concentration with a K_m^{app} = 571 ± 74 μM and k_{cat}^{app} = 1.4 ± 0.090 s^{-1}. (**Figure 2-5**). Importantly, the F359W catalyzed reaction is not cooperative in oxygen when dehydroepiandrosterone is utilized as the substrate. The F359W catalyzed reaction also shows a hyperbolic dependence on oxygen concentration with a K_m^{app} = 302 ± 38 μM and k_{cat}^{app} = 1.3 ± 0.072 s^{-1} (**Figure 2-5**). This result indicates that the kinetic cooperativity observed with cholesterol is lost when the rate(s) of kinetic step(s) subsequent to oxygen binding are reduced.

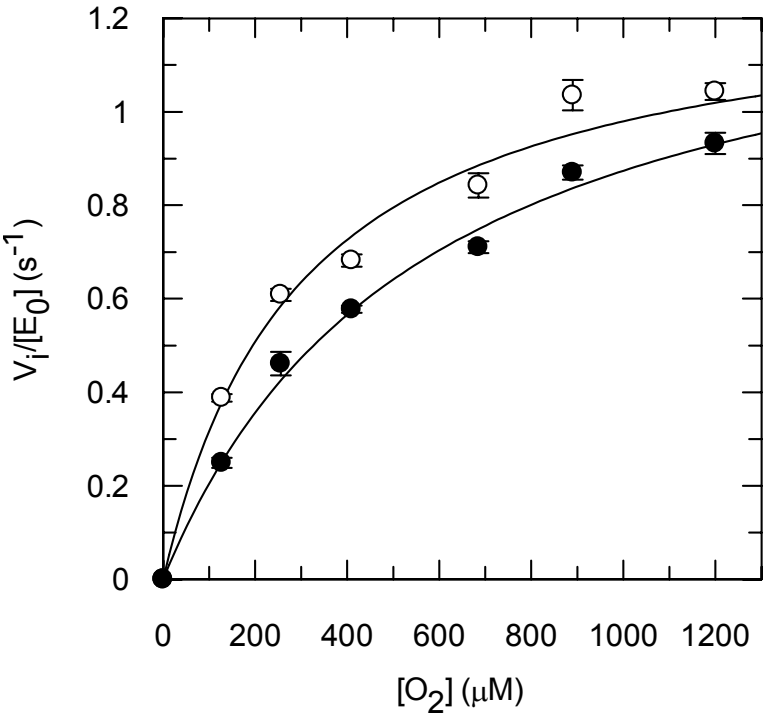

Figure 2-5: Initial velocities for wild-type cholesterol oxidase and F359W were measured over a range of O_2 concentrations with a fixed dehydroepiandrosterone concentration of 140 μM. and fit to equation (1). ○, WT; ●, F359W. The data shown are the average of two independent experiments, and the errors are the standard deviation of measurement.

3. Atomic resolution structure of the F359W mutant *

The crystal structure of the F359W mutant was refined to 0.95 Å resolution (**Table 2-4**). The mutant crystallizes in the same space group as the wild type enzyme and the overall structure of the mutant is the same. At this resolution in the wild-type structure, multiple conformations of amino acid residues were resolved into two distinct conformations. In conformation A, the tunnel between solvent and active site is closed. In conformation B, the tunnel residues are rotated out of the tunnel and an open passage is formed.[**16**]

In the wild-type structure, phenylalanine 359 occupies the two distinct conformations with equal occupancy, suggesting that the conformations are approximately equal in energy. In conformation A the phenylalanine side-chain fills the tunnel, and in conformation B, it undergoes a 18° rotation about χ_{1l} and the tunnel becomes solvent accessible. In the mutant structure, the indole ring of Trp359 is flipped into the tunnel in a position analogous to conformation A of phenylalanine 359 in the wild-type structure. A second conformation of tryptophan 359 is not detected in the electron density maps. The conformations of other tunnel residues and active site residues have less than a root-mean squared deviation from the wild-type structure. The rest of the residues that occupy two conformations in the wild-type structure also occupy two conformations in the F359W structure.

The observation of a single conformation in the mutant structure suggests that the tryptophan conformation analogous to conformation B of phenylalanine 359 is higher in energy than the observed tryptophan conformation. In addition,

* The crystallography experiments presented in this section were performed by Artem Lyubimov.

Table 2-4. Crystallographic data and refinement statistics for the F359W cholesterol oxidase structure.

Data collection	**F359W**
Space group	P21
Cell dimensions	
a, *b*, *c* (Å)	51.28, 72.87, 62.95
α, β, γ (°)	90.0, 105.11, 90.0
Resolution (Å)	46.7 – 0.95 (0.98 – 0.95)
R_{merge}	0.047 (0.48)
$I / \sigma I$	11.2 (1.9)
Completeness (%)	96.3 (67.6)
Redundancy	4.22 (2.56)
Refinement	
No. reflections (total)	1,141,795
No. reflections (unique)	270,322
R_{work} / R_{free}	14.0 / 17.5

rotation about χ_1 of tryptophan 359 cannot occur without simultaneous movement in the surrounding protein structure because unfavorable van der Waals contacts would occur during rotation. The increased steric bulk of the indole ring over that of a phenyl ring destabilizes conformation B and raises the barrier to its formation.

Manual modeling of the tryptophan χ_2 conformers reveals that an alternative conformation is possible upon -155° rotation. In this conformation, the tryptophan χ_1 angle is unchanged. The rotation results in the protrusion of the phenyl moiety of the indole ring towards the solvent rather than into the tunnel. In this conformation, a solvent accessible tunnel that extends to the active site is present.

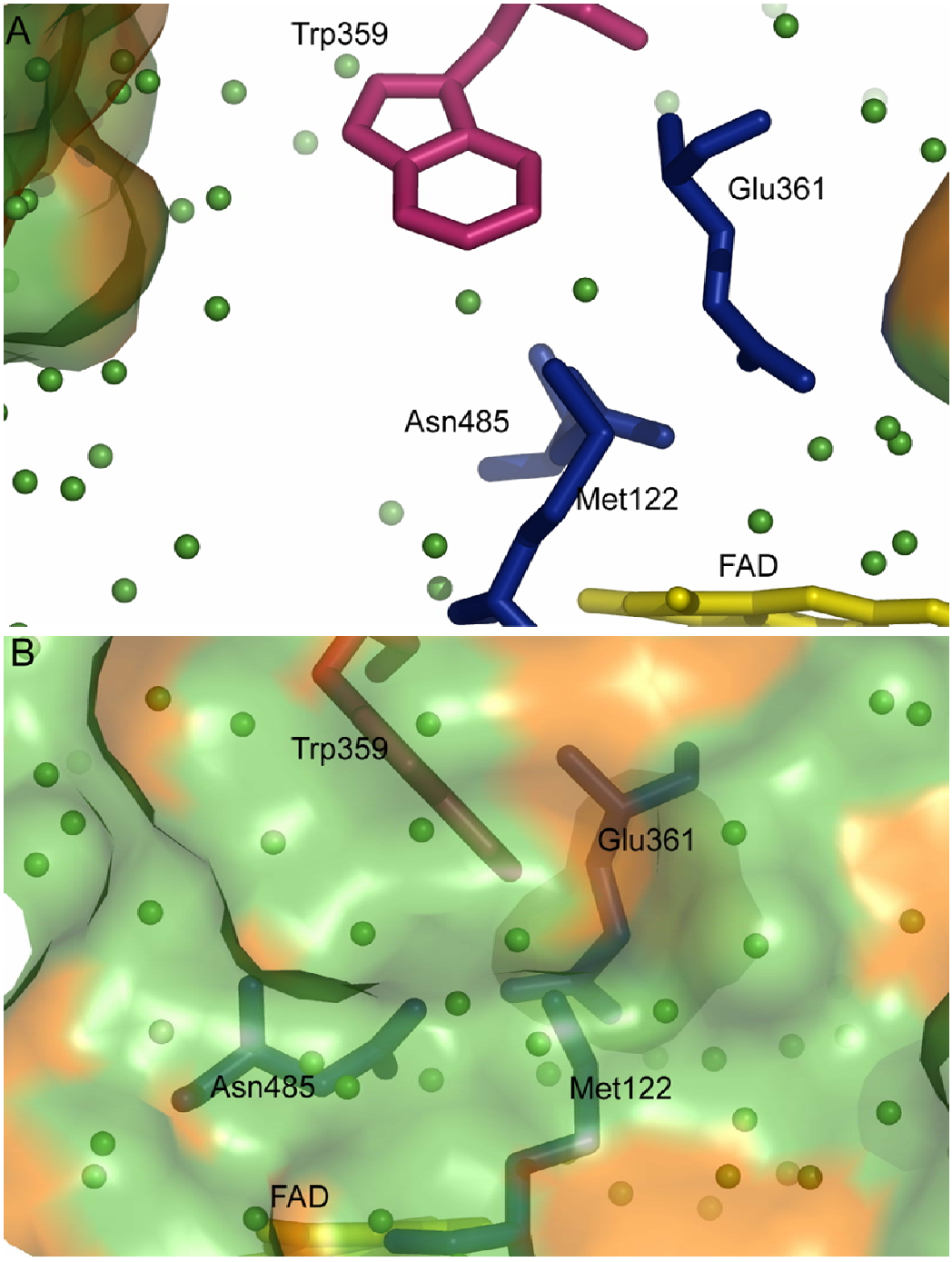

Figure 2-7: Surface representation of F359W mutant. Forest green, surface; Lawn green, water molecules. Key tunnel residues were labeled in blue and magenta. B is the resultant image after A was rotated 90° along the Y axis. Key tunnel residues were labeled. Images created using Pymol[**17**].

Discussion

Although, the mutation of phenylalanine 359 to tryptophan results in a 50-fold decrease in catalytic activity, the reduced enzyme is still oxidized by oxygen with multiple turnovers. The atomic resolution structure of the mutant with a tryptophan indole at position 359 has a blocked tunnel. If the mutation blocked the tunnel to such an extent that oxygen can no longer traverse the tunnel, and oxygen is forced to access the active site via the steroid-binding site, a ternary complex of oxygen and steroid would no longer be formed. Kinetically, a ping-pong mechanism of substrate binding would be observed. That is, the steroid binding, conversion, and release would have to occur before oxygen binding and turnover. However, the kinetic profile of the F359W mutant, as well as those of the other three mutants (**Figure 2-3**), are inconsistent with this mechanism and the model was not considered further.

The reactions catalyzed by the F359W, M122V and G347N mutants do not fit a classical ternary complex mechanism either. Instead, the mutations introduce positive cooperativity with respect to oxygen concentration. Cooperativity is generally associated with multi-subunit proteins that relay binding occupancy and structural conformation information between subunits, for example, as occurs upon binding of oxygen to hemoglobin. Cholesterol oxidase is a monomeric enzyme, and thus, it is distinctly improbable that the cooperativity results from multi-site binding of oxygen with successive changes in association constants and quaternary structure. The proposed oxygen-binding tunnel is large enough to accommodate two oxygen molecules. One could be bound as substrate and

the second as an allosteric effector. However, the F359W mutant tunnel is only large enough to accommodate half of one oxygen molecule (one water is observed in the electron density maps), and it is the mutant that shows positive cooperative behavior, not the wild-type enzyme. Furthermore, additional oxygen binding cavities were not observed in the mutant structure. Thus, a multi-site binding model was not consistent with either the structural data or the wild type kinetics.

Next, a kinetic cooperativity model was considered.[**22, 23**] Monomeric enzymes display kinetic cooperativity under non-equilibrium conditions that are often due to a slow protein conformational change. In this model, two different protein conformations, E and E', can bind O_2 followed by cholesterol to form a ternary complex, E'•O_2•cholesterol and the ternary complex reacts to form products (**Figure 2-8**). The reaction of E' is faster than the reaction of E. The protein conformation E' persists after product release and at high oxygen concentrations, oxygen can bind to E' before it has time to equilibrate to the more stable enzyme form, E. This kinetic trapping of E' by O_2 occurs because the two conformations, E and E', interconvert slowly and the rate of binding of O_2 is first-order in oxygen concentration. In this mechanism, the more active enzyme conformation E' appears to be remembered because it relaxes back to the E form so slowly and this type of kinetic cooperativity is known as mnemonic.[**23, 24**] There are two consequences of this mechanism. The first consequence is that the reaction kinetics only display cooperativity for the first or preferred substrate, and no cooperativity for the second substrate. In the case presented here, there

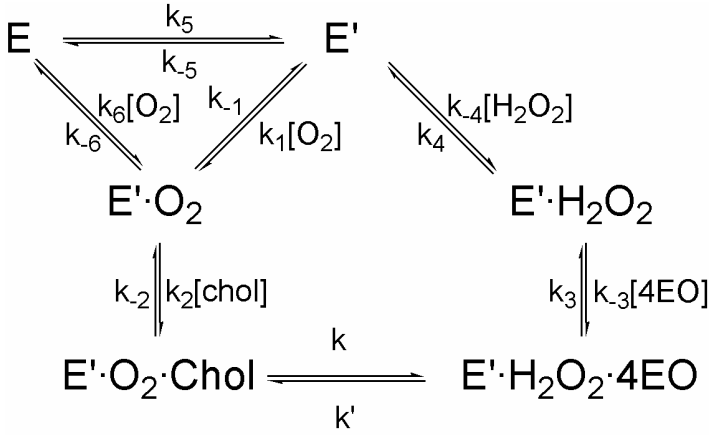

a

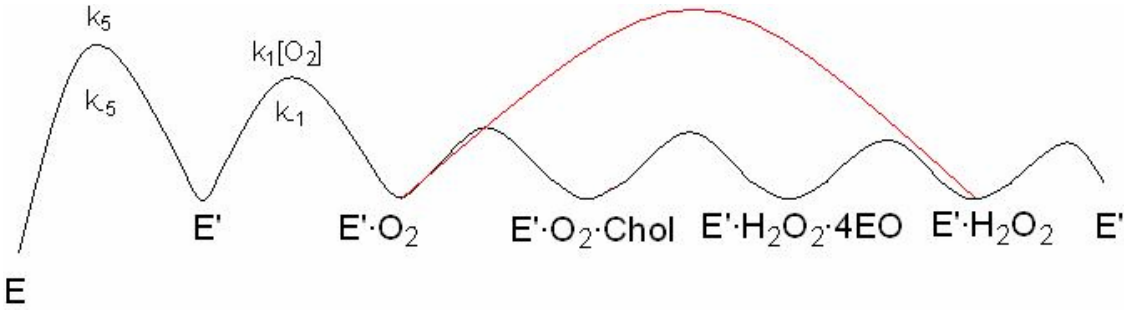

b

Figure 2-8: a, Mnemonic model for kinetically cooperative oxygen reaction in the mutant-catalyzed reactions. Adapted from the work of Cornish-Bowden and Ricard. [**22, 23**]. b, free energy diagram of the cooperativity model. Red peak represents the situation when a slow substrate such as DHEA is used.

is no cooperativity with respect to cholesterol. The second consequence is that the positive cooperativity will increase with increasing concentrations of the second substrate. Again, this is the case here (**Figure 2-4**); the Hill coefficient increases with increasing cholesterol concentration.

The mnemonic model is consistent with both the F359W structure and kinetics. The tunnel-closed conformation, (E in **Figure 2-8**) is the more stable, and the only experimentally observed, conformation. As oxygen passage through the tunnel is sterically blocked by the mutation, it is assumed that oxygen must bind by another means and this route is slower than the native binding mechanism through the tunnel. One possibility is diffusion through the protein by many different paths. After chemical conversion of cholesterol and O_2 to cholest-4-en-3-one and H_2O_2, respectively, the products are released. If the kinetic barrier to H_2O_2 diffusion through the protein is much higher than the barrier to H_2O_2 diffusion through the tunnel, the latter pathway will predominate. Upon H_2O_2 release, the tunnel will be open. Because the open and closed tunnel conformations interconvert slowly and are not in equilibrium in the presence of high oxygen concentrations, oxygen can bind via the tunnel. This binding pathway is faster than diffusion through the tunnel and cooperativity in time is observed. This mnemonic mechanism suggests that the F359W tunnel can be in an open conformation, but this conformation is much higher in energy than the closed form, and the open-closed interconversion is kinetically slow.

The precise structure of the F359W tunnel open conformation is not known. However, inspection of the crystal structure suggests that one possibility is rotation about χ_2 to “flip” the tryptophan indole out towards solvent. This conformation would be less stable than the ‘indole in’ conformation because the phenyl is oriented towards solvent water, rather than the indole that can

hydrogen bond. In addition, the barrier to flipping would be high because of steric interactions with the surrounding protein.

An alternative model is that oxygen only binds by diffusion through the protein and that hydrogen peroxide is only released by diffusion. In this case, there is not a defined pathway of binding, but many paths would contribute to oxygen binding. If the binding pathways were random, it would be very unlikely that the conformation of the enzyme (E' in **Figure 2-8**) released upon hydrogen peroxide exit would be in the optimal conformation for oxygen binding.

We cannot completely exclude an alternative mechanism in which the substrates bind in random order, and the flux through the oxygen binding first pathway versus the cholesterol binding first pathway shifts upon changing oxygen concentration.[**25, 26**] This mechanism requires that substrate binding not be at equilibrium, that is, steps subsequent to ternary complex formation are fast relative to substrate binding. The implication that results is that mutation of tunnel residues slows down substrate binding and our conclusions about the importance of a protein tunnel through which oxygen binds are unchanged.

An examination of other enzymes in the glucose-methanol-choline oxidoreductase superfamily tells us how well the tunnel feature is conserved. Although they catalyze different reactions, all six enzymes compared contain one molecule of bound FAD. Some tunnel residues are conserved upon structure alignments of GMC-oxidoreductase enzymes (**Figure 2-9**). The structures are matched by their FAD cofactors (**Figure 2-9** a). F359 from ChoA is best aligned with Trp568 of cellobiose dehydrogenase from *Phanerochaete chrysosporium*

and Phe351 of glucose oxidase from *Aspergillus niger*. All other enzymes aligned contain at least one aromatic residue within 5 Å from Phe359 of ChoA. It can thus be suggested that an aromatic side chain is often involved in controlling the switch of major structural or conformational change, since their movements are relatively dramatic compared to linear side chains. As a matter of fact, two Phe residues were found to lie at an interruption position where a potential tunnel could be formed in two of the enzymes aligned: cellobiose dehydrogenase from *Phanerochaete chrysosporium* and pyranose 2-oxidase from *Trametes multicolor* **(Figure 2-10)**. Further prediction is not possible because these two structures were solved at low resolutions. About other ChoA tunnel residues, G347 of ChoA is aligned with hydrophobic residues such as Ile and Leu in other enzymes. There is no clear pattern of what type of residues V189 is aligned to. In conclusion, an aromatic residue such as Phe is always the key in controlling tunnel open/close.

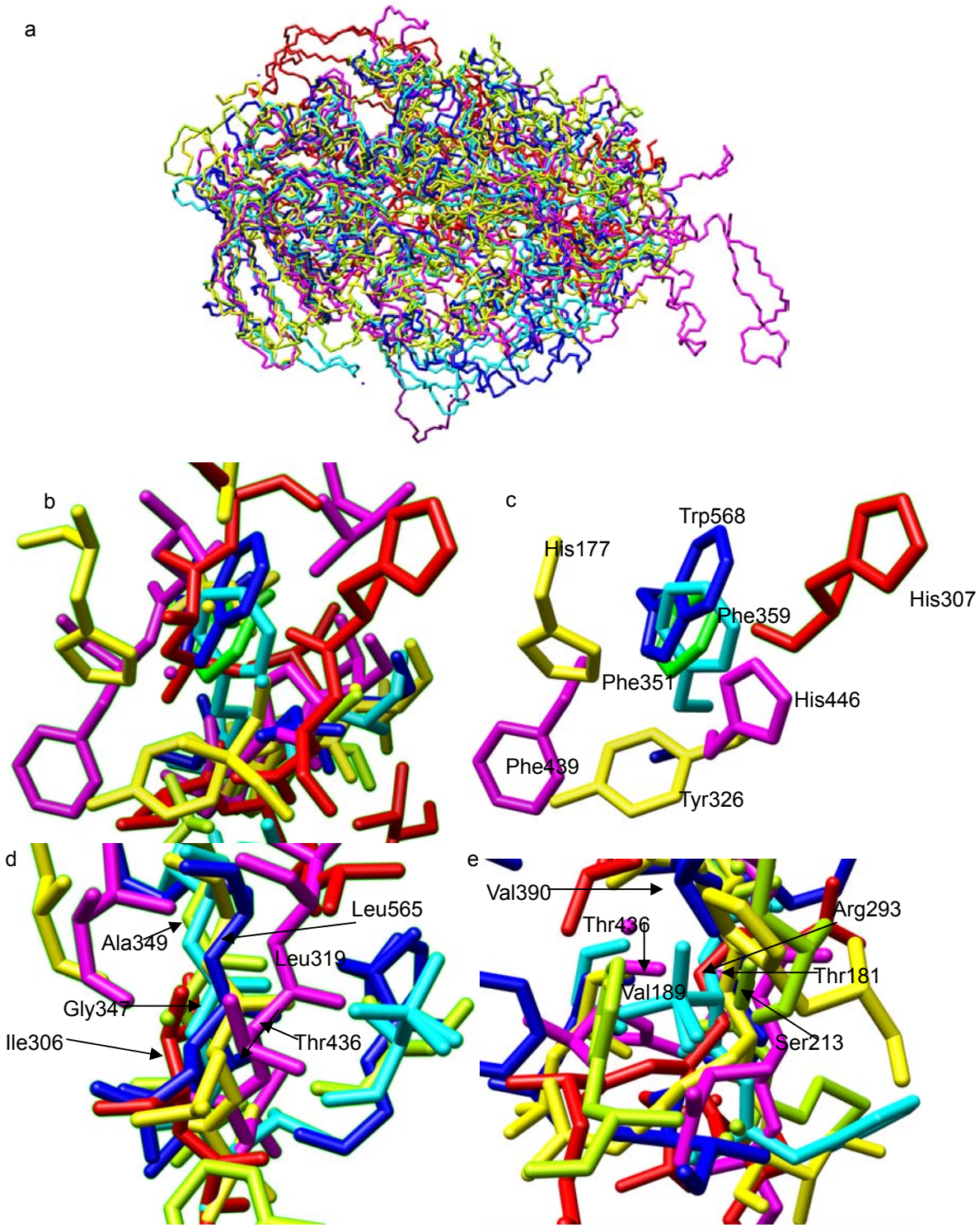
a
b
c
Trp568
His177
His307
Phe359
Phe351
His446
Phe439
Tyr326
d
Leu565
Ala349
Leu319
Gly347
Ile306
Thr436
e
Val390
Arg293
Thr436
Thr181
Val189
Ser213

Figure 2-9 Structure alignments of ChoA with other GMC oxidoreductases. a). all enzymes are matched by the positions of their FAD cofactors. Light green, glucose oxidase from *Aspergillus niger* (PDB entry 1CF3); yellow, hydroxynitrile lyase from almond (PDB entry 1JU2); blue, cellobiose dehydrogenase from *Phanerochaete chrysosporium* (PDB entry 1KDG); cyan, cholesterol oxidase from *Streptomyces* (ChoA, PDB entry 1B4V); purple, pyranose 2-oxidase from *Trametes multicolor* (PDB entry 1TT0); red, D-amino acid oxidase from *Homo sapiens*. b-e), residues that are within 3 Å distance from either Phe359 (b, c), Gly347 (d) or Val189 (e) of ChoA in the alignments are shown. Aromatic residues of b) are separated and labelled in c) for clarification. Structurally homologous residues to either Gly347 or Val189 are labeled in d) and e), respectively.

a

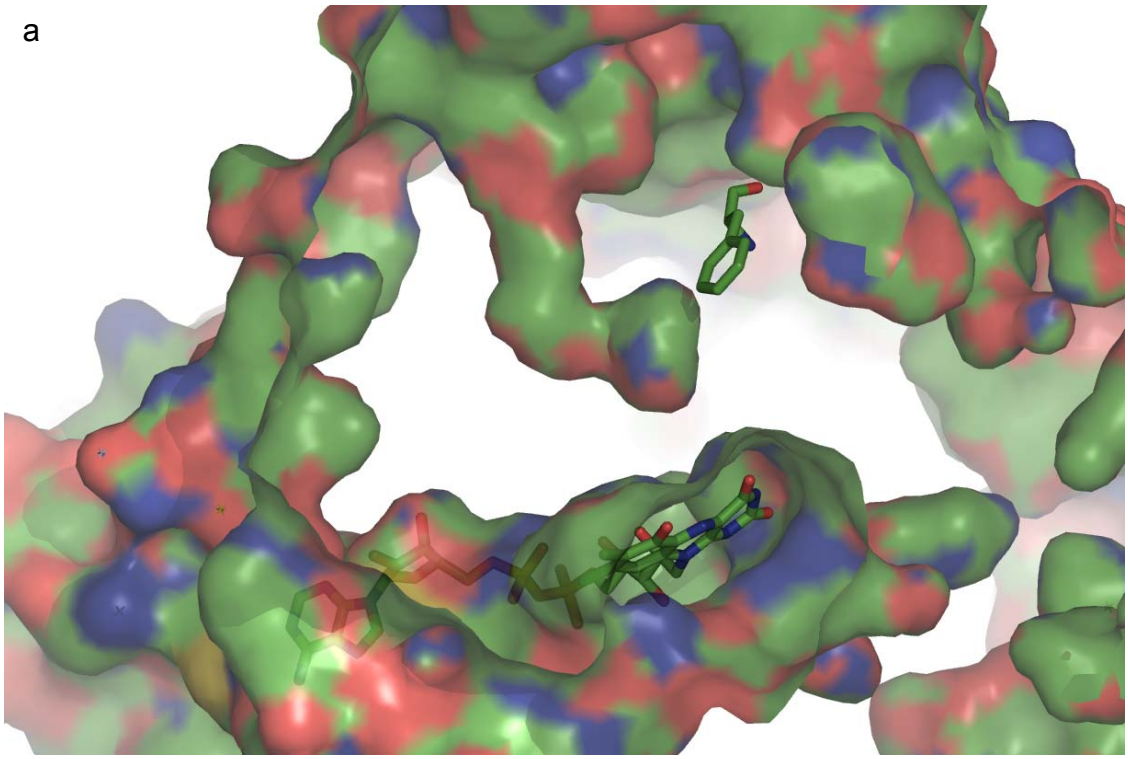

b

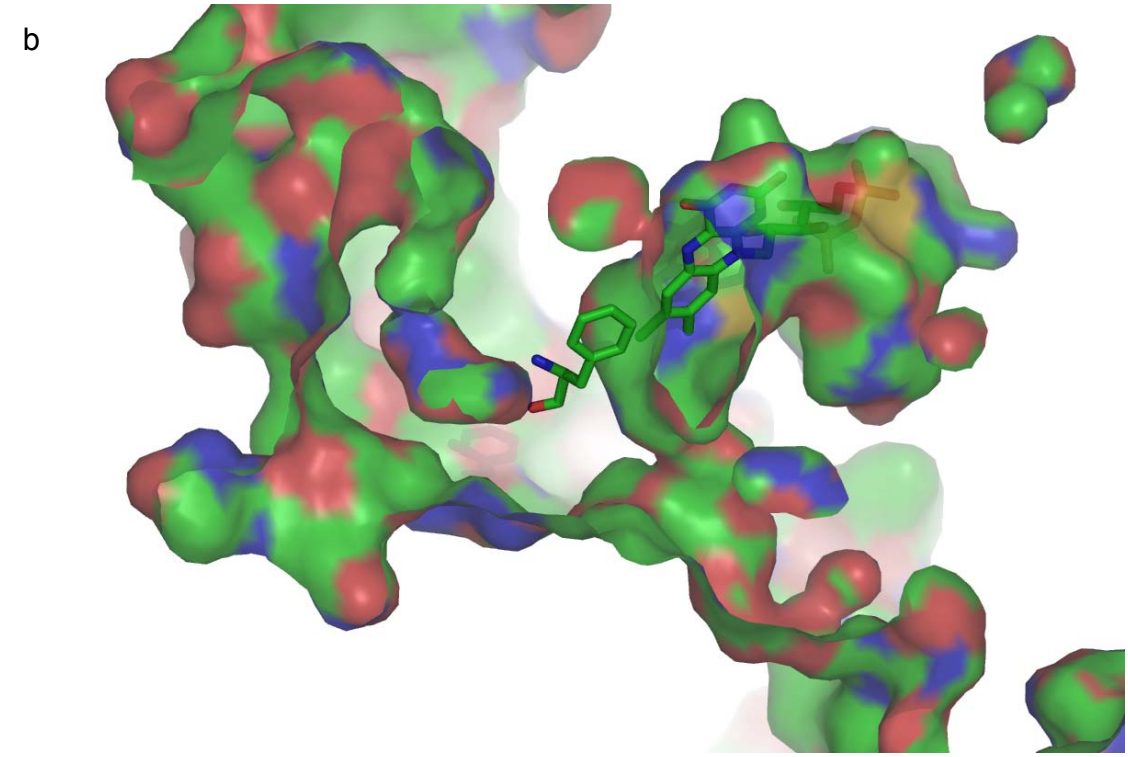

Figure 2-10 Potential "tunnel" in other GMC oxidoreductases. a) cellobiose dehydrogenase from *Phanerochaete chrysosporium* (PDB entry 1KDG); b) pyranose 2-oxidase from *Trametes multicolor* (PDB entry 1TT0); Tunnel surfaces were constructed by removing waters in the structure and then filling with solvent-accessible surfaces using Pymol. The FAD cofactors and the Phe residues that exist at where the potential tunnel discontinues are shown in sticks.

In conclusion, hydrophobic tunnels have been observed in other protein structures, and their function as gas-binding tunnels hypothesized. The mutagenesis, kinetic and structural studies presented here provide functional evidence for the utility of the hydrophobic tunnel that reaches ~18 Å between the solvent accessible surface and the active site of cholesterol oxidase (**Figure 2-11**). This tunnel provides oxygen access to the enzyme active site. That is, there is a specific binding pathway for oxygen to reach the reduced flavin cofactor. Similar oxygen binding tunnels have been observed in other protein structures, and are likely to function in a similar fashion. Their evolutionary selection is presumably derived from the need for temporal control as well as regiospecific control over oxygen delivery to reactive intermediates in enzyme-catalyzed reactions.

On the other hand, the hydrophobic tunnel might be functionally more important when used as an exit for hydrogen peroxide. Peroxide or similarly oxidizing reagents can cause degenerative diseases such as coronary heart disease [**33**], aging [**34**] and cancer [**35**]. Hydrogen peroxide can also react with amino acid side chains which leads to mutations of protein structures [**36**]. Although a channel for H^+/H_2O output can still be formed in cytochrome oxidases when oxygen is reduced to water instead of hydrogen peroxide [**37**], reactions

catalyzed by these enzymes will yield various types of intermediates that are partially reduced oxygen species [**38**]. Thus, It is possible that these hydrophobic tunnels were evolved to prevent reactivity of the product as well as oxidative reagents from damaging the enzymes.

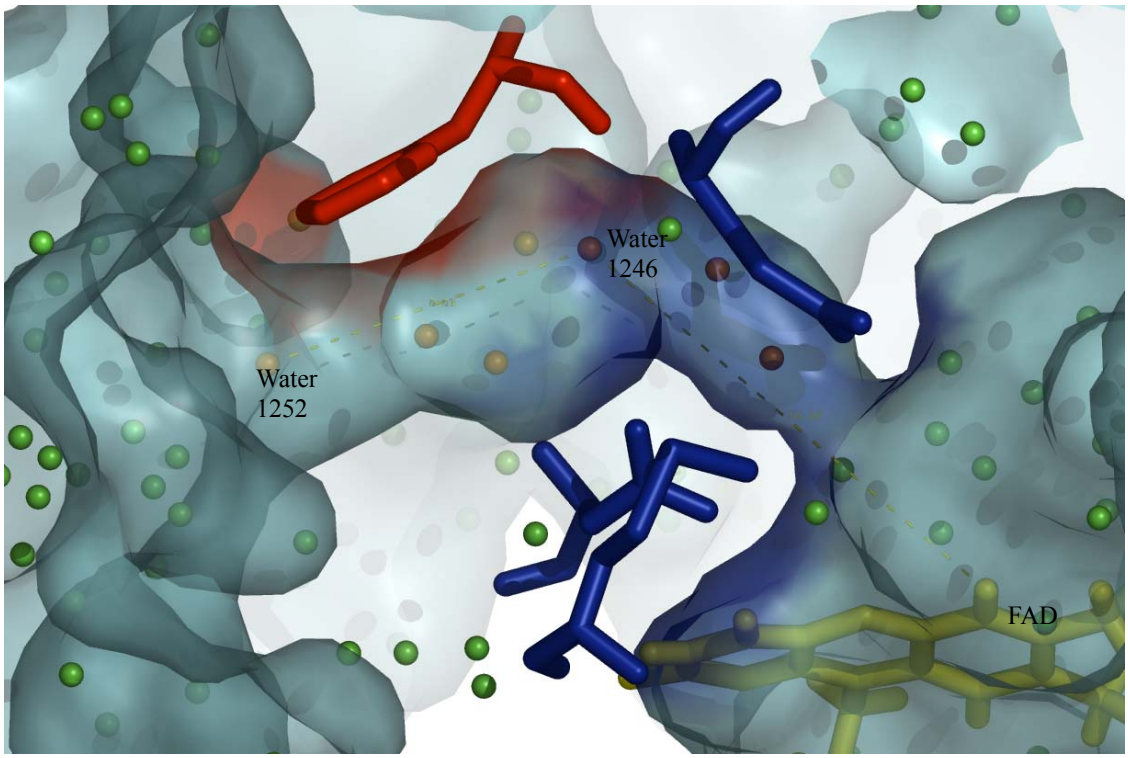

Figure 2-11 Length of the tunnel. Distances were drawn as yellow dashed lines. Water 1252 to water 1246: 7.74 Å; water 1246 to the hydrogen of C6 on the isoalloxazine ring: 10.66 Å.

References

1. F. M. Raushel, J. B. Thoden and H. M. Holden, Enzymes with molecular tunnels, *Acc. Chem. Res.* **36** (2003), no. 7, 539-548.
2. C. C. Hyde, S. A. Ahmed, E. A. Padlan, E. W. Miles and D. R. Davies, Three-dimensional structure of the tryptophan synthase alpha 2 beta 2 multienzyme complex from Salmonella typhimurium, *J. Biol. Chem.* **263** (1988), no. 33, 17857-17871.
3. F. M. Raushel, J. B. Thoden and H. M. Holden, The amidotransferase family of enzymes: molecular machines for the production and delivery of ammonia, *Biochemistry* **38** (1999), no. 25, 7891-7899.
4. X. Huang and F. M. Raushel, Restricted passage of reaction intermediates through the ammonia tunnel of carbamoyl phosphate synthetase, *J. Biol. Chem.* **275** (2000), no. 34, 26233-26240.
5. A. Volbeda and J. C. Fontecilla-Camps, Crystallographic evidence for a CO/CO(2) tunnel gating mechanism in the bifunctional carbon monoxide dehydrogenase/acetyl coenzyme A synthase from Moorella thermoacetica, *J. Biol. Inorg. Chem.* **9** (2004), no. 5, 525-532.
6. X. Tan, A. Volbeda, J. C. Fontecilla-Camps and P. A. Lindahl, Function of the tunnel in acetylcoenzyme A synthase/carbon monoxide dehydrogenase, *J. Biol. Inorg. Chem.* **11** (2006), no. 3, 371-378.
7. M. J. Knapp and J. P. Klinman, Kinetic studies of oxygen reactivity in soybean lipoxygenase-1, *Biochemistry* **42** (2003), no. 39, 11466-11475.
8. M. J. Knapp, F. P. Seebeck and J. P. Klinman, Steric control of oxygenation regiochemistry in soybean lipoxygenase-1, *J. Am. Chem. Soc.* **123** (2001), no. 12, 2931-2932.
9. M. P. Mims, A. G. Porras, J. S. Olson, R. W. Noble and J. A. Peterson, Ligand binding to heme proteins. An evaluation of distal effects, *J. Biol. Chem.* **258** (1983), no. 23, 14219-14232.
10. M. Schmidt, K. Nienhaus, R. Pahl, A. Krasselt, S. Anderson, F. Parak, G. U. Nienhaus and V. Srajer, Ligand migration pathway and protein

dynamics in myoglobin: a time-resolved crystallographic study on L29W MbCO, *Proc. Nat. Aca. Sci.* **102** (2005), no. 33, 11704-11709.

11. A. Ostermann, R. Waschipky, F. G. Parak and G. U. Nienhaus, Ligand binding and conformational motions in myoglobin, *Nature* **404** (2000), no. 6774, 205-208.
12. R. F. Tilton, Jr., I. D. Kuntz, Jr. and G. A. Petsko, Cavities in proteins: structure of a metmyoglobin-xenon complex solved to 1.9 A, *Biochemistry* **23** (1984), no. 13, 2849-2857.
13. I. M. Moustafa, S. Foster, A. Y. Lyubimov and A. Vrielink, Crystal structure of LAAO from Calloselasma rhodostoma with an L-phenylalanine substrate: insights into structure and mechanism, *J. Mol. Biol.* **364** (2006), no. 5, 991-1002.
14. R. Coulombe, K. Q. Yue, S. Ghisla and A. Vrielink, Oxygen access to the active site of cholesterol oxidase through a narrow channel is gated by an Arg-Glu pair, *J. Biol. Chem.* **276** (2001), 30435-30441.
15. Y. Montet, P. Amara, A. Volbeda, X. Vernede, E. C. Hatchikian, M. J. Field, M. Frey and J. C. Fontecilla-Camps, Gas access to the active site of Ni-Fe hydrogenases probed by X-ray crystallography and molecular dynamics, *Nat. Struct. Biol.* **4** (1997), no. 7, 523-526.
16. P. Lario, N. S. Sampson and A. Vrielink, Sub-atomic resolution crystal structure of cholesterol oxidase: What atomic resolution crystallography reveals about enzyme mechanism and the role of the FAD cofactor in redox activity, *J. Mol. Biol.* **326** (2003), 1635-1650.
17. W. L. DeLano, The PyMOL Molecular Graphics System, (2006).
18. N. S. Sampson, Dissection of a flavo-enzyme active site: the reaction catalyzed by cholesterol oxidase, *Antioxi. Red. Sign.* **3** (2001), 839-846.
19. Y. Ye, P. Lario, A. Vrielink and N. S. Sampson, The presence of a hydrogen bond betwen asparagine 485 and the p system of FAD modulates the redox potential in the reaction catalyzed by cholesterol oxidase, *Biochemistry* **40** (2001), 13779-13787.

20. N. S. Sampson and I. J. Kass, Isomerization, but not oxidation, is suppressed by a single point mutation, E361Q, in the reaction catalyzed by cholesterol oxidase, *J. Am. Chem. Soc.* **119** (1997), 855-862.
21. A. Lyubimov, L. Chen, N. S. Sampson and A. Vrielink, Probing the role of Asn485 in oxidation catalysis by mutagenesis and atomic resolution crystallography, *submitted* (2007).
22. J. Ricard and A. Cornish-Bowden, Co-operative and allosteric enzymes: 20 years on, *Eur. J. Biochem. / FEBS* **166** (1987), no. 2, 255-272.
23. A. Cornish-Bowden and M. L. Cardenas, Co-operativity in monomeric enzymes, *J. Theor. Biol.* **124** (1987), no. 1, 1-23.
24. J. Li, A. Vrielink, P. Brick and D. M. Blow, Crystal structure of cholesterol oxidase complexed with a steroid substrate: implications for flavin adenine dinucleotide dependent alcohol oxidases, *Biochemistry* **32** (1993), 11507-11515.
25. G. Pettersson, Mechanistic origin of the sigmoidal rate behaviour of glucokinase, *Biochem. J.* **233** (1986), no. 2, 347-350.
26. G. Pettersson, Mechanistic origin of the kinetic cooperativity of hexokinase type L1 from wheat germ, *Eur. J. Biochem. / FEBS* **154** (1986), no. 1, 167-170.
27. T. Lamark, I. Kaasen, M. W. Eshoo, P. Falkenberg, J. McDougall and A. R. Strom, DNA sequence and analysis of the bet genes encoding the osmoregulatory choline-glycine betaine pathway of Escherichia coli, *Mole. Microbiol.* **5** (1991), no. 5, 1049-1064.
28. K. R. Frederick, J. Tung, R. S. Emerick, F. R. Masiarz, S. H. Chamberlain, A. Vasavada, S. Rosenberg, S. Chakraborty, L. M. Schopfer and et al., Glucose oxidase from Aspergillus niger. Cloning, gene sequence, secretion from Saccharomyces cerevisiae and kinetic analysis of a yeast-derived enzyme, *J. Biol. Chem.* **265** (1990), no. 7, 3793-3802.
29. I. P. Cheng and J. E. Poulton, Cloning of cDNA of *Prunus serotina* (R)(+)mandelonitrile lyase and identification of putative FAD-binding site, *Plant. Cell. Physiol.* **34** (1993), 1139-1143.

30. Y. Sakai and Y. Tani, Cloning and sequencing of the alcohol oxidase-encoding gene (AOD1) from the formaldehyde-producing asporogeneous methylotrophic yeast, Candida boidinii S2, *Gene* **114** (1992), no. 1, 67-73.
31. T. Ishizaki, N. Hirayama, H. Shinkawa, O. Nimi and Y. Murooka, Nucleotide sequence of the gene for cholesterol oxidase from a Streptomyces sp, *J. Bact.* **171** (1989), no. 1, 596-601.
32. Bjarne Knudsen, T. Knudsen, M. Flensborg, H. Sandmann, M. Heltzen, A. Andersen, M. Dickenson, J. Bardram, P. J. Steffensen, S. Mønsted, T. Lauritzen, R. Forsberg, A. Thanbichler, J. D. Bendtsen, L. Görlitz, J. Rasmussen, D. Tordrup, M. Værum, M. N. Ravn, CLC Protein Workbench, (25. jun 2007).
33. R. Stocker and J. F. Keaney, Jr., Role of oxidative modifications in atherosclerosis, *Physiol. Rev.* **84** (2004), no. 4, 1381-1478.
34. I. Ben-Porath and R. A. Weinberg, The signals and pathways activating cellular senescence, *Inter. J. Biochem. Cell Biol.* **37** (2005), no. 5, 961-976.
35. P. Storz, Reactive oxygen species in tumor progression, *Front. Biosci.* **10** (2005), 1881-1896.
36. S. D. Maleknia, N. Reixach and J. N. Buxbaum, Oxidation inhibits amyloid fibril formation of transthyretin, *FEBS J.* **273** (2006), no. 23, 5400-5406.
37. C. Koutsoupakis, E. Pinakoulaki, S. Stavrakis, V. Daskalakis and C. Varotsis, Time-resolved step-scan Fourier transform infrared investigation of heme-copper oxidases: implications for O2 input and H_2O/H^+ output channels, *Biochim. Biophy. Acta* **1655** (2004), no. 1-3, 347-352.
38. C. Varotsis and G. T. Babcock, Photolytic activity of early intermediates in dioxygen activation and reduction by cytochrome oxidase., *J. Am. Chem. Soc.* **117** (1995), 11260–11269.

Chapter 3

The interplay between potentiometry and structural biology: probing the role of Asn485 in the catalysis of cholesterol oxidase by two mutant enzymes: N485L and N485D

I. Introduction

1. Active site residues and structures of cholesterol oxidase

The Detailed catalytic mechanism of cholesterol oxidase from *Streptomyces* (ChoA) was studied using a combination of crystallography and kinetic techniques.[**1-4**] Catalysis proceeds Michaelis complex formed between the active site residues and the substrate.[**5**] A model of this complex is shown in **Figure 3-1**. In this model, the C-H bond from the substrate molecule (DHEA in this case) is aligned with the lowest unoccupied molecular orbital (LUMO) of the FAD so as to maximize orbital overlap and thus facilitate catalysis. In fact, in the crystal structures a water molecule aligns over the π-orbital of the cofactor isoalloxazine ring (N5 position) [**2**]. This water molecule is thought to serve as a mimic of the substrate hydroxyl group in the structure.

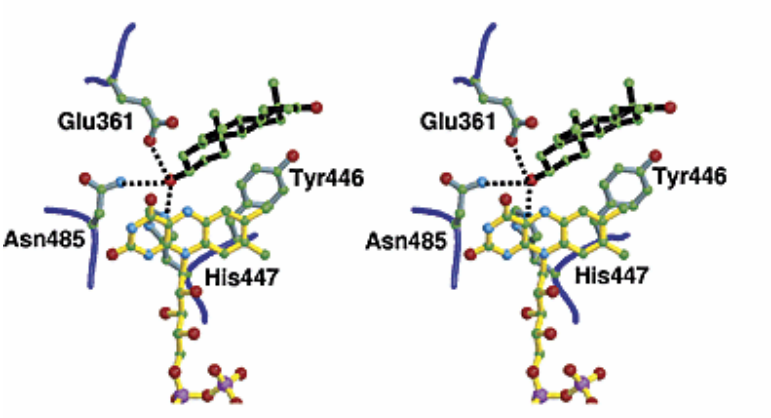

Figure 3-1 Stereo figure of a model for the Michaelis complex in ChoA (pdb entry 1MXT).[**2**] Adopted from reference [**5**].

His 447 is conserved in all enzymes in the GMC oxidoreductase family **(Figure 2-11)**. Its importance has also been demonstrated by mutagenesis and kinetical studies.[**1**] In the atomic resolution structure of ChoA, His447 is protonated at NE2 over a broad range of pHs.[**5**] The role of this conserved residue is to form hydrogen bond with the substrate hydroxyl group and participate in the positioning of the substrate with respect to the cofactor and Glu361 residue because the hydrogen atom from the substrate hydroxyl group needs to point toward Glu361 (**Scheme 3-1**).

Cholesterol oxidase catalyzes a unique isomerization reaction following the oxidation step. This feature is not shared by other GMC-oxidoreductases possibly due to the fact that oxidation of cholesterol will produce an intermediate, cholest-5-en-3-one, that is highly susceptible to peroxidation which will result in a series of side products[**6**]. In the isomerization, the C-H bond at C4 position is cleaved and one hydrogen is transferred to 6 position to form a new double-bond at α,β position. The crystal structure supported the general base hypothesis because Glu361 was found to be positioned over the plane of the substrate (**Scheme 3-1**) [**3, 7**]. Isotope transfer and mutagenesis studies suggested the involvement of a base in the isomerization.[**8, 6, 9**]

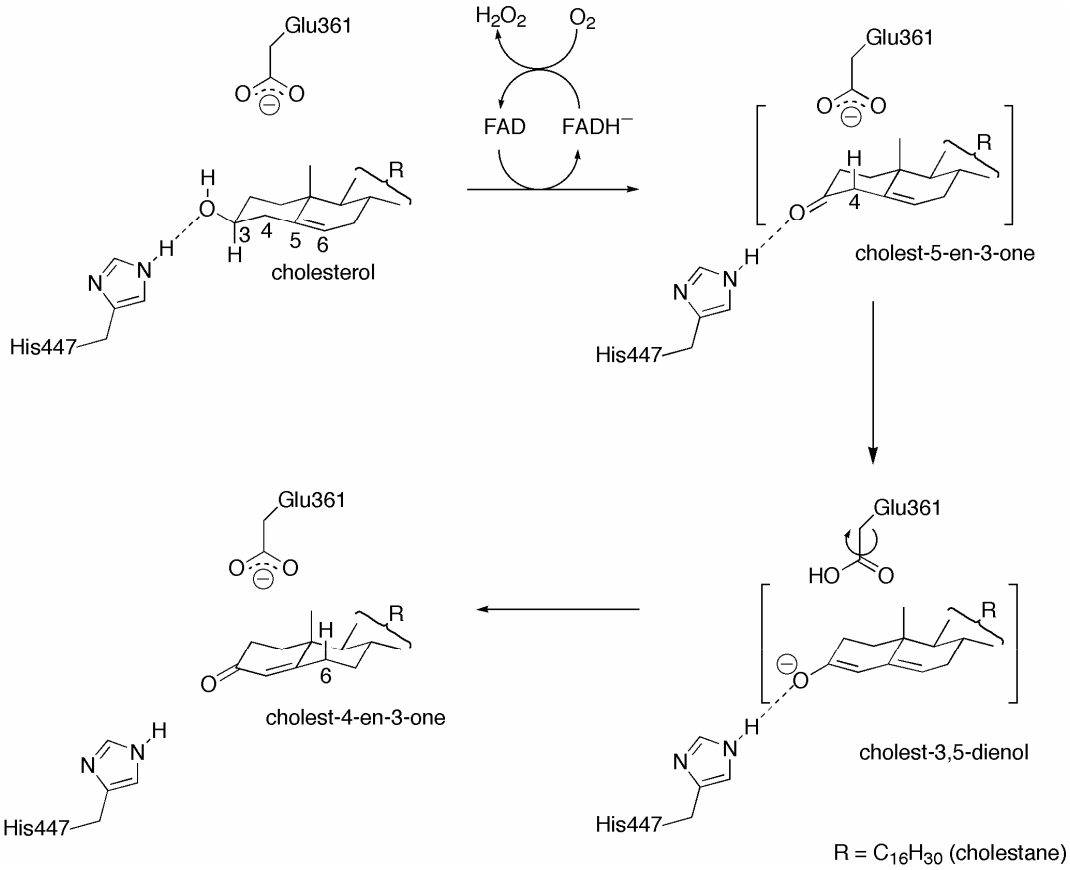

Scheme 3-1 Key active site residues involve in the catalysis of ChoA. [**10**]

2. An N-H···π interaction stabilizes the reduced flavin

The asparagine residue at position 485 in ChoA was postulated to play an important role in catalysis because it is located at the active site and is within hydrogen bonding distance of the substrate.[**3**] Kinetic and crystallographic studies were carried out to elucidate its role in catalysis.[**11**] It was found that mutation of asparagines to leucine resulted in a 1300-fold decrease in k_{cat}/K_m of the oxidation step but only 60-fold for the isomerization. Hydride (from the C3a) transfer at 3α position is still partially rate-limiting for the mutant. The reduction in catalytic rate was attributed to the reduction in redox potential (-76 mV) for the Leu mutant. An explanation of this reduction in potential was provided by crystal structure where it was found that an N-H···π interaction between Asn485 and the cofactor was removed by mutation into a Leu.[**11**] An amide-π interaction could reduce the overall thermodynamic energy by 2~3 kcal/mol through stabilization of the reduced FAD.[**12**]

An atomic resolution structure of the WT enzyme refined to 0.95 Å provided a better understanding toward the involvement of the Asn485 residue than the original 1.5 Å structure of N485L mutant.[**2**] Two populated conformational states for 82 amino acids were observed in the atomic structure. Asn485 was found to adopt two different side-chain conformations at liganded and un-liganded states of the enzyme. When in the liganded conformation, Asn485 and a few other hydrophobic residues form a tunnel that is pointed toward the solvent accessible surface for oxygen entry. This phenomenon could be explained mechanistically: the reduced FAD cofactor will require Asn485 to form an N-H···π interaction to

stabilize its extra charge as well as the need for molecular oxygen to cycle it back to its oxidized form (**Scheme 3-1**, **Figure 3-2**).

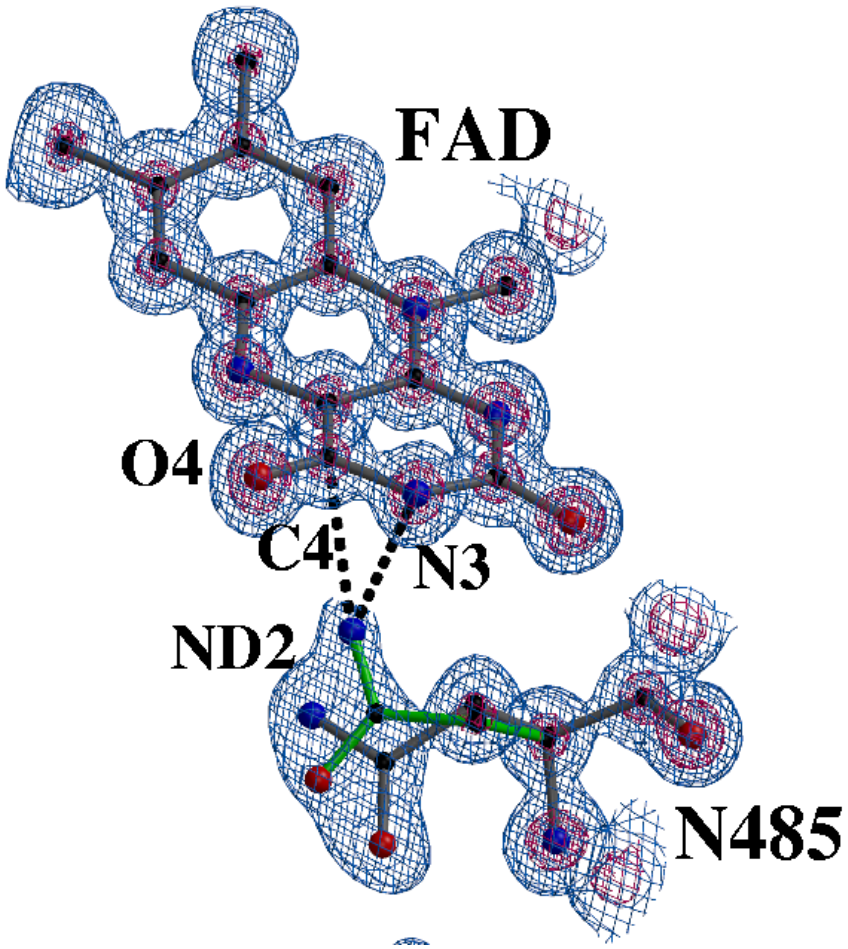

Figure 3-2 Side chain of Asn485 adopts two different conformations. The conformation appeared in green is the liganded conformation. Its interactions with the cofactor were shown as dotted lines.[**2**]

3. Potentiometry and its application in enzymology

Reduction potential is the tendency of a chemical species to acquire electrons and thereby be reduced. Each species has its own intrinsic reduction potential; the more positive the potential, the greater the affinity for electrons and tendency to be reduced. Reduction potentials are defined relative to the standard hydrogen electrode (SHE) which is arbitrarily given a potential of 0.00 volts. Some common oxi-reduction reactions and their redox potentials are listed in **Table 3-1**.

Half-reaction	Eo (V)
$Li^+(aq.) + e- \rightarrow Li(solid)$	−3.05
$2\ H_2O(liquid) + 2e^- \rightarrow H_2(gas) + 2\ OH^-(aq.)$	-0.83
$2H^+(aq.) + 2e^- \rightarrow H_2(gas)$	0.00
$O_2(gas) + 4H^+ + 4e^- \rightarrow 2H_2O$	+1.23

Table 3-1 Half-reactions and their corresponding potentials. E_0, potential; aq., aqueous solution.[**13**]

Redox centers are a common place within enzymes where storing and transferring of electrons occur during catalysis.[**14**] Metals and organic cofactors such as flavins are major components of redox centers. The free energy required to oxidize or reduce these redox centers is an important parameter of catalysis and its determination is key to elucidation of the mechanism. The redox potential of these redox centers can be readily converted to free energy. For example, there are 24 electrons involved in the cellular respiration process. The potential of oxygen being reduced to water is 1.23 V. We can thus calculate its free energy by using the Faraday constant (**Scheme 3-2**).

$$C_6H_{12}O_6 + 6O_2 \longrightarrow 6CO_2 + 6H_2O + \text{energy (36 ATP)}^*$$

$$\Delta G = -nFE$$

$$= -(24)(23.062)(1.23) = -686 \text{ kcal}$$

Scheme 3-2 Free energy of the cellular respiration process.

* The biology web. http://faculty.clintoncc.suny.edu/faculty/Michael.Gregory/default.htm

Another significant contribution of redox potential studies is that we can detect subtle changes in the protein environment surrounding the redox center, as well as how enzymes modulate the redox property of the cofactor. For instance, pKas of residues in the active sites of some enzymes can be assigned based on ionization (potential) states of the redox centers.[**15**] In another case, the two-electron midpoint potential of FAD is shifted 74 mV more negative as a result of tighter binding to the reduced form by its surrounding apoprotein.[**16**] This type of higher affinity can be attributed to the formation of covalent interaction and hydrogen bonding with the reduced cofactor.

The active site asparagine residue was mutated to Asp in this study to further probe the role of electrostatics during catalysis. The mutant was examined by a combination of kinetics, potentiometry and crystallographic techniques. Similar experiments were repeated for the N485L mutant. The crystal structure of the Leucine mutant was refined to atomic resolution for a detailed comparison with structures from WT and N485D.

II. Results

1. Steady-state kinetics and potentiometry at pH 7

Steady-state kinetic parameters at pH 7.0 were recorded for WT, N485D and N485L enzymes (**Table 3-2 and Table 3-3**). Mutations on the Asn residue decreased kcat of oxidation by 650 (N485D) ~1100 (N485L) fold. Apparent Km values were affected < 2 fold within experimental error. The isomerization step, as probed by using cholest-5-en-3-one as the substrate, was diminished only 6~20 fold. Hydride transfer, which is partially rate-limiting in the WT enzyme, is still determining the date in the mutants at pH 7.0 (**Table 3-4**). However, it is no longer rate-determining for the N485D mutant at pH 5.1 because the isotope effects decreases to 1.2 from 2.5 at pH 7.0.

Potentiometric experiments were done in an anaerobic spectroelectrochemical cell following the method of Stankovich.[**17**] The potentials of individual one-point reduction (E1, E2) for the WT enzyme were recorded. However, due to limited stability of semiquinone in the mutants, only the mid-point potential was obtained for N485D and N485L enzymes. The potential of the enzyme was poised using a redox dye, the E_m of which is within 30 mV of the enzyme. The potentials were measured with an Ag/AgCl electrode and corrected to the standard hydrogen electrode. The concentrations of oxidized, semiquinone and reduced flavin enzyme species were determined spectroscopically at each measured potential. As summarized in **Table 3-5**, E1 corresponds to the one-electron reduction potential of the cofactor to the

semiquinone form and E2 indicates the potential of the second electron reduction, which converts semiquinone of the cofactor to its reduced form. The midpoint potential of the WT enzyme is within the range of potentials that are observed for most flavoproteins (0~-150 mV) at pH 7.0. The E_m of N485D and N485L are reduced -80 and -85 mV from that of WT, respectively.

Table 3-2. Michaelis-Menten rate constants of the oxidation reaction.

pH	Enzyme	Oxidation [a]			
		k_{cat} (s^{-1})	K_m (μM)	k_{wt}/ k_{mutant}	k_{cat}/ K_m pH 5.1/pH 7.0
7.0	WT	47 ± 4.0	2.7 ± 0.28	n.a.	
	N485D	0.073 ± 0.0048	6.6 ± 1.2	644	
	N485L	0.044 ± 0.0051	4.6 ± 1.9	1068	
	WT	46 ± 3.6	6.7 ± 1.4	n.a.	0.44
5.0	N485D	1.4 ± 0.16	6.3 ± 2.1	33	20
	N485L	0.035 ± 0.0044	6.2 ± 2.2	1314	0.59

[a] measured by H_2O_2 formation and cholesterol as substrate.

Table 3-3. Michaelis-Menten rate constants of the isomerization reaction.

pH	Enzyme	Isomerization [a]			
		k_{cat} (s^{-1})	K_m (μM)	k_{wt}/k_{mutant}	k_{cat}/K_m pH 5.1/pH 7.0
7.0	WT	61 ± 3.9	7.2 ± 1.4	n.a.	n.a.
	N485D	10 ± 0.47	7.2 ± 0.87	6.1	n.a.
	N485L	3.2 ± 0.3	18 ± 0.6	19	n.a.
	WT	64 ± 3 [b]	6.2 ± 0.7 [b]	n.a.	1.2
5.0	N485D	1.1 ± 0.086	5.9 ± 1.3	58	0.134
	N485L	2.5 ± 0.16	8.5 ± 1.1	26	0.78

[a] measured by cholest-4-en-3-one formation at 240 nm and cholesten-5-en-3-one as substrate.
[b] Kass, I., Biochemistry, 37 (51), 17990-18000

Table 3-4. Primary isotope effects for wild type and mutant cholesterol oxidases as a function of pH

pH	Enzyme	$^{D}V^{a}$	$^{D}V/K^{a}$
5.1	WT	1.9 ± 0.1	1.6 ± 0.1
	N485D	1.2 ± 0.1	1.2 ± 0.1
	N485L	2.4 ± 0.2	2.4 ± 0.2
7.0	WT	2.2 ± 0.1[b]	2.2 ± 0.1[b]
	N485D	2.5 ± 0.2	2.5 ± 0.2
	N485L	2.2 ± 0.1[b]	2.2 ± 0.1[b]

[a] measured by H_2O_2 formation and 3-[^{2}H]-cholesterol as substrate. [b] from reference [**11**]

Table 3-5. Redox potentials of wild type and mutant enzyme as a function of pH

pH	Enzyme	E1 (mV)	E2 (mV)	Em (mV)	Em^{mutant} - Em^{WT} (mV)	$Em^{pH\ 5}$ – $Em^{pH\ 7}$ (mV)[a]
7.0	WT	-97 ± 8[b]	-165 ± 4[c]	-131	n.a.[d]	n.a.
	N485D	n.m.[g]	n.m.	-211 ± 6[h]	-80	n.a.
	N485L	n.m.	n.m.	-216 ± 2[h]	-85	n.a.
5.0	WT[e]	-28 ± 1	-117 ± 3	-73	n.a	58
	N485D	n.m.	n.m.	-82 ± 4[f]	-9	125
	N485L	n.m.	n.m.	-103 ± 4[f]	-30	112

[a] decrease in Em from that of WT. [b] the average and standard deviation of 4 experiments (dye used are: I2S X2 and ANQ X2) [c] the average and standard deviation of 3 experiments (dye used are: ANQ X2 and CV X1) [d] not applicable [e] the average and standard deviation of 2 experiments each (E1: I4S X2; E2: CV X2) [f] the average and standard deviation of two experiments (dye used are: riboflavin X1; CV X1) [g] not measurable [h] the average and standard deviation of 2 experiments (dye used is: riboflavin X2)

2. Kinetic and potentiometric measurements at pH 5.1

Both the kinetic and thermodynamic parameters of WT and mutant enzymes were measured at pH 5.1 and compared to those of pH 7. For the WT enzyme and the N485L mutant, the rate of oxidation was unchanged at pH 5.0 whereas for N485D, the low pH results in a 20-fold increase in the rate of oxidation compared to pH 7.0 (**Table 3-2**). The isomerization step in the WT enzyme remained unchanged over the range of pH 4.5 – 10.6.[**18**] In contrast, for N485D, isomerization decreased 8-fold at pH 5.1 compared to pH 7.0. The midpoint reduction potentials for WT and mutant enzymes were 60-125 mV more positive when the pH was lowered to 5 (**Table 3-4**). The change in potential observed between pH 5 and pH 7 was greater for the mutants than for the WT enzyme (**Table 3-4**).

Examination of the visible spectra of WT and N485D at both pH 7 and pH 5 resulted in differences at various regions. Spectra of both enzymes red shifted due to increased protonation level when the pH was lowered (**Figure 3-3**). Spectrum shifts were observed in the WT enzyme from 385 nm to 388 nm and 467 nm to 468 nm; N485D had bigger shifts, from 380 nm to 389 nm and 465 nm to 467 nm. N485D appeared to be affected more by the change in pH.

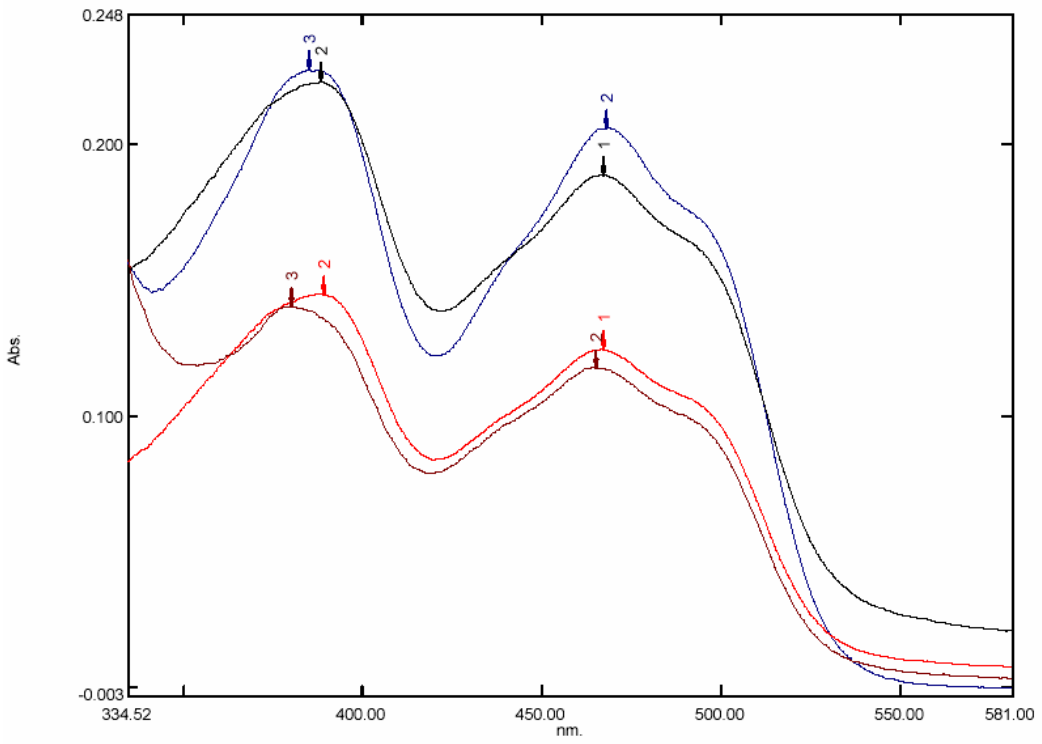

Figure 3-3 Spectra overlay of WT and N485D mutant enzymes at visible region. Blue, WT at pH 7; Black, WT at pH 5; Brown, N485D at pH 7; Red, N485D at pH 5.

3. Atomic resolution structure of N485L mutant

The crystal structure of the N485L mutant was obtained previously at 1.5 Å resolution [**19**], but was later refined to 0.92 Å atomic resolution by Vrielink et. al.[**10**]. Multiple side chain conformations were observed in the improved structure. Since the atomic resolution structure of the WT enzyme is already available, a much more detailed comparison of the mutant structure with that of the WT gave insights into the electrostatic effects of Asn485 in the catalysis.[**2**]

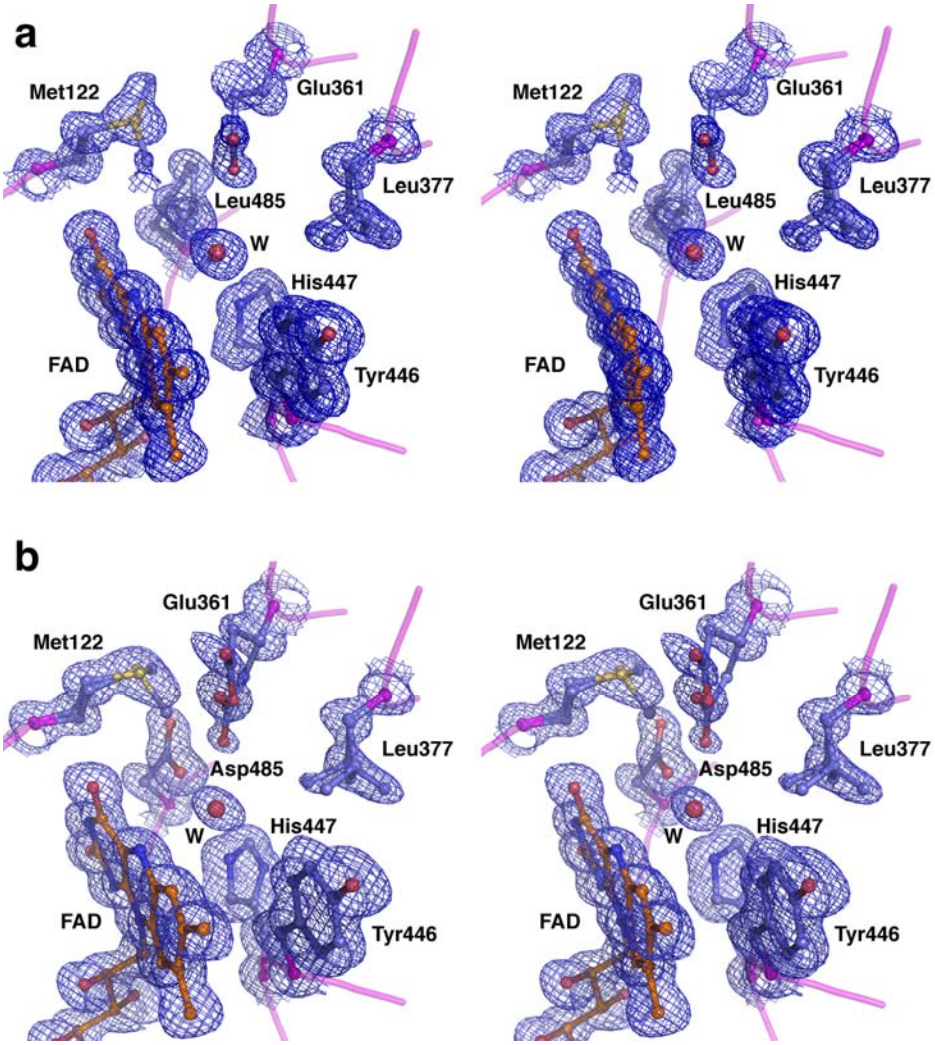

Figure 3-4 Electron density at the active sites of WT and mutant enzymes. a) N485L mutant; b) N485D mutant. $2F_o$-F_c electron density (blue cloud) is contoured at 1.0σ. Ball-and-stick models were used to illustrate the active site residues and the FAD cofactor.[**10**]

One additional conformation arises from the atomic structure of N485L, in addition to the original side chain conformation observed in the 1.5 Å resolution structure. These two conformations are separated by a rotation of 180° along χ2 axis. Consequently, the methyl group at the end of the side chain is placed in two different positions (**Figure 3-4**). However, both of two side chain conformations observed point away from the cofactor pocket due to lack of H-bond donors which causes N485L to lose stabilization of the reduced FAD (**Figure 3-5 a,b**). In the lower resolution structure of N485L, Met122 has only one conformation. One more conformation of its side chain is now visible under atomic resolution although conformation B is dominant in the population (**Figure 3-5 b**).

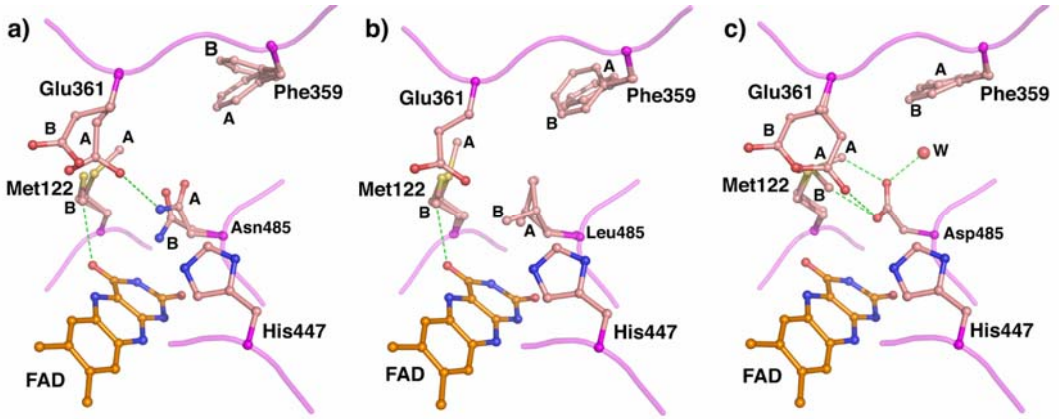

Figure 3-5 Active sites of the WT and mutant enzymes. a) wild-type; b) N485L; c) N485D. Portions other than the isoalloxazine ring was omitted for the cofactor. Green dashed lines represent hydrogen bonds.[**10**]

It is now obvious that the apparent two conformations of Phe359 in the WT structure are correlated with the side chain conformations of Asn485. When the amide of Asn485 moves closer to the cofactor to stabilize extra negative charge (conformer B), conformer A of Phe359 rotates nearly 90° to become conformer B and thus form a hydrophobic tunnel that connects the active site to outside solvent (**Figure 3-6**). [**2**] However, the movement of Leu485 is greatly restricted in the N485L mutant (**Figure 3-5**). As a result, Phe359 in the mutant is not able to rotate to the tunnel open position. The tunnel remains closed because the side chain phenyl ring needs to maintain maximal van der Waals contact with Leu485.

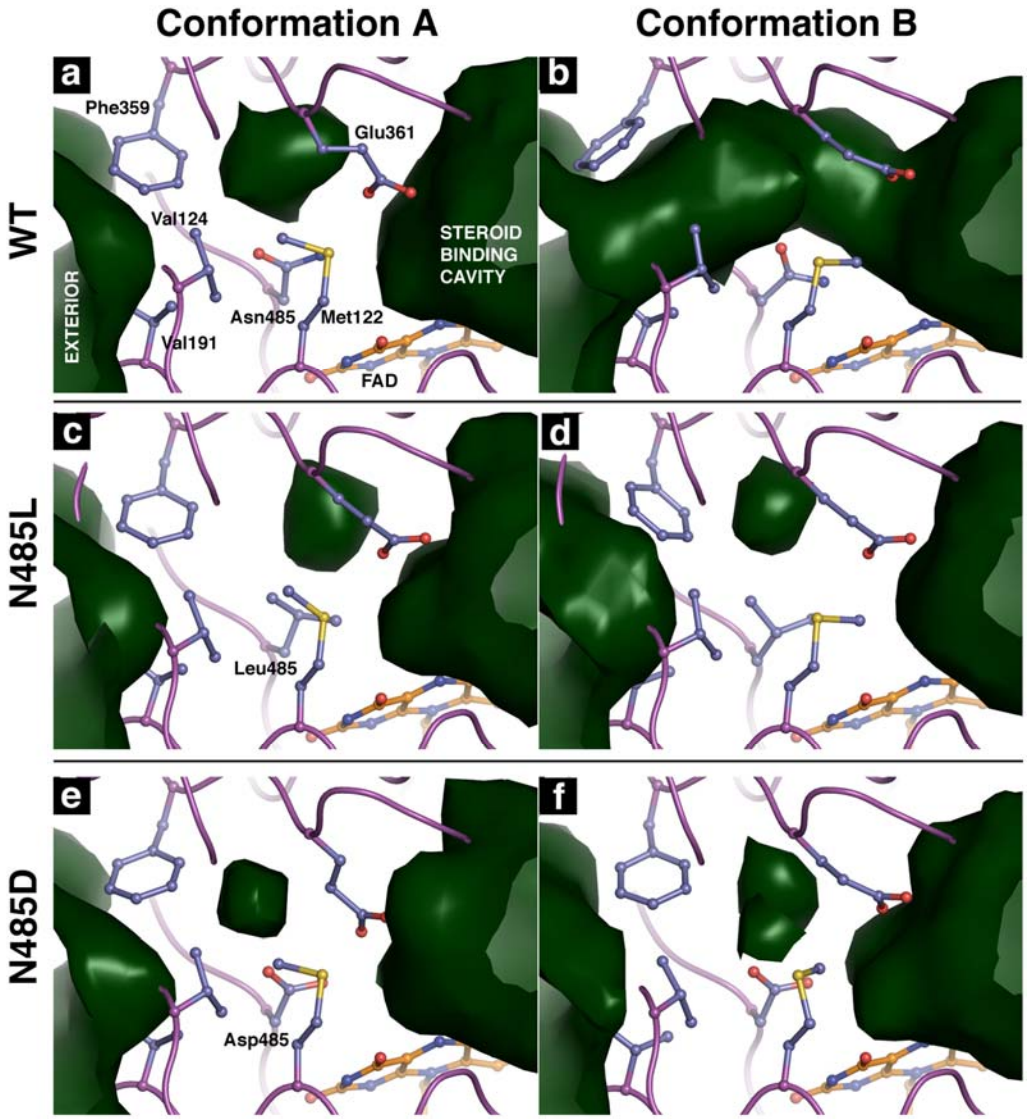

Figure 3-6 The hydrophobic tunnel for oxygen is affected by mutations on Asn485. a-f) solvent-accessible surface in the active site. Key tunnel residues were labeled as ball-and-stick models. The tunnel is either closed when the residue at 485 position adopts conformation A (a,c,e) or open in conformation B (b,d,f).[**10**]

4. Atomic resolution structure of N485D mutant

One of the two side chain conformations of Asn485 observed in the native structure disappears in the Asp mutant structure refined to 1.0 Å resolution. Conformer B of Asn485 which corresponds to the tunnel open conformation is no longer present when Asn was mutated to an Asp. The carboxylate group now rotates away from the cofactor at all times (**Figure 3-5 a,c**). The aspartate side chain communicates with Phe359 through a water molecule (Wat1241) found in a hydrophobic pocket formed by the phenyl ring of Phe359 and two other valines. Phe359 adopts two conformations (**Figure 3-5 c**), one of which (conformer B) interacts with Wat1241 using its side chain π electrons. Wat1241 in turn forms a hydrogen-bond with the aspartate. Overall, the Asp mutant disrupts the active site environment by introducing extra negative charge and forming interactions with residues outside the active site and the reduced FAD is no longer stabilized.

Met122 in the N485D mutant structure is found in two conformations both of which point toward the side chain negative charge of Asp485. CE-Met122 is within 2.5-3 Å distance with both OD1 and OD2 of Asp485. This type of distance is in the range of CH···O hydrogen bond interactions which in this case is formed between methyl carbon of Met122 and the aspartate carboxylate moiety of Asp485. Also, one conformation of the Glu361 side chain is in hydrogen bonding distance of Asp485. Two conformers of Glu361 in the N485D structure were illustrated in a model where Met122 adopts different conformations but both are involved in an interaction with the negative charge of the carboxylate (**Figure 3-7**).

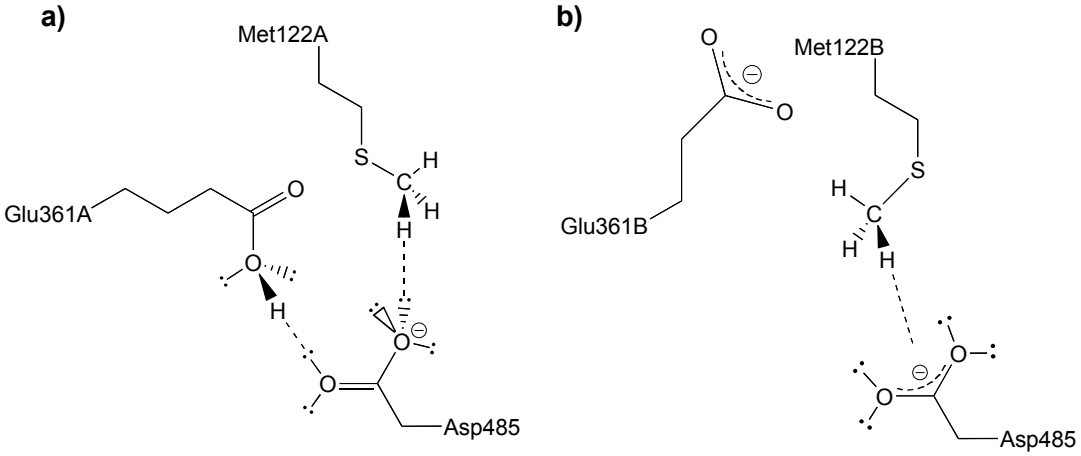

Figure 3-7 Hydrogen bonding network between Asp485 and Met122, Glu361. a) conformation A; b) conformation B.[**10**]

III. Discussion

Asparagine 485 plays important roles in catalysis by establishing an NH•••π interaction between the amide and the pyrimidine ring of the reduced cofactor.[**11**] Mutations of this residue to either an Asp or a Leu removed this interaction and thus caused loss of oxidation catalysis by 600-1200 fold at normal pH of 7.0. In the potentiometric studies, the amount of semiquinone formed was so little in the mutant due to the loss of the NH•••π interaction that E1 and E2 of were not sufficiently separated to be measured.

Kinetic studies were conducted at a lowered pH of 5.1 to see how changes of protonation level in the environment affect the catalysis by the enzymes (WT and mutants). Mutation from an Asn to an Asp perturbed the active site electrostatic environment (**Figure 3-4**) and thus caused a decrease in k_{cat} of the oxidation half-reaction at pH 7.0 but not as much reduction at pH 5.1. The carboxylate side chain of Asp485 in the mutant displays partial amide behavior when it becomes partially protonated at low pH. On the other hand, the Leu mutant activity is not rescued by lowering pH since it has a hydrophobic side chain.

The potentials of WT and two mutant enzymes are separated by 70~90 mV at pH 7.0 but both mutants are able to recover their redox potential at pH 5.1 to only 10~30 mV lower than that of WT. Increase of oxidizing power for all three enzymes can be attributed to a much more facile reduction of the cofactor at lower pH due to a positively elevated electrostatic environment, as indicated by

the UV/visible spectra at different pHs (**Figure 3-3**). The WT and mutant spectra are much more similar at pH 5 as a result of red-shifted N485D spectrum. The potentials of the FAD cofactor are known to be susceptible to changes of protonation level because similar increases of redox potentials at lower pH was seen in glucose oxidase (this work and reference [**17**]) and flavin mononucleotide [**20**]. Although crystal structures of the WT enzyme obtained at pH 5 and 7 did not show significant differences [**21**], it is speculated that Asn485 could play a role in modulating the potentials of the cofactor.

Redox potentials of the enzymes display a dependency on pH by +30~60 mV per reduced pH unit. According to Stankovich et al.[**14**], when FAD's pKa1 < pH < pKa2, the reduction reaction is a two-electron, one-proton transfer which will have a 29 mV slope in the potential-pH dependence curve. This appears to be the case for WT ChoA which transfers a hydride at neutral pH and is supported by the titration data (**Table 3-4**). However, a positively charged amino acid side chain near the flavin could increase pKa1 of the cofactor and thus make pH < pKa1, which will result in a two-electron, two-proton reaction that is consistent with the behavior of N485D. The residue that promotes the pKa1 of flavin might not be Asp485, since a neutral residue such as Leu485 has a similar effect. It could be a residue that establishes interactions with the isoalloxazine ring as a result of active site disruption caused by Asn485 mutations.

The atomic resolution structure of N485D at pH 5.2 suggests a mechanism via which the isomerization reaction is impaired 60 fold by the mutation. Glu361 plays a role in the isomerization reaction by facilitating the transfer of hydrogen

from 4- position to the 6 position on the steroid moiety of cholesterol substrate.[**8**] Asp485 forms a strong hydrogen bond with conformer A of Glu361 in the mutant structure thus placing it away from its catalytic position over β plane of the substrate (**Figure 3-7**).

Overall, mutagenesis studies targeting the Asn485 residue in the WT enzyme has demonstrated its importance in contributing to both thermodynamic and kinetic competencies of the enzyme. Removing the NH•••π interaction by mutating Asn to either an Asp or Leu abolishes the catalysis by destabilizing the reduced cofactor, as supported by the more negative redox potentials observed in the mutants. Atomic resolution structures also reveal that decrease in catalytic efficiency is a result of mis-positioning of the Glu361 residue in the mutants. The Asp mutant displaying Asn-like activity at lower pH suggests that a carboxylic side chain could recover partial amide property when the protonation level in the environment elevates.

IV. References

1. I. J. Kass and N. S. Sampson, Evaluation of the role of His^{447} in the reaction catalyzed by cholesterol oxidase, *Biochemistry* **37** (1998), 17990-18000.
2. P. I. Lario, N. Sampson and A. Vrielink, Sub-atomic resolution crystal structure of cholesterol oxidase: what atomic resolution crystallography reveals about enzyme mechanism and the role of the FAD cofactor in redox activity, *J. Mol. Biol.* **326** (2003), no. 5, 1635-1650.
3. Q. K. Yue, I. J. Kass, N. S. Sampson and A. Vrielink, Crystal structure determination of cholesterol oxidase from Streptomyces and structural characterization of key active site mutants, *Biochemistry* **38** (1999), no. 14, 4277-4286.
4. Y. Yin, P. Liu, R. G. Anderson and N. S. Sampson, Construction of a catalytically inactive cholesterol oxidase mutant: investigation of the interplay between active site-residues glutamate 361 and histidine 447, *Arch. Biochem. Biophys.* **402** (2002), no. 2, 235-242.
5. N. S. Sampson and A. Vrielink, Cholesterol oxidases: a study of nature's approach to protein design, *Acc. Chem. Res.* **36** (2003), no. 9, 713-722.
6. N. S. Sampson and I. J. Kass, Isomerization, but not oxidation, is suppressed by a single point mutation, E361Q, in the reaction catalyzed by cholesterol oxidase, *J. Am. Chem. Soc.* **119** (1997), 855-862.
7. J. Li, A. Vrielink, P. Brick and D. M. Blow, Crystal structure of cholesterol oxidase complexed with a steroid substrate: implications for flavin adenine dinucleotide dependent alcohol oxidases, *Biochemistry* **32** (1993), 11507-11515.
8. I. J. Kass and N. S. Sampson, The importance of Glu^{361} position in the reaction catalyzed by cholesterol oxidase, *Bioorg. Med. Chem. Lett.* **8** (1998), 2663-2668.
9. I. J. Kass and N. S. Sampson, The isomerization catalyzed by *Brevibacterium sterolicum* cholesterol oxidase proceeds stereospecifically

with one base, *Biochem. Biophys. Res. Commun.* **206** (1995), 688-693.

10. L. Chen, A. Lyubimov, N. S. Sampson and A. Vrielink, Probing the role of asn485 in oxidation catalysis by mutagenesis and atomic resolution crystallography, *submitted* (2007).
11. Y. Yin, N. S. Sampson, A. Vrielink and P. I. Lario, The presence of a hydrogen bond between asparagine 485 and the pi system of FAD modulates the redox potential in the reaction catalyzed by cholesterol oxidase, *Biochemistry* **40** (2001), no. 46, 13779-13787.
12. M. Formaneck, Li, G., Zhang, X. and Cui, Q.,, Calculating accurate redox potentials in enzymes with a combined QM/MM free energy perturbation approach, *J. Theor. Comput. Chem.* **1** (2002), no. 53-67.
13. A. S. Donald T. Sawyer, Julian L. Roberts, Jr., Electrochemistry for chemists, *New York : Wiley, c1995.* **2nd ed.** (1995).
14. M. Stankovich, Bioelectrochemistry, *Encyclop. Electrochem.* **9** (2002), no. 15, 487-509.
15. L. H. Bradley and R. P. Swenson, Role of glutamate-59 hydrogen bonded to N(3)H of the flavin mononucleotide cofactor in the modulation of the redox potentials of the Clostridium beijerinckii flavodoxin. Glutamate-59 is not responsible for the pH dependency but contributes to the stabilization of the flavin semiquinone, *Biochemistry* **38** (1999), no. 38, 12377-12386.
16. J. D. Pellett, K. M. Sabaj, A. W. Stephens, A. F. Bell, J. Wu, P. J. Tonge and M. T. Stankovich, Medium-chain acyl-coenzyme A dehydrogenase bound to a product analogue, hexadienoyl-coenzyme A: effects on reduction potential, pK(a), and polarization, *Biochemistry* **39** (2000), no. 45, 13982-13992.
17. M. T. Stankovich, An anaerobic spectroelectrochemical cell for studying the spectral and redox properties of flavoproteins, *Anal. Biochem.* **109** (1980), no. 2, 295-308.
18. I. Kass, J. and N. S. Sampson, The importance of Glu^{361} position in the reaction catalyzed by cholesterol oxidase., *Bioorg. Med. Chem. Let.* **8** (1998), 2663-2668.

19. Y. Yin, N. S. Sampson, A. Vrielink and P. I. Lario, The presence of a hydrogen bond between asparagine 485 and the pi system of FAD modulates the redox potential in the reaction catalyzed by cholesterol oxidase, *Biochemistry* **40** (2001), no. 46, 13779-13787.
20. S. G. Mayhew, The effects of pH and semiquinone formation on the oxidation-reduction potentials of flavin mononucleotide. A reappraisal, *Eur. J. Biochem. / FEBS* **265** (1999), no. 2, 698-702.
21. A. Y. Lyubimov, P. I. Lario, Moustafa, I. and A. Vrielink, Atomic resolution crystallography reveals how changes in pH shape the protein microenvironment., *Nat. Chem. Biol.* **2** (2006), no. 5, 259-264.

Chapter 4

Experimental methods

I. Materials and methods

II. References

I. Materials and methods

Materials

Bovine serum albumin (BSA), cholesterol and dyes for redox titration experiments were purchased from Sigma (St. Louis, MO). Triton X-100 was purchased from Aldrich Fine Chemical Co., (Milwaukee, WI). Restriction endonucleases, T4 DNA ligase and calf intestinal alkaline phosphatase were purchased from New England Biolabs (Beverly, MA). Oligonucleotides were purchased from IDT, Inc. (Coralville, IA). All other chemicals and solvents, of reagent or HPLC grade, were supplied by Fisher Scientific (Pittsburgh, PA). Water for assays and chromatography was distilled, followed by passage through a Barnstead NANOpure filtration system.

Buffers and media

10X PBS: 137 mM NaCl, 4.3 mM Na_2HPO_4, 2.5 mM KCl, 1.4 mM KH_2PO_4 in ddi H_2O; 10x HEPES: 1.37 M NaCl, 0.06 M D(+) Glucose, 0.05 M KCl, 0.007 M $Na_2HPO_4 \cdot 7H_2O$, 0.2 M HEPES (pH 7.1); LB Media: 10 g tryptone, 5 g yeast extract, 5 g NaCl, 1 mL of 1 N NaOH in 1L of ddi H_2O; Buffer A: 50 mM sodium phosphate, pH 7.0; Buffer B: 50 mM sodium phosphate, pH7.0 • 2 mM $(NH_4)_2SO_4$.

General Methods

Restriction digests and ligations were performed according to procedures described below. The plasmids were purified with the Wizard Plus DNA Purification System (Promega, Madison, WI). A Shimadzu UV2101 PC Spectrophotometer was used for assays and acquisition of UV spectra. Fluorescence measurements were taken on a Spex Fluorolog 3-21

spectrofluorometer.

Construction of pCO300 and other mutant expression plasmids

A 214 base oligonucleotide was made by PCR using 2 primers. Primer 1 contained the designated mutation site and a *Stu*I site (5'-ggCTggggCCCCAACggTAACATCATgACCgCCCgggC CAACCACATgTggAACCCCACCggCgCCC-3'). Primer 2 corresponded to the anticoding strand and contained a *Hin*dIII site (5'-gCTCACAAgCTTACgACgCCgTgACgTCCTgCTTgATgA TgCgCTCgACgTTCCgCTCggCCAgCgCCgTgATggTCACgAACgggAggACgCCg ACgg-3'). With these 2 primers and using *Xho*I-restricted pCO202 [1] as a template, 35 cycles of PCR were performed with iProof polymerase (Bio-Rad Laboratories, Hercules, CA) at an annealing temperature of 72 °C. The PCR fragment was digested with *Stu*I and *Hin*dIII, purified, and subcloned into pCO200 [1] that had been similarly digested to yield the N485D ChoA mutant expression plasmid pCO300. Other mutants, pCO301 (M122V), pCO302 (G347N) and pCO303 (F359W) were prepared in a similar fashion with the following primers and restriction sites used: pCO301, 5'-gCCAgTgAATTCgAgCTCggTACCCggggACCCCgAgCTT-3' (SacI) and 5'-CCTCgAAgTACgAgCgCTTgggCTCCACggCAACgCCgCCgTTgACgAgCgA-3' (AfeI); pCO302, 5'-ggAACCCCACCggCgCCCACCAgTCCTCCATCCCCgCCCTCAATATCgACgCg TgggAC-3' (SgrAI) and 5'-GCTCACAATTCCACACAA-3' (HindIII); pCO303, 5'-CggCATCgACgCgTgggACAACAgCgACTCCTCggTCTgggCggAgATCgCCCCCA

TgCC-3' (MluI) and 5'-gCTCACAATTCCACACAA-3' (HindIII). For pCO304 (V189M), site-directed mutagenesis was carried out according to the QuickChange protocol from Strategene (La Jolla, CA). Basically, 2 complimentary primers, 5'-ACgTTggggACgAACATggTgCCgAgACCg-3' and 5'-CggTCTCggCACCATgTTCgTCCCCAACgT-3', each carrying the mutation site, were used to PCR the pCO200 template. Then the PCR fragments were digested with DpnI, and transformed into XL1-Blue competent cells for plasmid preparation. Sequencing of these clones was conducted at the Stony Brook sequencing facility using an ABI 3730 Genetic Analyzer (Applied Biosystems, Foster City, CA).

Protein purification of wt and mutant cholesterol oxidases

Cell paste of E. coli BL21(DE3)plysS was obtained from 1 L of 2 x YT-ampicillin (200 µg/mL) medium grown at 28 ºC for 10 h after addition of IPTG (100 µg/mL) at A_{600} = 0.6 by centrifugation at 4,000 g for 30 min. The pellet was resuspended in buffer A and lysed by French press at 18,000 psi. All subsequent steps were conducted at 4 °C. Cell debris was removed by centrifugation at 135,000 g for 60 min. The supernatant was precipitated with 1.0 M $(NH_4)_2SO_4$ and the pellet was discarded. $(NH_4)_2SO_4$ was added to the supernatant to a final concentration of 2 M. The pellet was obtained by centrifugation at 4,000 g. This pellet was resuspended in buffer A (5 mL) and desalted using dialysis (nMWCO 6,000-8,000) against buffer A. The dialysate was loaded onto a column of DEAE-cellulose (30 mm x 25 cm, DE-52, Whatman) preequilibrated with buffer A. Fractions were collected by elution with buffer A

(100 mL). Fractions containing cholesterol oxidase (as determined by SDS-PAGE) were combined and concentrated by $(NH_4)_2SO_4$ precipitation (3.0 M). The pellet was redissolved in buffer A to give a final concentration between 10 to 20 mg/mL of protein and it was further purified on a butyl-Sepharose column (30 mL butyl-Sepharose-4 Fast Flow, XK 16/40, Pharmacia Biotech, Upsala, Sweden) preequilibrated with buffer B. The protein was eluted by running a linear gradient from 75% buffer B to 100% buffer A (160 mL). Fractions (4 mL) were collected and the elution profile was monitored at A_{280}. Fractions were assayed for content and purity by SDS-PAGE. Fractions containing pure cholesterol oxidase (>98%) were combined and ultrafiltered (YM30 membrane) into buffer A.

UV and fluorescence steady-state kinetic assays of WT and mutant cholesterol oxidases

Solutions of cholesterol oxidase were prepared in buffer A. For steady-state enzyme kinetics, the initial velocities of WT and mutant cholesterol oxidases were measured in the following way. The formation of conjugated enone was followed as a function of time at 240 nm (ε_{240} =12,100 M^{-1} cm^{-1}). Triton X-100 was added to buffer A to a final concentration of 0.025% (w/v) along with 0.01% (w/v) BSA. The detergent micelles were allowed to form at 37 °C for 10 min, cholesterol was added and the solution was equilibrated for 10 min. The reaction was initiated by adding cholesterol oxidase (WT or mutant). Independent sets of data were fit simultaneously to the hyperbolic form of the Michaelis-Menten equation using Kaleidagraph (Synergy Software, Reading, PA).

Steady-state two-substrate kinetics

The UV A_{240} assay was used except that the assay solution (sodium phosphate, Triton X-100, BSA, cholesterol and isopropanol) was saturated with different concentrations of oxygen. Mixtures of oxygen and nitrogen at different ratios were generated using a two gas mixer (Aalborg Corporation, Orangeburg, NY) and the concentration of oxygen. The assay solution was pumped under vacuum and purged with the appropriate gas mixture every 10 min over a period of 2 h. The oxygen concentration in the assay buffer was monitored using an oxygen meter (YSI model 53, Yellow Springs Instruments, Yellow Springs, Ohio). The oxygen meter was calibrated using the NADH/catalase system where 2 equivalents of NADH (concentration known) corresponded to one equivalent of oxygen. (**Scheme 4-1**)

$$2NADH + O_2 \xrightarrow{\text{catalase}} 2NAD^+ + H_2O_2$$

Scheme 4-1 Calibration of the oxygen meter

Redox potential measurements

Potentiometric titrations were performed to determine the midpoint potential of wild-type and mutant cholesterol oxidases. A spectralelectrochemical cell was made by Tom Stefanek from the glass technology service of University of Minnesota. Methyl viologen (100 μM) was used as the mediator dye to transfer electrons from the electrode to the protein and the redox indicator dye (**Figure 4-**

1). For wild-type cholesterol oxidase (~30 μM), indigo disulfonate and cresyl violet were used as redox indicator dyes. For N485D and N485L mutant cholesterol oxidases (~30 μM), phenosafranin was used. Before each titration, the enzyme solutions (in 50 mM sodium phosphate, pH 7.0) underwent 12 cycles of pumping under vacuum and argon purging over 2 h to reach anaerobic conditions. Then the electrodes (working, auxiliary and reference electrodes) were inserted into the spectroelectrochemical cell under positive argon pressure and the titration was initiated by adding electrons from a potentiostat (Model 800B, CH Instruments, Austin, TX). After each addition of electrons, the system was allowed to equilibrate at 25°C for 30 min then a spectrum was recorded as well as the potential (**Figure 4-2**). The redox indicator dye was titrated under the same condition as the enzyme and their spectra were subtracted to obtain the spectra of enzyme alone. The concentrations of all species of the enzyme were calculated from the spectra and their molar absorptivities, and were plotted versus the equilibrium potential of the system using **Equation 4-1**. The potential of the enzyme, $E^{\circ\prime}_{enzyme}$, equaled to the value of the Y intercept.

$$E_{cell} = E^{\circ\prime}_{enzyme} + 0.059 \log [ox/red] \qquad \textbf{Equation 4-1}$$

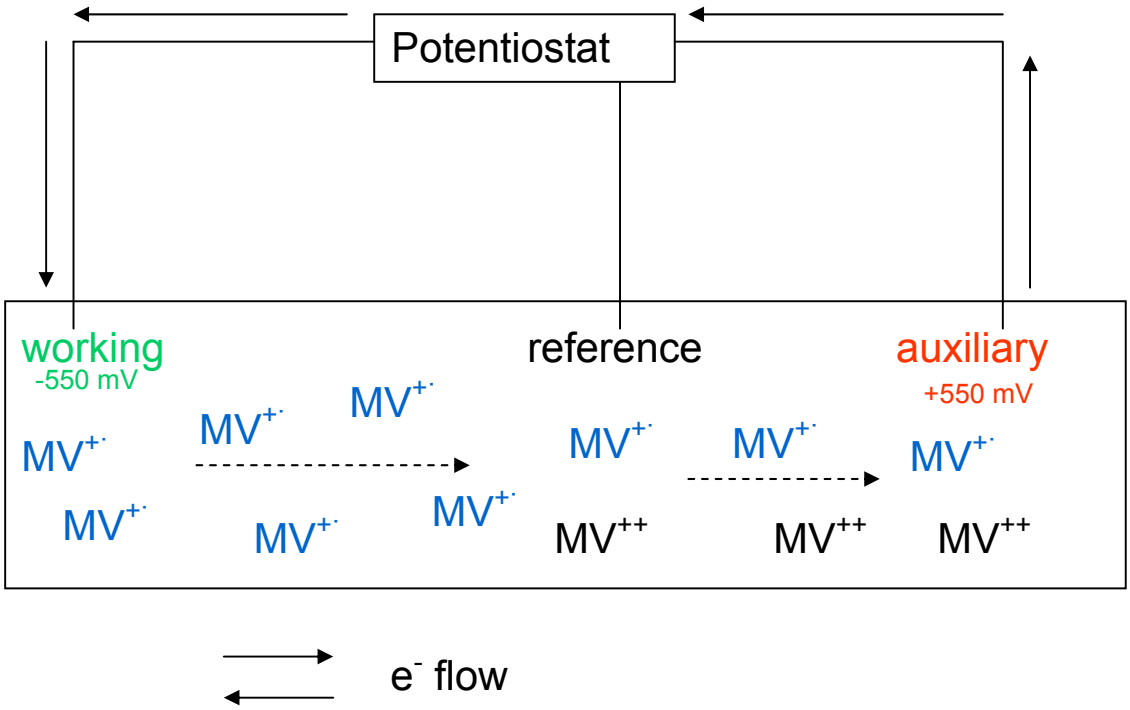

Figure 4-1 Electron flow in the spectraelectrochemical cell.

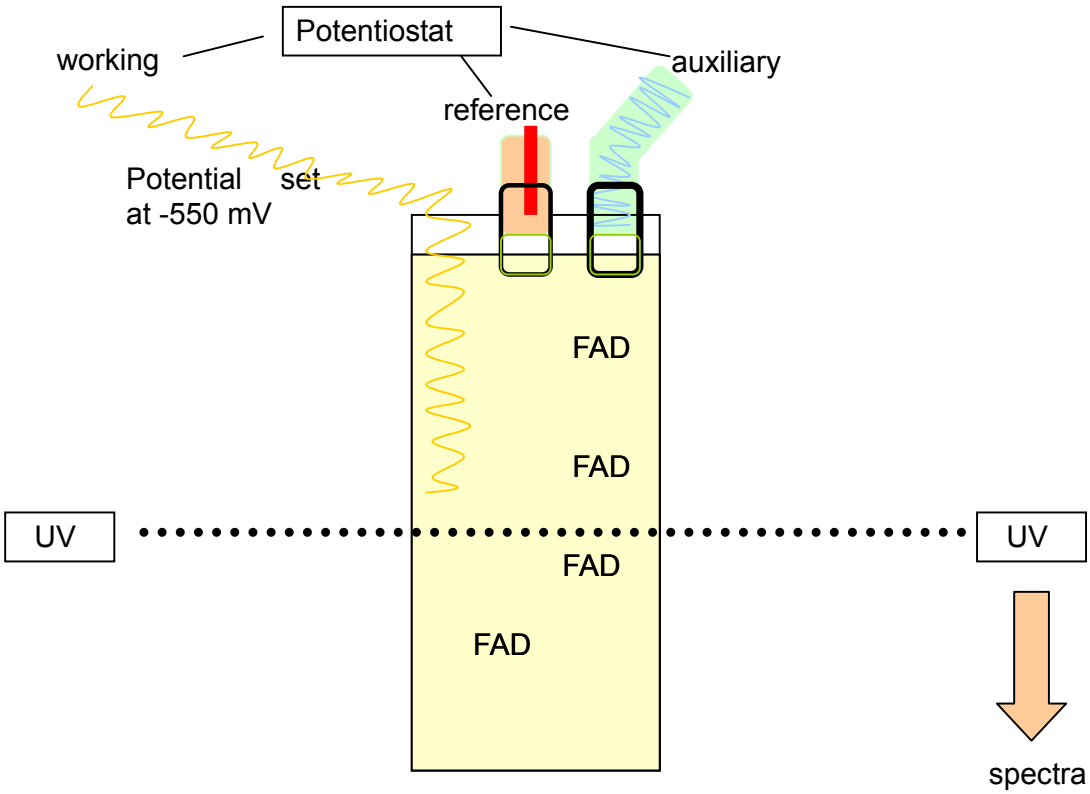

Figure 4-2 Illustration of a typical titration.

II. References

1. I.J. Kass, and N.S. Sampson, The importance of Glu^{361} position in the reaction catalyzed by cholesterol oxidase. *Bioorg. Med. Chem. Lett.*, 1998. **8**: p. 2663-2668.
2. Q.K. Yue, et al., Crystal Structure Determination of Cholesterol Oxidase from *Streptomyces* and Structural Characterization of Key Active Site Mutants. *Biochemistry*, 1999. **38**: p. 4277-4286.
3. Z. Otwinowski and W. Minor, *Processing of X-Ray Diffraction Data Collected in Oscillation Mode.*, in *Meth. Enz.*, C.W.J. Carter and R.M. Sweet, Editors. 1997, Academic Press: Boston. p. 307-325.
4. G.N. Murshudov, A.A. Vagin, and E.J. Dodson, Refinement of macromolecular structures by the maximum-likelihood method. *Acta Cryst. Sec. D-Biol. Cryst.*, 1997. **53**: p. 240-255.
5. P. Emsley and K. Cowtan, Coot: model-building tools for molecular graphics. *Acta Cryst. D Biol. Cryst.*, 2004. **60**(Pt 12 Pt 1): p. 2126-32.
6. G.M. Sheldrick and T.R. Schneider, *SHELXL: High-resolution refinement*, in *Meth. Enz.*, C.W.J. Carter and R.M. Sweet, Editors. 1997, Academic Press: Boston. p. 319-343.
7. A.A. Vaguine, J. Richelle, and S.J. Wodak, SFCHECK: a unified set of procedures for evaluating the quality of macromolecular structure-factor data and their agreement with the atomic model. *Acta Cryst. D Biol. Cryst.*, 1999. **55 (Pt 1)**: p. 191-205.
8. R.A. Laskowski et al., PROCHECK: A program to check the stereochemical quality of protein structures. *J. App. Cryst.*, 1993. **26**: p. 283-291.
9. Collaborative Computational Project, N., The CCP4 suite: programs for protein crystallography. *Acta Cryst. D*, 1994. **50**: p. 760-763.
10. J.A. Christopher, SPOCK: The Structural Properties Observation and Calculation Kit (Program Manual). in *Center for Macromol. Design*. 1998, Texas A&M University: College Station.
11. P. Kraulis, MOLSCRIPT: A program to produce both detailed and

schematic plots of protein structures. *J. Appl. Crystallogr.*, 1991. **24**: p. 946-950.

12. E.A. Merritt, and D.J. Bacon, Raster3D: Photorealistic Molecular Graphics, in *Meth. Enz., B*, J. Carter, C.W. and R.M. Sweet, Editors. 1997, Academic Press: New York. p. 505-525.
13. W.L. DeLano, The PyMOL Molecular Graphics System. 2002, DeLano Scientific: San Carlos, CA, USA.
14. H.M. Berman, et al., The Protein Data Bank. *Nuc. Acids Res.*, 2000. **28**: p. 235-242.

Appendix

I. Procedures for titrations to determine redox potentials
II. Plasmid map for cloning variant cholesterol oxidases
III. Pairwise sequence alignments of WT ChoA with other GMC oxidoreductases

I. Procedures for titrations to determine redox potentials

-from reference [**1**] and more recently, [**2**] with minor adjustments

Part 1 Materials preparation

1.1 Mediator titrant and redox indicators

Generally methyl viologen (MV^{++} Fisher, AC22732-0010) is used as the mediator. The concentration is 100 μM. A 5 mM stock solution is recommended.
Indigo disulfonate (I2S, Sigma, 34172-166), indigo tetrasulfonate (I4S, sigma, 340596), cresyl violet (CV, sigma C-1791), phenosafranin (PSR, sigma 199648), 2-amino-1,4-naphthoquinone (ANQ, sigma R238597) and riboflavin (sigma R-4500) are the redox indicator dyes used in the potentiometric titrations. The concentration ranges from 2-10 μM depending on the ε of the dye (dye's absorbance at λmax should not be too far away from that of the enzyme)

1.2 Glassware and argon line

Contact Tom Stefanek from the glass technology service of University of Minnesota for all glasswares related to the titrations. Three "main bodies" are needed: titration cuvette, storage cell and calibration cell. The later two are essentially identical in appearance. Numerous joints and caps are accompanied, they are listed in the illustrations attached. The argon line was setup according to Fig.2 of reference [**2**] and a scanned image is also attached in this protocol. The gas purifier can be purchased from Fisher (10-594A).

1.3 Accessories

Fine gold and silver wires can be purchased from W.E. Mowrey company (651-646-1895), gauge size 24. A solder set (gun and wire, diameter 1/8") as well as copper wire (gauge 16) and epoxy are from local ACE hardware store or home depot. Teflon shrink tubing (MF-2027) and vycor tips (MF-2064) are bought from Bioanalytial systems, Inc. Syringe tubing is from Fisher (427406). Instead of regular grease, Apiezon type N high-vacuum grease should be used (fisher 14-638-15D) A glass stirring bar is optional. Peel off the Teflon layer of a normal stirring bar, take the magnet inside. Then melt a glass Pasteur pipette and seal the magnet with glass. Make sure there is no leak – this is tricky because otherwise there will be electron leaking into the metal during titrations. (I don't seem to be able to seal it completely so the glass stiring bar is not used in my experiments)

1.4 Instruments

A UV-vis spectrometer and a potentiostat (CHI instruments, model 800B) are needed.

Part 2 Making Electrodes

2.1 Working electrode

Solder a straight gold wire with a bent copper wire, let cool and then epoxied into the glass joint. Be sure to cover the solder (no metal should be exposed) and not letting the epoxy fall into the chamber below the glass joint. As seen in Figure 1:

Figure 1

The epoxy takes 24 hr to fully solidify after which time the gold wire can be curved using appropriate size of copper wire, needle, etc. by winding the gold wire around it.

2.2 Reference electrode

The tips of the reference and auxiliary electrodes are made by assembling the vycor (treated by boiling in first 30% H_2O_2 for 3-4 h and then water, until the glass goes clear before use) with the heat-shrinking tubing, and then blow with a heat fan until the tubing stops shrinking or the vycor turns turbid-white. See Figure 2.

Figure 2

Make the cap of the reference electrode in a way similar to the working electrode, but use silver wire instead. Then dip the silver wire in HCl:HNO3 (3:1) solution repeatedly until the color of the wire stops changing or no bubbles appears. Now inject into the electrode 0.1 M KCl solution saturated with AgCl (degassed). The syringe is made as shown in Figure 3 (tubing is from Clay Adams, Parsipanny, NJ, polyethylene PE-20).

Figure 3

Now grease the joints and insert the cap into the solution-filled electrode sleeve, tighten with rubber bands (Figure 4).

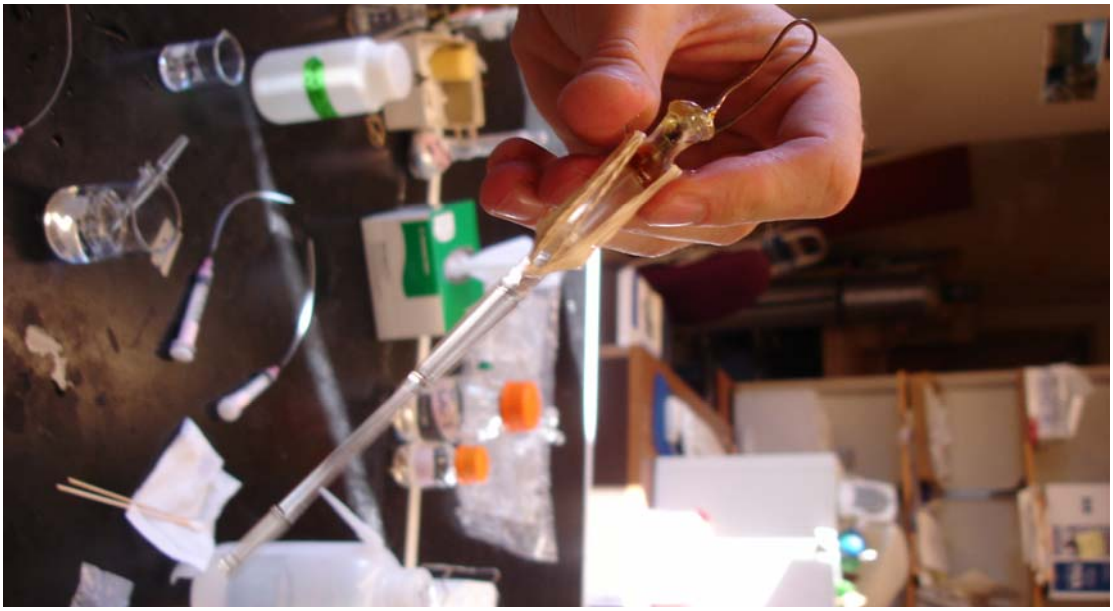

Figure 4

2.3 Auxiliary electrode

Auxiliary electrode is made in the same way as reference electrode except that 1) the silver wire is NOT treated in the acid mixture 2) curve the silver wire 3) the solution is NOT saturated with AgCl.

Part 3 Titrations and data analysis

3.1 Preparations

One day before titrations all electrodes should be placed in the storage cells (filled with 1 mM MV). The MV solution should be degassed by applying a straight vacuum and then filled with argon. Under positive pressure of argon, insert 3 electrodes. Add electrons at -550 mV until the solution turns blue. Leave it o/n to make sure the electrodes are in a reducing environment.
Blank the UV with buffer only, then take an initial scan of the enzyme only. If it is a potentiometric measurement, add the dye and scan again. Otherwise seal the cuvette with caps and take it for degassing. Lean the cuvette to increase the solution's contact with the gas phase. Open the vacuum gently until gas bubbles are emerging out of the solution. Then close vacuum, turn on argon line gently so that no solution will be disturbed but just bubbles will disappear. Then leave it under argon for 10 min. Repeat 12 times. Invert the cuvette briefly to mix between each flushing.
Leave the argon on and open the cap for auxiliary electrode (make sure there is still positive pressure by checking whether the bubbler is bulbbing). Insert the auxiliary electrode and do the reference and working electrodes (should extend all the way to the bottom of the cuvette) in the same way. Tighten everything with rubber bands. (Figure 5)

Figure 5

3.2 Coulometric titration

Set potential at -550 mV (-825 mV on the potentiostat because the reference is ~+275 mV) and start adding electron to the enzyme. Amount of electrons added will be recorded by the potentiostat. After the desire amount of electrons are added, release the potential and shake the cuvette to mix. Wait until absorbance stops changing (normally takes 30-40 min) and then take a spectrum. Repeat until the enzyme is reduced completely. Note that 3-5 mCu of electrons will be consumed to reduce the trace amount of oxygen even after degassing.
According to the Faraday constant, 10 μM enzyme will require 10.6 mCu electrons in a two-electron reduction (5.5 mL volume). The enzyme concentration can thus be calculated from the amount of electrons added. ε at different wavelengths can

also be obtained in the following ways:

1) ε of ox and red can be readily calculated from the spectra but % semiquinone will be needed for calculation of semiquinone ε
2) make a plot of A370 vs. n, e.g. figure 6
3) make linear curves out of two limbs of the curve and identify intermediate points (pink). Two lines intercept at 100% semiquinone. εseq.370 can be obtained. εseq.390 can be calculated similarly.
4) calculate [ox], [seq] and [red], subsequently % seq and εseq.470, εseq.500 at each pink point and average

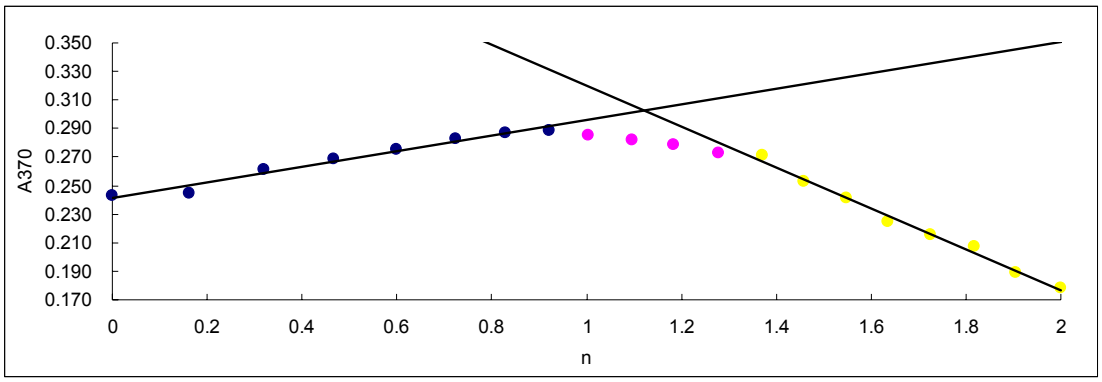

Figure 6

3.3 Potentiometric titration

The potentiometric titration follows the same procedure as coulometric titration, except that

1) add dye to the enzyme before degassing
2) it might or might not takes longer time to equilibrate between each addition of electrons. Again, monitor the absorbances until constant.
3) Potentials are recorded (on the software menu, control -> open circuit potential) after each reduction.

Then the ox, seq and red at each titration are calculated using corresponding ε. Nernst plots are drawn based on the potentials recorded at each titration.

3.4 After titration

The volume and pH of the titration mixture must be recorded. The potential of the reference electrode is checked after every titration by the following method:

1) in 50 mL H_2O, add 871 mg K_3PO_4, 27 mg $K_3[Fe(CN)_6]$ and 35 mg $K_4[Fe(CN)_6]$, adjust to pH 7.0 w/ 1N HCl, transfer to calibration cell
2) Vacuum briefly and then fill w/ N_2, let it flow over the solution for 5 min
3) Insert electrodes and incubate w/ solution at 40 °C for 10 min, protect from light at all times
4) Measure the potential, it should be around +150 mV (the reference electrode is 150 mV more negative than the +425 mV ferri/ferro cyanide)

Part 4 Maintenance

Once made, the reference electrode needs to be re-made about once per year. Solution in the auxiliary electrode need to be re-filled with fresh, degassed KCl before every experiment. Constantly check the metal wires for any grease build up and if that's the case, clean with cyclohexane. Check the epoxy of every electrode from time to time and make sure there is no leakage.

References:

1. M. T. Stankovich, An anaerobic spectroelectrochemical cell for studying the spectral and redox properties of flavoproteins, *Anal. Biochem.* **109** (1980), no. 2, 295-308.
2. M. Stankovich, Bioelectrochemistry, *Encyclopedia of Electrochemistry* **9** (2002), no. 15, 487-509.

Attached: Glassware joint sizes and argon line illustration

UNIVERSITY OF MINNESOTA
GLASS TECHNOLOGY SERVICES

PRINT NO _____ DATE FILED _____
JOB ORDER NO _____ DATE _____
DEPARTMENT _____ BUDGET NO _____
NAME _____ PHONE NO. _____

Please make drawing on space below

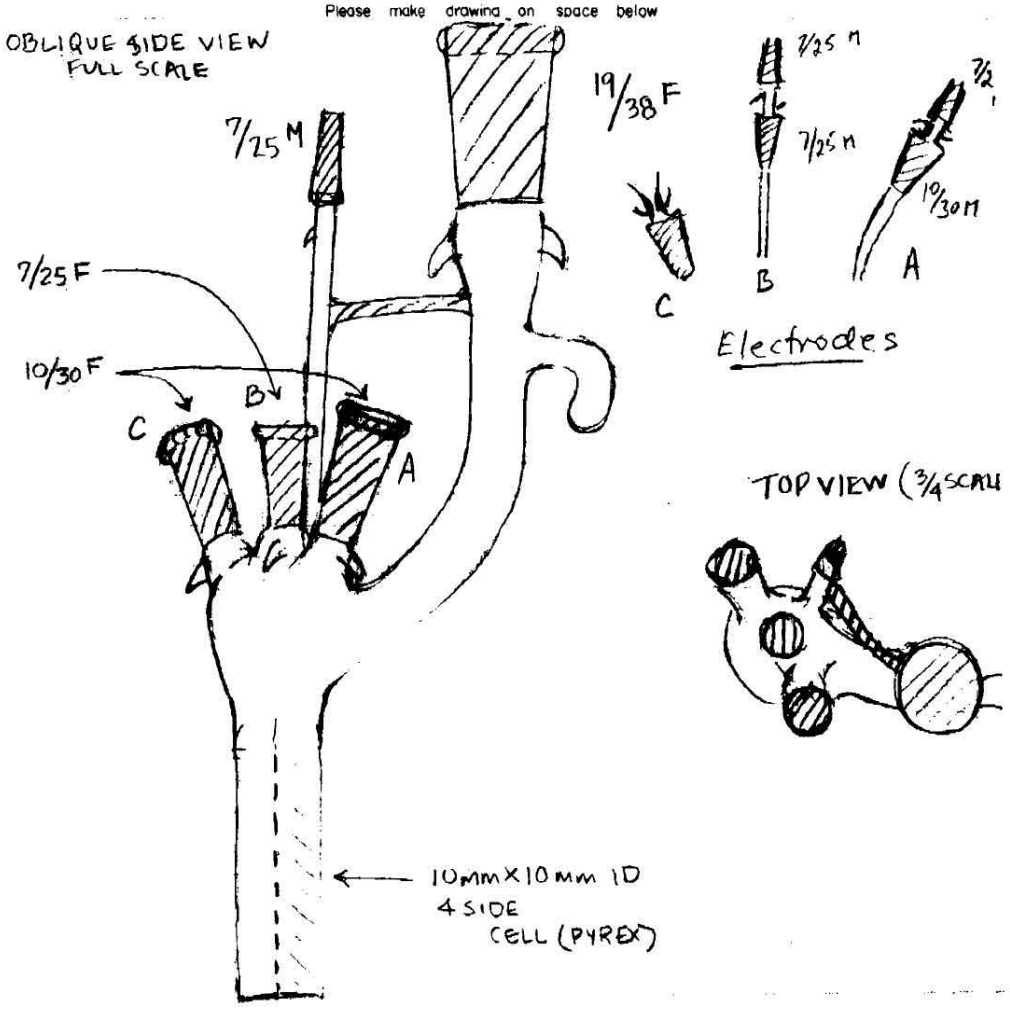

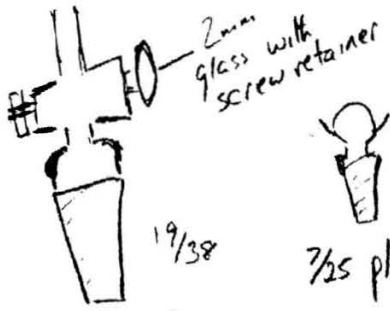

stopcock - 19/38 M

I make the glass components only. The wires etc that are attached are done by the customer.

CHEMISTRY GLASS SHOP

UNIVERSITY OF MINNESOTA
BUS ADM FORM 998

ACCOUNT NO. - F/D/B	CLAIM NO.
DEPARTMENT NAME: Chemistry Stony Brook University	
NAME: [illegible]	PHONE: 632-7953
DESCRIPTION: Storage cell + electrode.	DATE REC'D / BY

optical electrochemical cell & electrodes
as per attached diagrams & table. Also please make
2 storage cells that will fit 1 electrode.

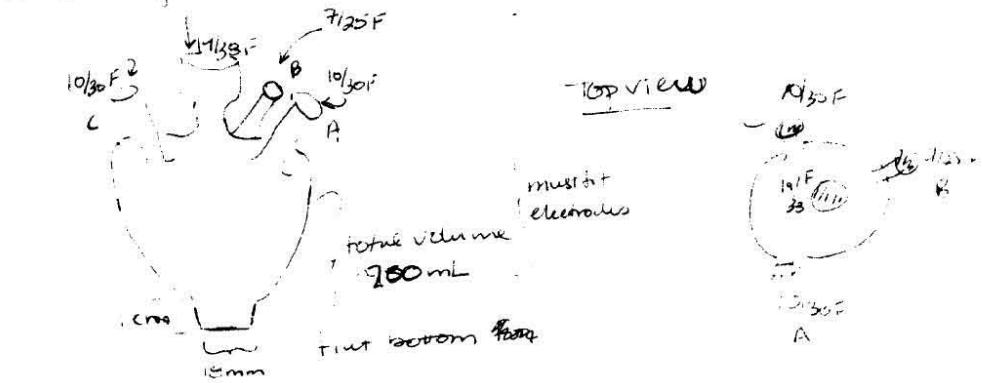

Quantity	Code	Description	Dollar	Date	Time	By

Date Completed_____

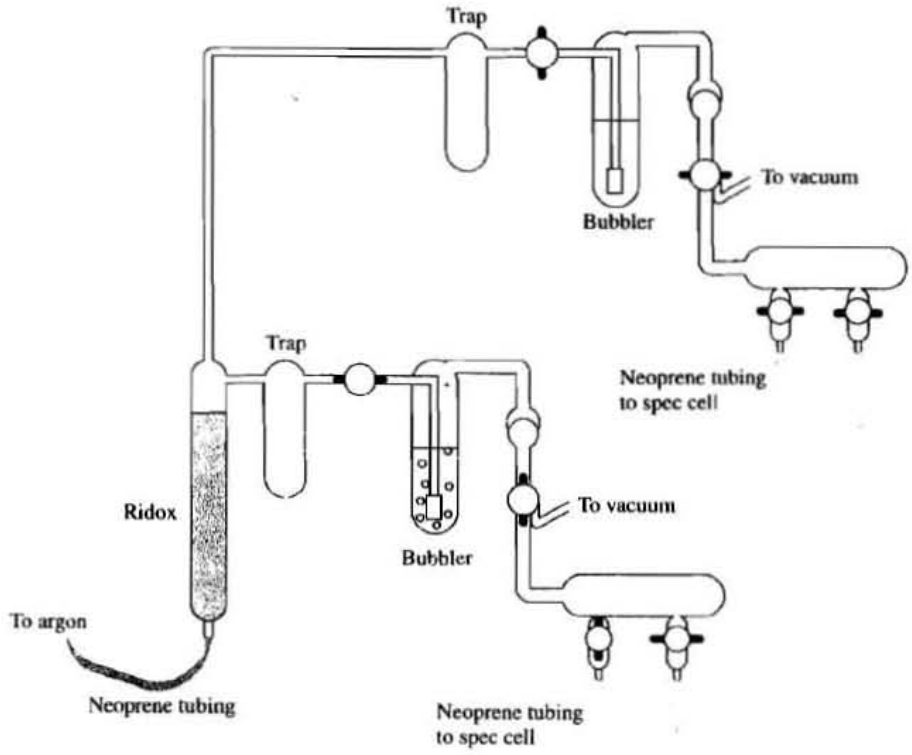

Fig. 2 Argon line.

II. Plasmid map for cloning variant cholesterol oxidases

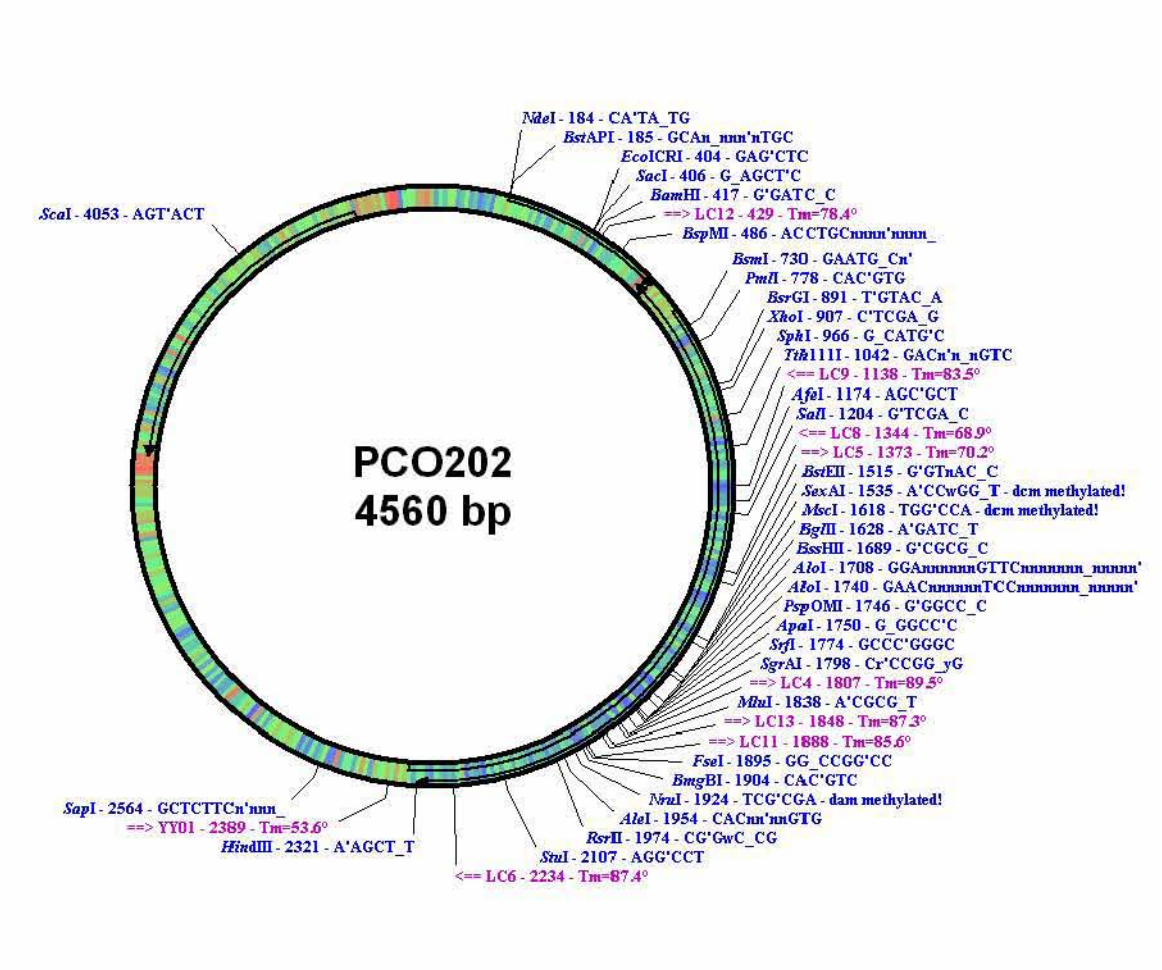

III. Pairwise sequence alignments of WT ChoA with other GMC oxidoreductases

1. ChoA and cellobiose dehydrogenase from *Phanerochaete chrysosporium*

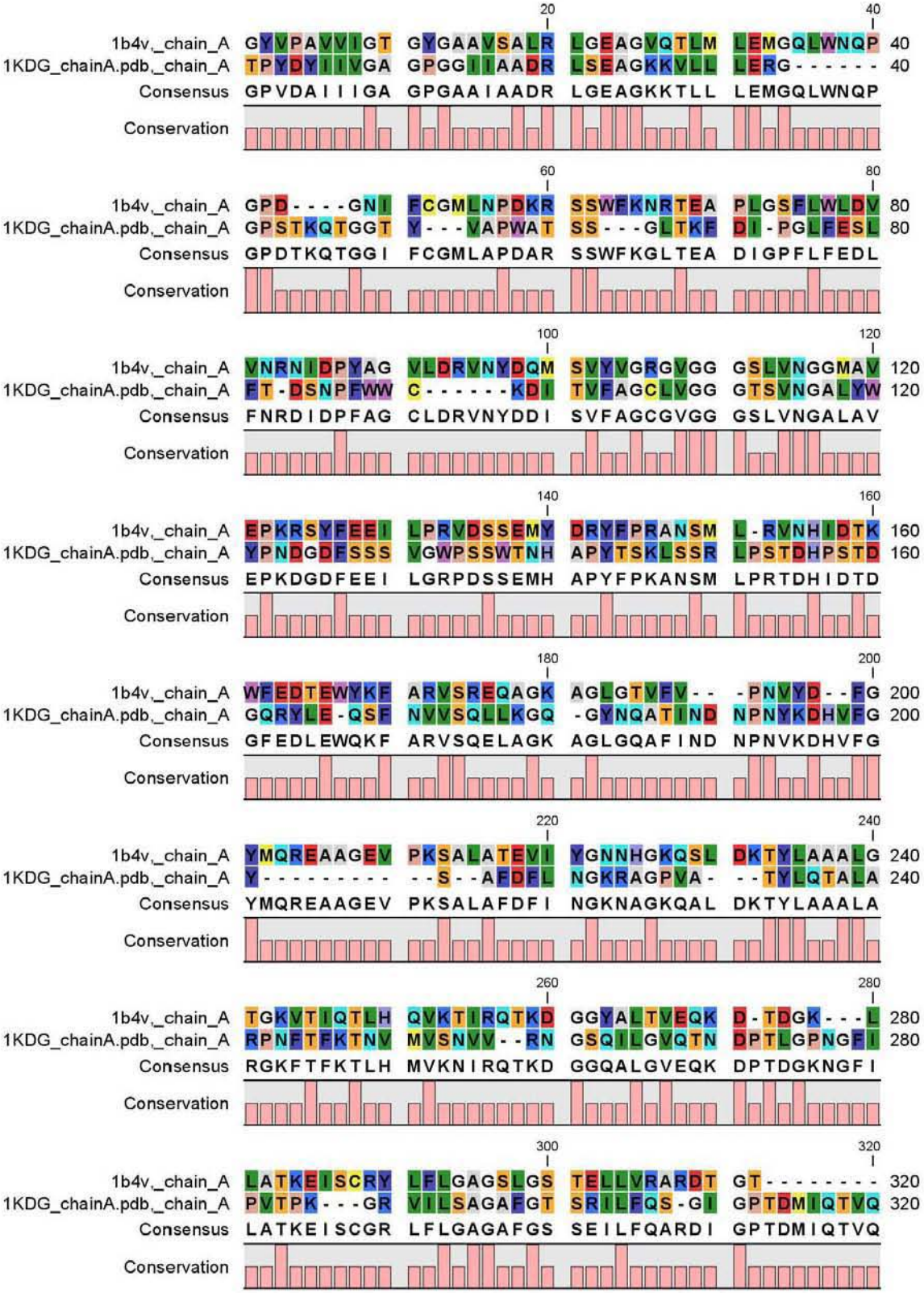

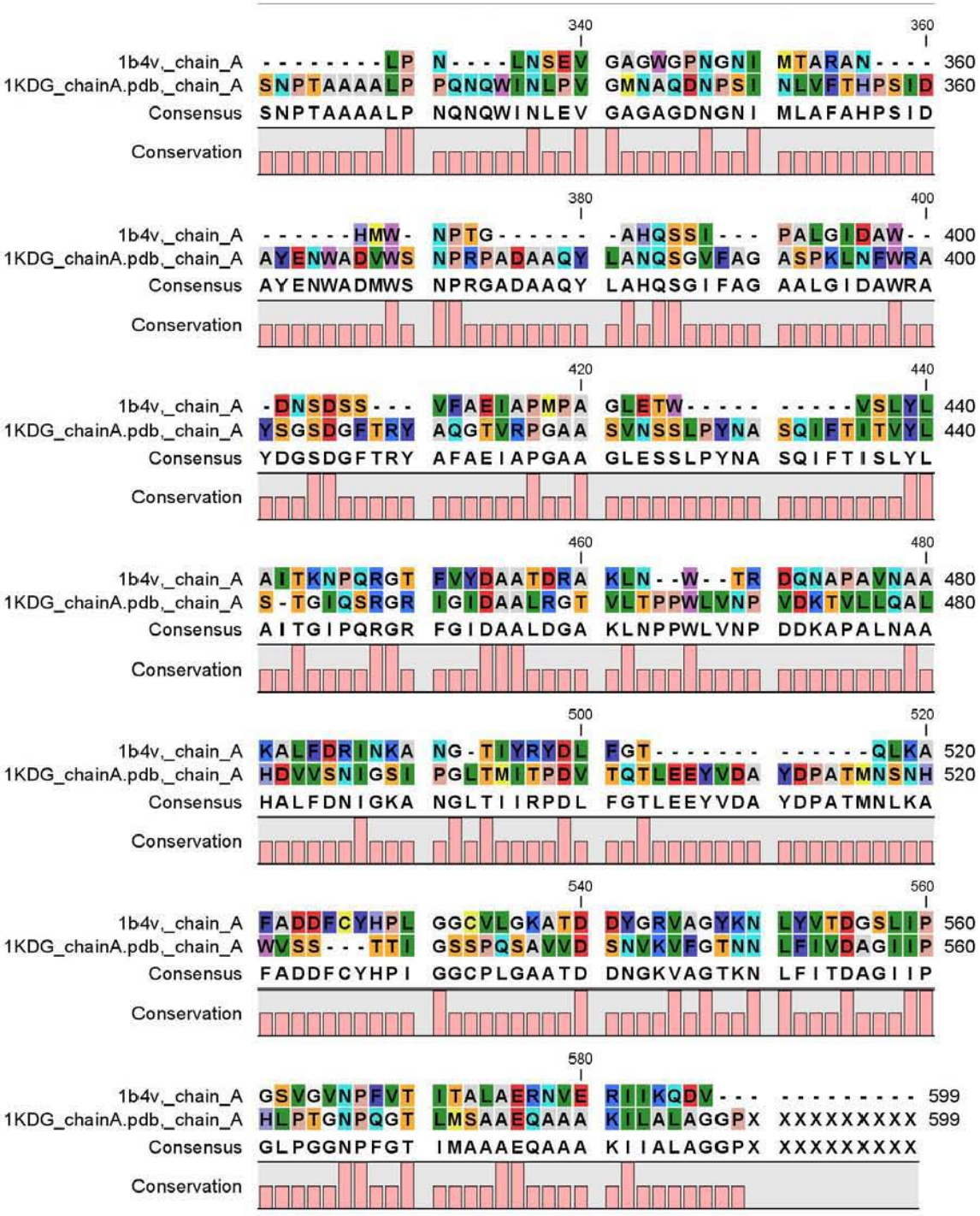
340
360
1b4v,_chain_A - - - - - - - - LP N - - - - LNSEV GAGWGPNGNI MTARAN - - - - 360
1KDG_chainA.pdb,_chain_A SNPTAAAAALP PQNQWINLPV GMNAQDNPSI NLVFTHPSID 360
Consensus SNPTAAAALP NQNQWINLEV GAGAGDNGNI MLAFAHPSID
Conservation
380
400
1b4v,_chain_A - - - - - - HMW - NPTG - - - - - - - AHQSSI - - - PALGIDAW - - 400
1KDG_chainA.pdb,_chain_A AYENWADVWS NPRPADAAQY LANQSGVFAG ASPKLNFWRA 400
Consensus AYENWADMWS NPRGADAAQY LAHQSGIFAG AALGIDAWRA
Conservation
420
440
1b4v,_chain_A - DNSDSS - - - VFAEIAPMPA GLETW - - - - - - - - - - VSLYL 440
1KDG_chainA.pdb,_chain_A YSGSDGFTRY AQGTVRPGAA SVNSSLPYNA SQIFTITVYL 440
Consensus YDGSDGFTRY AFAEIAPGAA GLESSLPYNA SQIFTISLYL
Conservation
460
480
1b4v,_chain_A AITKNPQRGT FVYDAATDRA KLN - - W - - TR DQNAPAVNAA 480
1KDG_chainA.pdb,_chain_A S - TGIQSRGR IGIDAALRGT VLTPPWLVNP VDKTVLLQAL 480
Consensus AITGIPQRGR FGIDAALDGA KLNPPWLVNP DDKAPALNAA
Conservation
500
520
1b4v,_chain_A KALFDRINKA NG - TIYRYDL FGT - - - - - - - - - - - - QLKA 520
1KDG_chainA.pdb,_chain_A HDVVSNIGSI PGLTMITPDV TQTLEEEYVDA YDPATMNSNH 520
Consensus HALFDNIGKA NGLTIIRPDL FGTLEEYVDA YDPATMNLKA
Conservation
540
560
1b4v,_chain_A FADDFCYHPL GGCVLGKATD DYGRVAGYKN LYVTDGSLIP 560
1KDG_chainA.pdb,_chain_A WVSS - - - TTI GSSPQSAVVD SNVKVFGTNN LFIVDAGIIP 560
Consensus FADDFCYHPI GGCPLGAATD DNGKVAGTKN LFITDAGIIP
Conservation
580
1b4v,_chain_A GSVGVNPFVT ITALAERNVE RIIKQDV - - - - - - - - - - 599
1KDG_chainA.pdb,_chain_A HLPTGNPQGT LMSAAEQAAA KILALAGGPX XXXXXXXXX 599
Consensus GLPGGNPFGT IMAAAEQAAA KIIALAGGPX XXXXXXXXX
Conservation

2. ChoA and D-amino acid oxidase from *Homo sapiens*

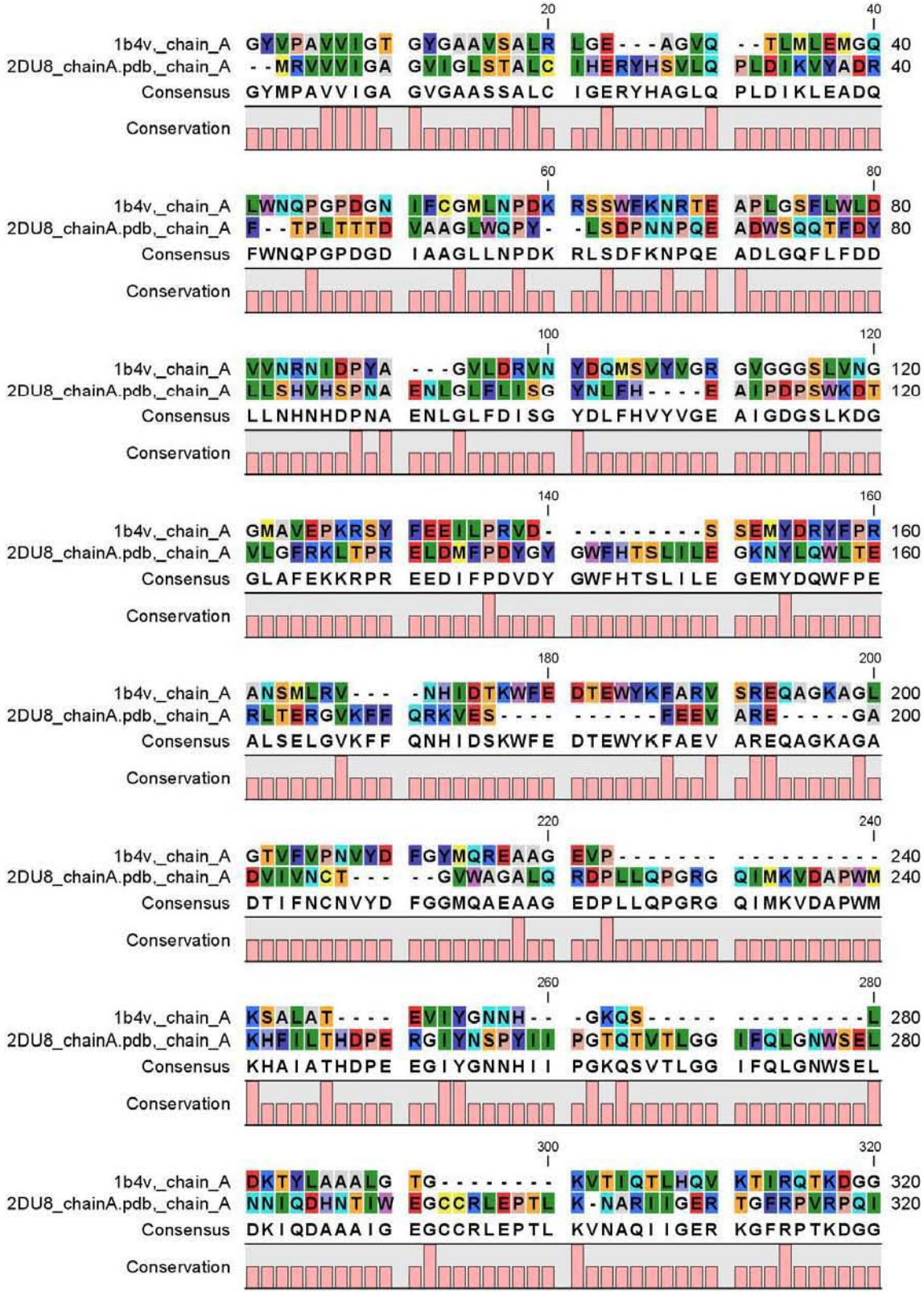

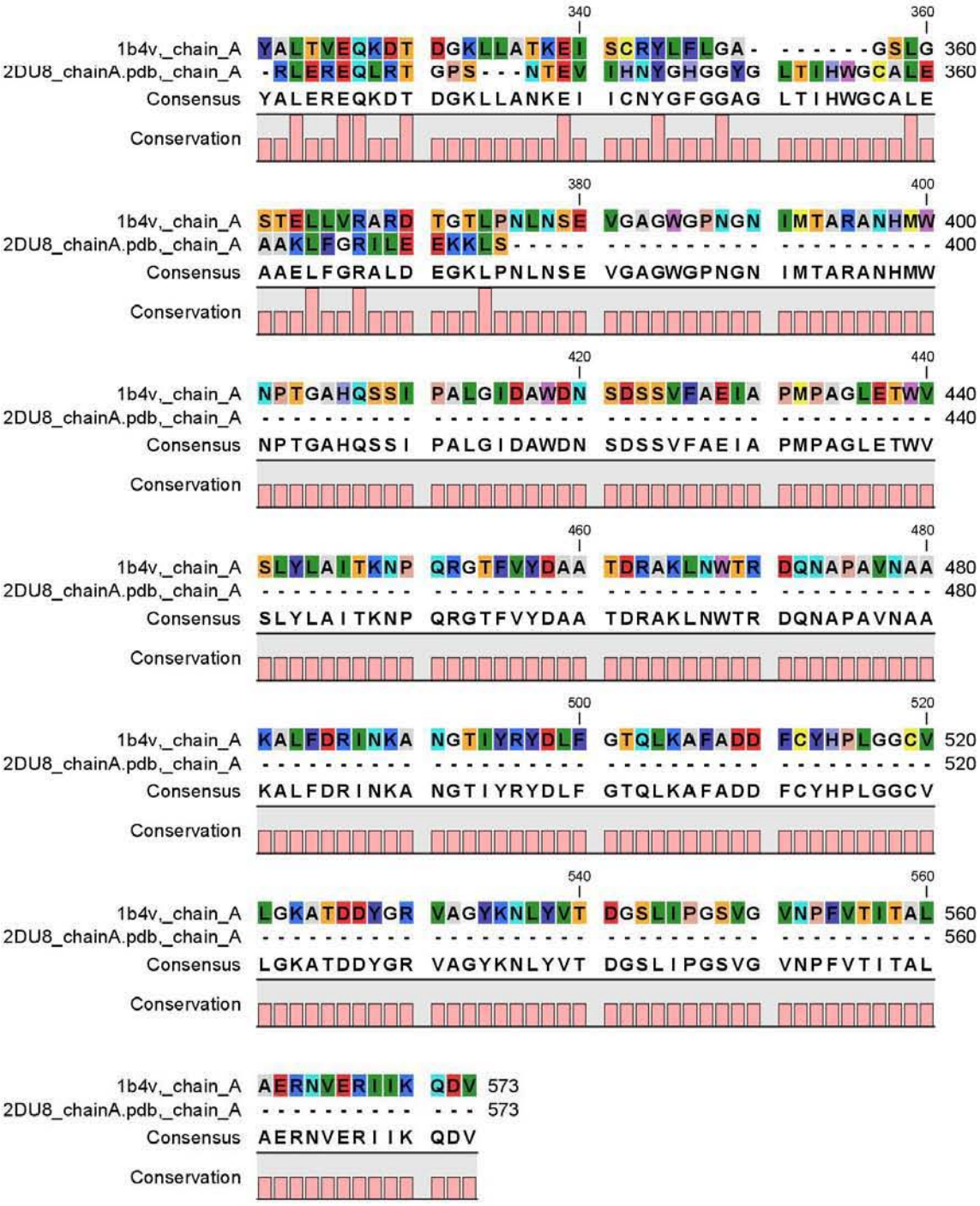
340
360
1b4v,_chain_A YALTVEQKDT DGKLLATKEI SCRYLFLGA- ------GSLG 360
2DU8_chainA.pdb,_chain_A -RLEREQLRT GPS---NTEV IHNYGHGGYG LTIHWGCALE 360
Consensus YALEREQKDT DGKLLANKEI ICNYGFGGAG LTIHWGCALE
Conservation
380
400
1b4v,_chain_A STELLVRARD TGTLPNLNSE VGAGWGPNGN IMTARANHMW 400
2DU8_chainA.pdb,_chain_A AAKLFGRILE EKKLS----- ---------- ---------- 400
Consensus AAELFGRALD EGKLPNLNSE VGAGWGPNGN IMTARANHMW
Conservation
420
440
1b4v,_chain_A NPTGAHQSSI PALGIDAWDN SDSSVFAEIA PMPAGLETWV 440
2DU8_chainA.pdb,_chain_A ---------- ---------- ---------- ---------- 440
Consensus NPTGAHQSSI PALGIDAWDN SDSSVFAEIA PMPAGLETWV
Conservation
460
480
1b4v,_chain_A SLYLAITKNP QRGTFVYDAA TDRAKLNWTR DQNAPAVNAA 480
2DU8_chainA.pdb,_chain_A ---------- ---------- ---------- ---------- 480
Consensus SLYLAITKNP QRGTFVYDAA TDRAKLNWTR DQNAPAVNAA
Conservation
500
520
1b4v,_chain_A KALFDRINKA NGTIYRYDLF GTQLKAFADD FCYHPLGGCV 520
2DU8_chainA.pdb,_chain_A ---------- ---------- ---------- ---------- 520
Consensus KALFDRINKA NGTIYRYDLF GTQLKAFADD FCYHPLGGCV
Conservation
540
560
1b4v,_chain_A LGKATDDYGR VAGYKNLYVT DGSLIPGSVG VNPFVTITAL 560
2DU8_chainA.pdb,_chain_A ---------- ---------- ---------- ---------- 560
Consensus LGKATDDYGR VAGYKNLYVT DGSLIPGSVG VNPFVTITAL
Conservation
1b4v,_chain_A AERNVERIIK QDV 573
2DU8_chainA.pdb,_chain_A ---------- --- 573
Consensus AERNVERIIK QDV
Conservation

3. ChoA and glucose oxidase from *Aspergillus niger*

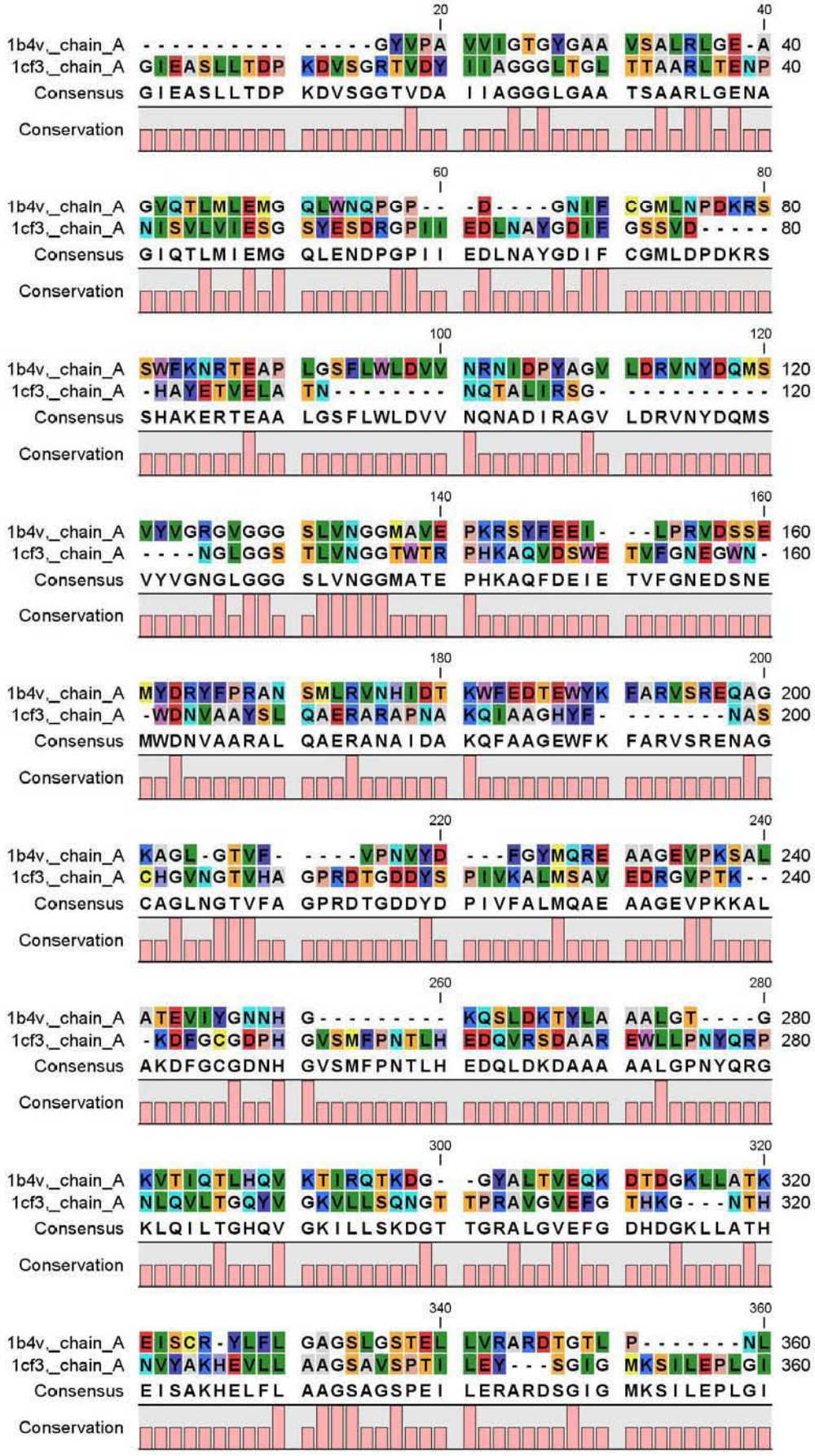

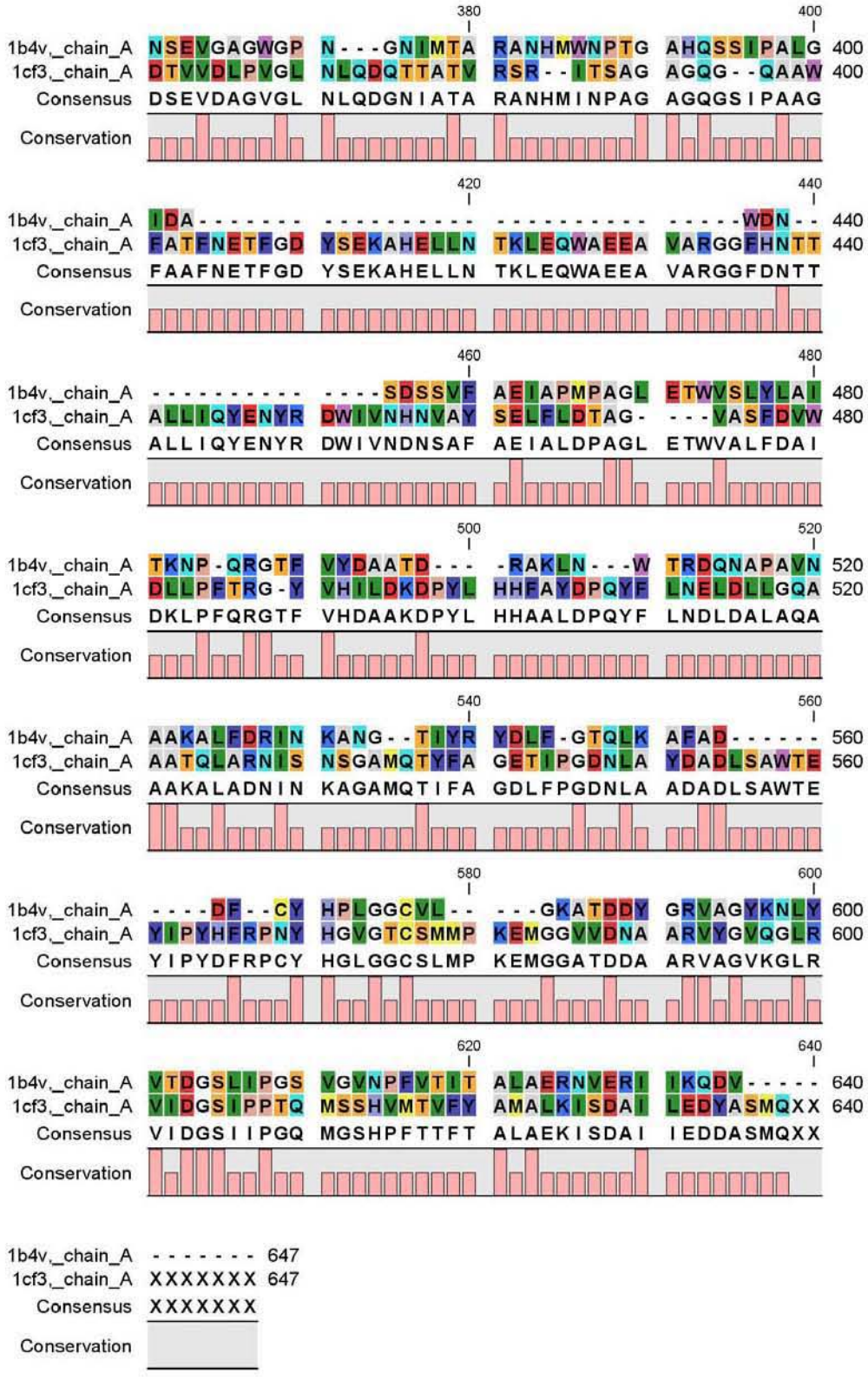
380
400
1b4v._chain_A NSEVGAGWGP N---GNIMTA RANHMWNPTG AHQSSIPALG 400
1cf3._chain_A DTVVDLPVGL NLQDQTTATV RSR--ITSAG AGQG--QAAW 400
Consensus DSEVDAGVGL NLQDGNIATA RANHMINPAG AGQGSIPAAG
Conservation
420
440
1b4v._chain_A IDA------- ---------- ---------- -----WDN-- 440
1cf3._chain_A FATFNETFGD YSEKAHELLN TKLEQWAEEA VARGGFHNTT 440
Consensus FAAFNETFGD YSEKAHELLN TKLEQWAEEA VARGGFDNTT
Conservation
460
480
1b4v._chain_A ---------- ----SDSSVF AEIAPMPAGL ETWVSLYLAI 480
1cf3._chain_A ALLIQYENYR DWIVNHNVAY SELFLDTAG- ---VASFDVW 480
Consensus ALLIQYENYR DWIVNDNSAF AEIALDPAGL ETWVALFDAI
Conservation
500
520
1b4v._chain_A TKNP-QRGTF VYDAATD--- -RAKLN---W TRDQNAPAVN 520
1cf3._chain_A DLLPFTRG-Y VHILDKDPYL HHFAYDPQYF LNELDLLGQA 520
Consensus DKLPFQRGTF VHDAAKDPYL HHAALDPQYF LNDLDALAQA
Conservation
540
560
1b4v._chain_A AAKALFDRIN KANG--TIYR YDLF-GTQLK AFAD------ 560
1cf3._chain_A AATQLARNIS NSGAMQTYFA GETIPGDNLA YDADLSAWTE 560
Consensus AAKALADNIN KAGAMQTIFA GDLFPGDNLA ADADLSAWTE
Conservation
580
600
1b4v._chain_A ----DF--CY HPLGGCVL-- ---GKATDDY GRVAGYKNLY 600
1cf3._chain_A YIPYHFRPNY HGVGTCSMMP KEMGGVVDNA ARVYGVQGLR 600
Consensus YIPYDFRPCY HGLGGCSLMP KEMGGATDDA ARVAGVKGLR
Conservation
620
640
1b4v._chain_A VTDGSLIPGS VGVNPFVTIT ALAERNVERI IKQDV----- 640
1cf3._chain_A VIDGSIPPTQ MSSHVMTVFY AMALKISDAI LEDYASMQXX 640
Consensus VIDGSIIPGQ MGSHPFTTFT ALAEKISDAI IEDDASMQXX
Conservation
1b4v._chain_A -------- 647
1cf3._chain_A XXXXXXX 647
Consensus XXXXXXX
Conservation

4. ChoA and hydroxynitrile lyase from almond

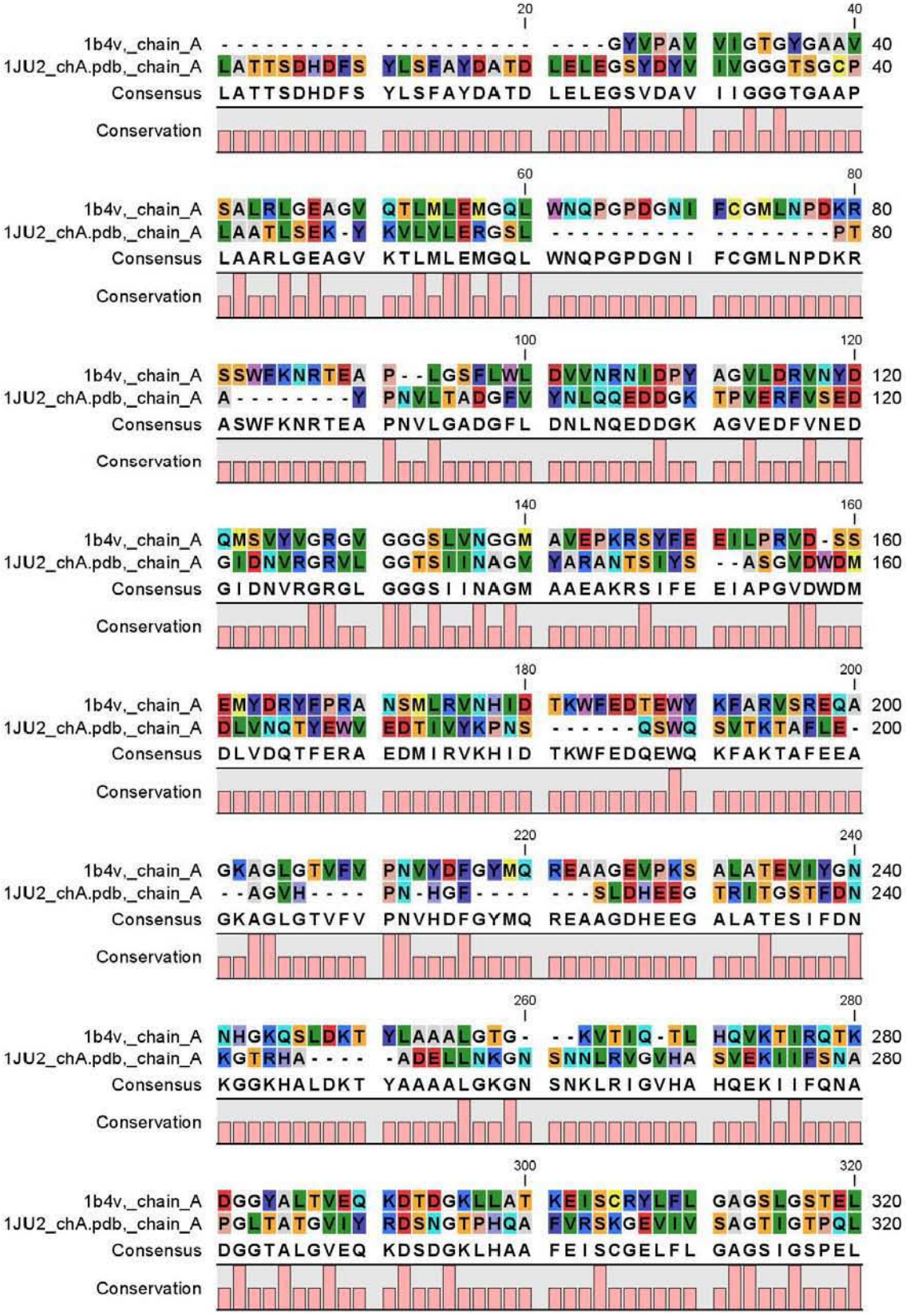

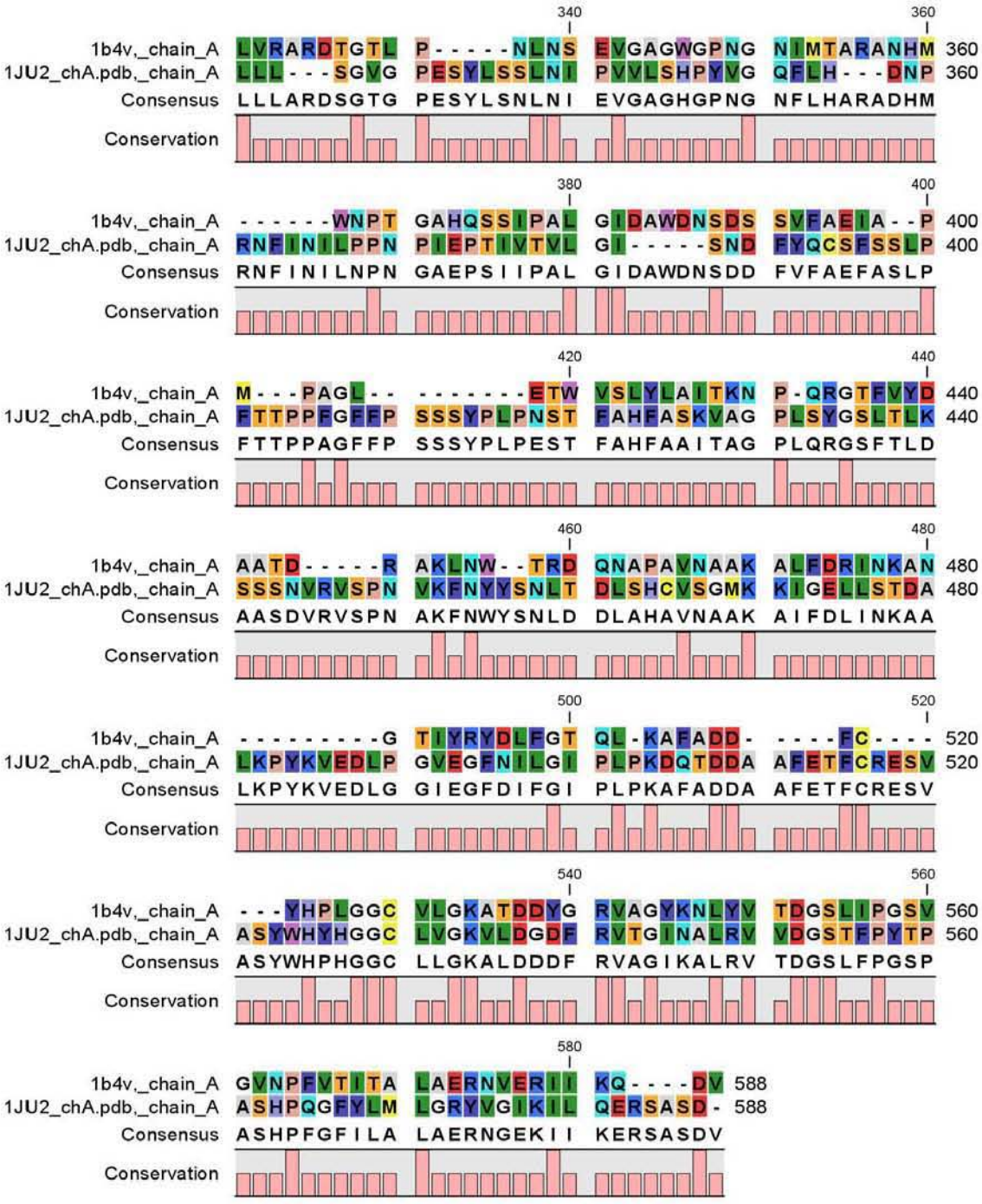
340
360
1b4v,_chain_A LVRARDTGTL P-----NLNS EVGAGWGPNG NIMTARANHM 360
1JU2_chA.pdb,_chain_A LLL---SGVG PESYLSSLNI PVVLSHPYVG QFLH---DNP 360
Consensus LLLARDSGTG PESYLSNLNI EVGAGHGPNG NFLHARADHM
Conservation
380
400
1b4v,_chain_A ------WNPT GAHQSSIPAL GIDAWDNSDS SVFAEIA--P 400
1JU2_chA.pdb,_chain_A RNFINILPPN PIEPTIVTVL GI-----SND FYQCSFSSLP 400
Consensus RNFINILNPN GAEPSIIPAL GIDAWDNSDD FVFAEFASLP
Conservation
420
440
1b4v,_chain_A M---PAGL-- -------ETW VSLYLAITKN P-QRGTFVYD 440
1JU2_chA.pdb,_chain_A FTTPPFGFFP SSSYPLPNST FAHFASKVAG PLSYGSLTLK 440
Consensus FTTPPAGFFP SSSYPLPEST FAHFAAITAG PLQRGSFTLD
Conservation
460
480
1b4v,_chain_A AATD-----R AKLNW--TRD QNAPAVNAAK ALFDRINKAN 480
1JU2_chA.pdb,_chain_A SSSNVRVSPN VKFNYYSNLT DLSHCVSGMK KIGELLSTDA 480
Consensus AASDVRVSPN AKFNWYSNLD DLAHAVNAAK AIFDLINKAA
Conservation
500
520
1b4v,_chain_A ---------G TIYRYDLFGT QL-KAFADD- ----FC---- 520
1JU2_chA.pdb,_chain_A LKPYKVEDLP GVEGFNILGI PLPKDQTDDA AFETFCRESV 520
Consensus LKPYKVEDLG GIEGFDIFGI PLPKAFADDA AFETFCRESV
Conservation
540
560
1b4v,_chain_A ---YHPLGGC VLGKATDDYG RVAGYKNLYV TDGSLIPGSV 560
1JU2_chA.pdb,_chain_A ASYWHYHGGC LVGKVLDGDF RVTGINALRV VDGSTFPYTP 560
Consensus ASYWHPHGGC LLGKALDDDF RVAGIKALRV TDGSLFPGSP
Conservation
580
1b4v,_chain_A GVNPFVTITA LAERNVERII KQ----DV 588
1JU2_chA.pdb,_chain_A ASHPQGFYLM LGRYVGIKIL QERSASD- 588
Consensus ASHPFGFILA LAERNGEKII KERSASDV
Conservation

5. ChoA and pyranose 2-oxidase from *Trametes multicolor*

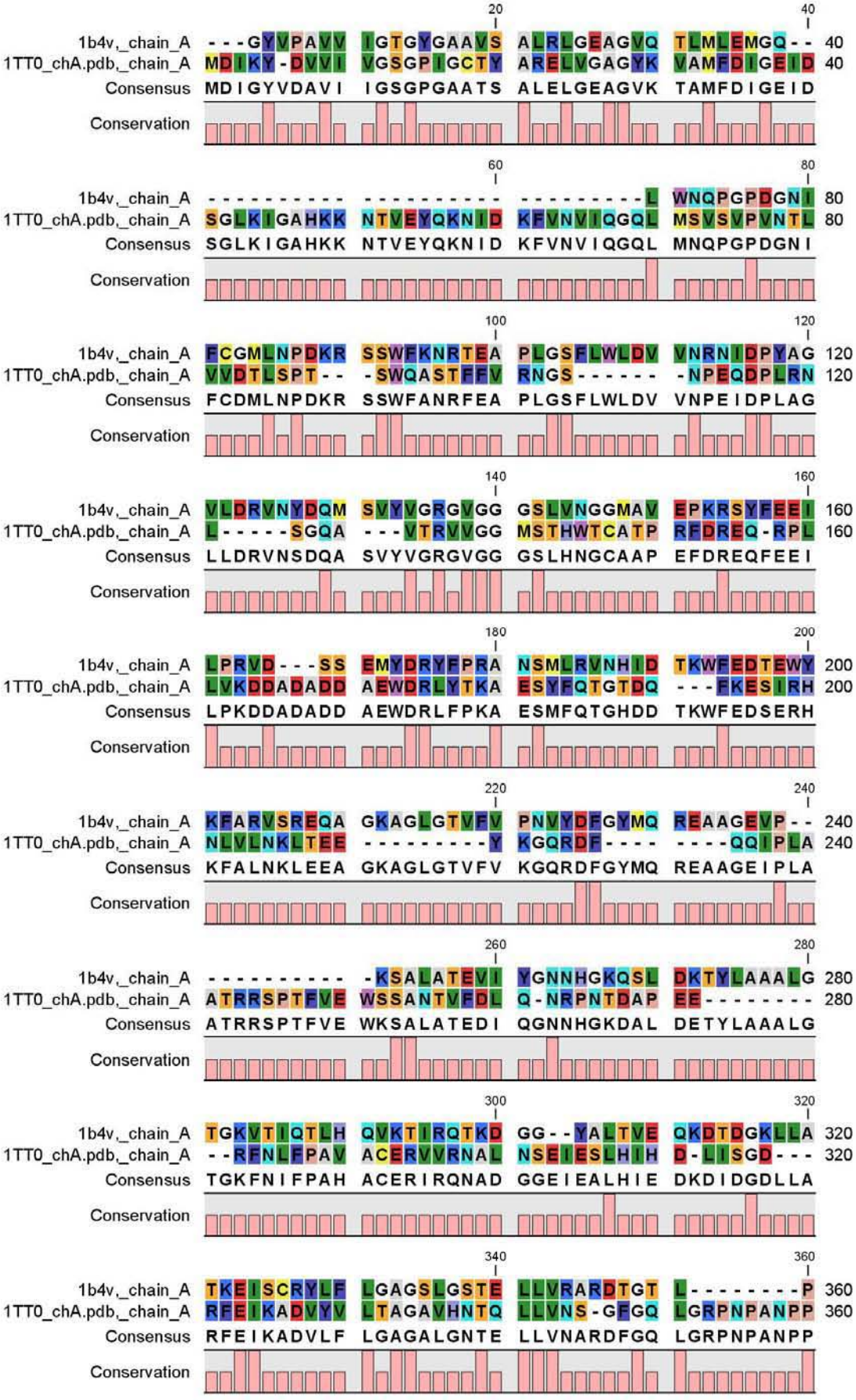

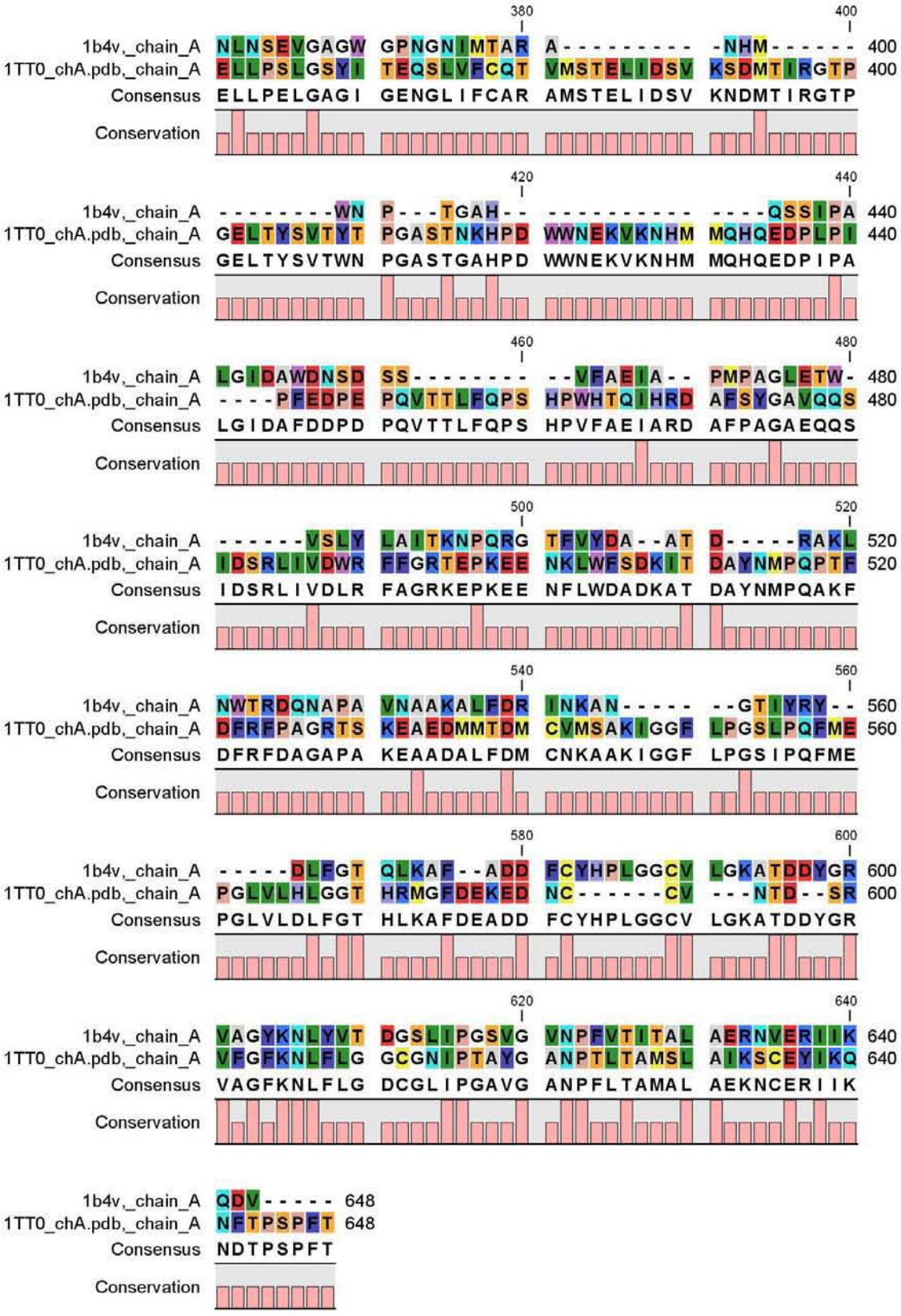
380
400
1b4v,_chain_A NLNSEVGAGW GPNGNIMTAR A---------- -NHM------ 400
1TT0_chA.pdb,_chain_A ELLPSLGSYI TEQSLVFCQT VMSTELIDSV KSDMTIRGTP 400
Consensus ELLPELGAGI GENGLIFCAR AMSTELIDSV KNDMTIRGTP
Conservation
420
440
1b4v,_chain_A --------WN P---TGAH-- ---------- ----QSSIPA 440
1TT0_chA.pdb,_chain_A GELTYSVTYT PGASTNKHPD WWNEKVKNHM MQHQEDPLPI 440
Consensus GELTYSVTWN PGASTGAHPD WWNEKVKNHM MQHQEDPIPA
Conservation
460
480
1b4v,_chain_A LGIDAWDNSD SS-------- --VFAEIA-- PMPAGLETW- 480
1TT0_chA.pdb,_chain_A ----PFEDPE PQVTTLFQPS HPWHTQIHRD AFSYGAVQQS 480
Consensus LGIDAFDDPD PQVTTLFQPS HPVFAEIARD AFPAGAEQQS
Conservation
500
520
1b4v,_chain_A ------VSLY LAITKNPQRG TFVYDA--AT D-----RAKL 520
1TT0_chA.pdb,_chain_A IDSRLIVDWR FFGRTEPKEE NKLWFSDKIT DAYNMPQPTF 520
Consensus IDSRLIVDLR FAGRKEPKEE NFLWDADKAT DAYNMPQAKF
Conservation
540
560
1b4v,_chain_A NWTRDQNAPA VNAAKALFDR INKAN----- --GTIYRY-- 560
1TT0_chA.pdb,_chain_A DFRFPAGRTS KEAEDMMTDM CVMSAKIGGF LPGSLPQFME 560
Consensus DFRFDAGAPA KEAADALFDM CNKAAKIGGF LPGSIPQFME
Conservation
580
600
1b4v,_chain_A -----DLFGT QLKAF--ADD FCYHPLGGCV LGKATDDYGR 600
1TT0_chA.pdb,_chain_A PGLVLHLGGT HRMGFDEKED NC------CV ---NTD--SR 600
Consensus PGLVLDLFGT HLKAFDEADD FCYHPLGGCV LGKATDDYGR
Conservation
620
640
1b4v,_chain_A VAGYKNLYVT DGSLIPGSVG VNPFVTITAL AERNVERIIK 640
1TT0_chA.pdb,_chain_A VFGFKNLFLG GCGNIPTAYG ANPTLTAMSL AIKSCEYIKQ 640
Consensus VAGFKNLFLG DCGLIPGAVG ANPFLTAMAL AEKNCERIIK
Conservation
1b4v,_chain_A QDV----- 648
1TT0_chA.pdb,_chain_A NFTPSPFT 648
Consensus NDTPSPFT
Conservation